THE SENSITIVITY OF NONDESTRUCTIVE TESTING IN DETECTING FREEZE-THAW DETERIORATION IN CONCRETE

Yutai Liu

The Department of Civil Engineering and Applied Mechanics
McGill University
Montreal, Canada

July 2015

A thesis submitted to McGill University in partial fulfillment of the requirements of the degree of Master of Engineering

ABSTRACT

In cold regions, freeze-thaw damage is considered one of the most important factors in concrete deterioration. Repeated freeze-thaw cycles can cause internal cracking, scaling and even complete disintegration of concrete if the concrete is not properly designed. For the purpose of detecting internal freeze-thaw damage at early stages and minimize the subsequent cost of repair, effective and convenient concrete testing techniques are of great importance.

The objective of this thesis was to evaluate the sensitivity of various nondestructive testing techniques in detecting freeze-thaw deterioration in concrete. Three nondestructive test (NDT) methods were investigated and compared in this thesis: the surface resistivity test (SR), the bulk resistivity test (BR) and the ultrasonic pulse velocity test (UPV). The pressure tension test (PT) has proven to be more sensitive in detecting the internal cracking of concrete compared to other tension tests. This thesis utilized this method to quantify the freeze-thaw damage in concrete specimens and further evaluate its applicability in evaluating the deterioration in concrete associated with cyclic freeze and thaw. Two concrete mixes of W/C 0.65 and 0.45 were prepared and cured for 28 days before being subjected to freeze-thaw cycling according to ASTM standard C666. NDT and pressure tension testing were carried out on the specimens to monitor deterioration over ongoing freeze-thaw cycles. The relationships between the test results of NDT and PT were studied. Test results showed that the three NDT methods exhibit various sensitivities and capabilities in detecting freeze-thaw damage in concrete. SR is very sensitive in detecting freeze-thaw damage, while BR and UPV are able to detect freeze-thaw deterioration only when the damage is more severe. In addition, testing showed that the surface resistivity is very sensitive to temperature change, an issue that must be considered when implementing this technique in the field.

SOMMAIRE

Dans les régions froides, les dégâts de gel-dégel sont considérés comme l'un des facteurs les plus importants de détérioration du béton. Des cycles de gel-dégel répétés peuvent provoquer, dans des bétons incorrectement conçu, des fissures internes, de l'écaillage voir même la désintégration complète du béton. Afin de détecter des dégâts internes de gel-dégel à des étapes préliminaires et de minimiser le coût de la réparation ultérieure, trouver des techniques de tests du béton efficaces et pratiques est d'une grande importance.

L'objectif de cette thèse était d'évaluer la sensibilité de diverses techniques de contrôle non destructif pour la détection des détériorations du béton due aux cycles de gel-dégel. Trois méthodes de contrôle non destructif (NDT) ont été étudiées et comparées dans cette thèse: l'essai de la résistivité de surface (SR), l'essai de la résistivité de volume (BR) et l'essai de vitesse d'impulsions ultrasoniques (UPV). L'essai de traction par pression (PT) est reconnu comme étant plus sensible pour la détection de fissuration interne du béton par rapport à d'autres essais de traction. Cette thèse a utilisé cette méthode pour quantifier les dégâts de gel-dégel dans les échantillons de béton et pour continuer d'évaluer l'applicabilité de cette méthode dans l'évaluation de la détérioration du béton soumis à des cycles de gel-dégel. Deux mélanges de béton de rapport eau/ciment (W/C) 0.65 et 0.45 ont été préparés et une cure de 28 jours a été faite avant que les échantillons soient soumis à des cycles de gel-dégel selon la norme ASTM C666. Les essais NDT et PT ont été régulièrement effectués sur les échantillons pour surveiller la détérioration au cours des cycles de gel-dégel. Les relations entre les résultats des essais NDT et PT ont été étudiées. Les résultats des essais ont montré que les trois méthodes de NDT présentent différentes sensibilités et capacités dans la détection des dégâts de gel-dégel dans le béton. SR est très sensible dans la détection des dégâts de gel-dégel, tandis que BR et UPV sont capables de détecter les détériorations de gel-dégel seulement lorsque les dégâts sont plus sévères. En outre, les essais ont montré que la résistivité de surface est très sensible aux changements de température, un enjeu qui doit être considéré lors de la mise en œuvre de cette technique en chantier.

ACKNOWLEDGEMENTS

The author would like to sincerely thank all those participated in the completion of this thesis as well as those involved in the experimental research.

First and foremost, I would like to thank sincerely my supervisor, Prof. Andrew J. Boyd. Without his insightful guidance and encouraging support, as well as his financial assistance, the completion of this thesis and experimental work wouldn't be possible. I would also like to acknowledge my colleagues, Andrew Komar and Omar Shaikhon, for their help and collaboration on this research. My sincere thanks also go to John Bartczak, along with the staff members of the materials laboratory of McGill University for their help in carrying out the experimental work.

Last but not least, I am mostly grateful for the love and support from my family and friends throughout the completion of my studies.

TABLE OF CONTENT

LIST OF FIGURES

LIST OF TABLES

INTRODUCTION

Concrete infrastructure is subjected to various kinds of deterioration throughout its service life. In most parts of Canada, concrete structures are subjected to cyclic freeze and thaw and this kind of damage is especially evident in old structures where air-entrained concrete was not used. In many regions of Canada, temperature can reach lower than -30°C in the winter and above 30°C degree in the summer. This extreme environmental condition is what makes concrete structures susceptible to freeze-thaw deterioration. Air entrainment was found to be beneficial in concrete exposed to freeze-thaw cycles in the 1940s (Ward & Langan, 1990). It is considered the most widely used method for the protection of concrete against freeze-thaw damage. With air-entrainment, the durability of concrete improves greatly against freeze-thaw cycling and thus it is a necessary inclusion in concrete structures exposed to freeze-thaw cycles. However, this does not exclude concrete from such damage or provide a life-long guarantee. It does, however, greatly extend the expected service life of structures. Potholes are most commonly seen in the pavements in Canada, which are mostly the results of cyclic freeze-thaw cycles and deicing salt. Edmonton is spending 5.9 million dollars on pothole repair in 2015 alone, and is investing 55 million per year on arterial road rehabilitation over the next 4 years (Mertz, 2015). As for the southern neighbor of Canada, the United States spends nearly $50 billion annually on repair of the infrastructure according to the National Research Council. (JValenza & Scherer, 2006)

For the purpose of detecting internal damage in concrete at early stages and minimize the subsequent cost of repair, effective and convenient concrete testing techniques are of great importance. Coring in existing structures is often utilized to determine concrete strength. However, coring is a destructive test method, which will leave flaws that will potentially require further repair afterward. Nondestructive testing is considered beneficial when it comes to long-term monitoring. It is completely nondestructive and noninvasive, much easier to implement, and more convenient compared to coring.

The objective of this work was to determine the ability of nondestructive testing (NDT) techniques to detect and monitor internal freeze-thaw damage. In this work, three nondestructive test methods: surface resistivity (SR), bulk resistivity (BR) and ultrasonic pulse resistivity (UPV) were utilized. Concrete specimens with different water-cement ratios were cast and exposed to freeze-thaw conditions following ASTM C666. In the meantime, destructive testing (using the pressure tension test (PT)) was performed on concrete samples to validate the sensitivity of the nondestructive test methods. An evident contrast of resistance to freeze-thaw deterioration was present in specimens with different water-cement ratio. In addition, the relationship between temperature and surface resistivity was investigated and found to be a significant factor affecting the implementation of surface resistivity in field conditions.

CHAPTER 1 LITERATURE REVIEW

1.1. Freeze-Thaw Deterioration

Concrete is composed of cement, water, fine aggregates and coarse aggregates, and admixtures are often added to improve its performance in the fresh and hardened states. If properly designed, cast and cured, concrete will withstand adverse weather conditions; cold climates, for example, where cyclic freeze-thaw is prevalent (Al‐Assadi, Casati, Fernández, & Gálvez, 2011).

Freeze-thaw deterioration occurs mainly in Northern climates where cyclic freeze-thaw is frequent (Figure 1). Liquid within concrete will expand when it freezes and induces contraction when it thaws (Chini, Muszynski, & Hicks, 2003). The 9% volume increase of liquid upon freezing causes internal hydraulic pressure in the concrete's capillary pores. If the hydraulic pressure exceeds the tensile resistance of the concrete, internal cracking will occur (POWERS, 1945). If this happens cyclically, it will diminish concrete durability significantly throughout the process.

Significant durability issues of structures were noticed in a major city in Canada in the late sixties. After a review and study on the existing construction practices, the main conclusion was drawn that the in-situ concrete did not have adequate amount of entrained air content. These results, together with a review of concurrent specifications in other metropolitan centers, became the foundation for the revision of concrete materials specifications in the seventies (Ward & Langan, 1990).

Figure 1: Typical example of concrete deteriorated from freeze-thaw actions (non-air entrained concrete railing)

Source: http://www.concrete-experts.com/pages/ft.htm

1.1.1 Freeze-Thaw Damage Mechanism

1.1.1.1 Hydraulic Pressure Theory

According to Powers (1945), the hydraulic pressure from the 9% volumetric expansion during the phase change of water to ice is the primary reason for freeze-thaw damage in concrete. The formation of ice in capillary pores requires additional space, and if the pores are already fully saturated, the excess water is forced into the adjacent pores, inducing hydraulic pressure. If the hydraulic pressure is greater than the tensile capacity of the concrete, frost damage occurs. However, this does not mean that a concrete specimen will fail completely when undergoing its first freezing. In fact, concrete is ordinarily not fully saturated and there is residual space in concrete for it to accommodate the expansion upon freezing.

At the beginning of a freezing cycle, the specimen surface is considered more saturated because it has been in contact with water for some time, and thus, the water to ice phase transition will start from the surface. Secondly, the water in bigger capillary pores near the surface will freeze first, and the unfrozen water will be propelled into the less saturated

pores, causing hydraulic pressure in the concrete. This process is illustrated with the help of Figure 2. A is the saturated surface region of a specimen; B is area with lower water content.

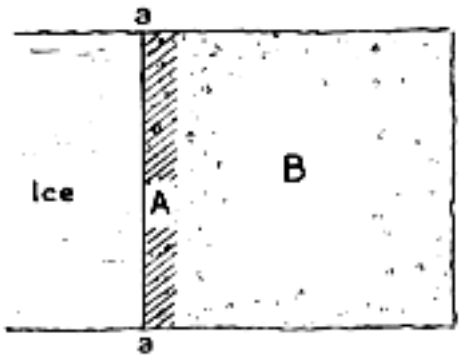

Figure 2: Process of freezing of a specimen

Source: (POWERS, 1945)

Freezing will first occur in Area A because it has a lower freezing point, and there is a temperature gradient between A and B. Subsequently, water in Region B will supercool. The mechanism behind this is that A has a higher water content than B and is at a lower temperature because it is closer to the exterior environment. When water in Region A starts to freeze, the free water will move toward Region B. Hence, hydraulic pressure is developed because the water is propelled through a compacted and porous material.

However, Even though it seems clear that hydraulic pressure is the reason for freeze-thaw damage, the hydraulic theory cannot account for all of the observations during freezing, especially with paste of high porosity and fully saturated (POWERS, 1975). There were cases where this theory could not account for all of the deterioration. Air-entrained cement paste contracted more than can be accounted for by thermal contraction during freezing. Contrary to the theory that ice formation develops as temperature decreases, non-air-entrained cement specimens continued to expand even though temperature was kept constant during freezing (Powers & Helmuth, 1953).

1.1.1.2 Osmotic Pressure Theory

Hydraulic pressure was not considered to be the only cause of paste volume change. It is hydraulic pressure and diffusion acting together that cause expansion (Powers & Helmuth, 1953). According to Powers' research in 1975 (POWERS, 1975), hydraulic pressure theory was based on inconclusive studies, focusing mainly on the cement paste structure and amount of ice formation.

It is known that a considerable amount of evaporable water in concrete is in the absorbed state, which is not freezable, and the rest is contained in capillaries as freezable water. Freezable water in capillary pores has different freezing points depending on the pore size. Water in smaller pores can have significantly lower freezing points compared to that in larger capillary pores. As is also known, the freezing point is lowered by impure solution in capillary pores, and dissolved alkali is usually found in concrete pore solution.

Powers found out that water in larger pores will freeze first during cooling to a temperature in the freezing range and freezable water in smaller pores remains unfrozen. The freezing process continues when temperature is lowered and less water remains unfrozen with lower temperature. Some of the water in the larger pores will remain unfrozen as well, owing to the dissolved alkalis. Freezing in concrete paste starts from an ice crystal and propagates from the rapid growth of dendritic ice crystal. Therefore, in an isolated cavity, the temperature has to be low enough to generate an ice crystal seed for the freezing to propagate.

Osmotic pressure is present when there is movement of unfrozen water toward the ice, or to more concentrated solution at the freezing sites. The occurrence of osmotic pressure depends on whether or not the cavity is full of solution and ice. Unfrozen capillary water is drawn to capillary pores where solution is more concentrated or an ice-containing cavity regardless of the solution concentration, including zero, i.e., pure water. Before causing

expansion, paste shrinks as unfrozen water is drawn to ice-containing cavities. Therefore, the observed change (expansion occurring after shrinkage during freezing) is the resultant of the two effects.

1.1.1.3 Litvan's Theory

Based on Litvan's theory (1973), water contained in capillary pores or adsorbed on the surface of concrete does not freeze without redistribution. Surface force restraining the mobility of water molecules is the reason why a crystal lattice is not formed, which is essential for ice formation.

The concept of vapor pressure is used to explain this mechanism. When cooled below 0 °C, water in concrete pores could turn into ice, or could stay as supercooled water due to surface force restricting it from forming ice. Supercooled water has a higher vapor pressure than ice, which results in a disequilibrium state. This pressure gradient expels water out of the pores into surroundings of the paste and desiccates the paste itself. The expelled water will freeze quickly once outside of the pore system. An equilibrium state is reestablished. Any further cooling will continue to disturb the equilibrium state and contribute to the desiccation of the paste.

Damage can occur in two forms according to Litvan (1973). The first one is that instead of being expelled out of the paste, water migrates to cracks or fissures in concrete. The water accumulates and fills the cracks completely. When water freezes into ice, the crack propagates and damage occurs. In general, damage firstly occurs in the weakest part of the concrete and propagates to the sound areas. The second damage form is that water freezes into ice before it can be fully expulsed from the paste due to the rapid cooling rate. In this case, ice blocks the channels and further damage is induced because of the subsequent internal pressure.

1.1.2 Factors Affecting Freeze-Thaw Deterioration

Frost damage in concrete could be concluded in two basic mechanisms. Volumetric change related to freezable water in concrete, and pressure induced by transport of water during freezing (Gerard Gabriel Litvan, 1980; Powers & Helmuth, 1953; Powers & Willis, 1950).

Given the physical processes involved, the durability of concrete subjected to frost damage is primarily determined by (1) the pore characteristics of concrete; (2) pore solution; (3) properties of cementing materials, aggregates and admixtures; (4) external conditions (B., 1989; Mindess, Young, & Darwin, 1981).

1.1.2.1 Pore Characteristics

Pore characteristics can be generalized as pore volume, pore size and pore spacing. The reason for the importance of pore characteristics is that they are closely related to the water transport properties of concrete. The water transport properties of pore structure in concrete rely on factors of void spacing, void size and the void connectivity. In non-air-entrained concrete, the transport of water may cause stress exceeding its tensile capacity if no enough air bubbles are present or the void volume is not enough. If the pore structure of concrete is properly designed for frost damage, excess water is expelled to nearby voids to relieve pressure (Leger & Tinawi, 1995). The capillary pores in concrete are filled with water as the freeze-thaw cycles increase and irreversible damage occurs until there is no residual room for the volumetric expansion. Concrete drying between freeze-thaw cycles releases space in capillary pores, but if no drying occurs, freeze-thaw damage is detrimental to concrete after a significant number of cycles (B., 1989; Mindess et al., 1981).

There are four types of pores in concrete based on their sizes: (1) gel pores (1.5–2.0 μm); (2) capillary pores (5–5000 μm); (3) macro pores resulting from entrained air; (4) macro pores resulting from inadequate compaction. Gel pore have no negative effect on concrete strength but are directly related to creep and shrinkage of concrete. Capillary pores and other larger pores are responsible for concrete strength and elasticity (Cai & Liu, 1998; Cordon, 1966; POWERS, 1945).

Pore spacing is widely regarded as the most important factor for concrete exposed to frost damage. From Powers' hydraulic pressure theory, pore distance instead of the total volume is the determining factor for protection, provided that total air volume is at least 1 percent. (POWERS, 1945). A direct relationship can be drawn between freeze-thaw damage and void spacing of concrete, and according to previous studies, a void spacing of less than 250 μm is believed to be adequate for concrete to resist freeze-thaw damage (Powers & Willis, 1950).

Concrete with a large number of small, well-distributed, air voids demonstrates a much-reduced rate of disintegration and internal damage upon freezing. This is due to residual room for expansion and limiting the spacing between pores, which will allow expelled water to move to them without generating high hydraulic pressures (POWERS, 1945). To achieve ideal concrete durability when subjected to freeze-thaw damage, porosity should be maintain at a very low level. Pores of large size and small size are preferable than those of medium size. Large pores are rarely fully saturated and water in small pores is only freezable at very low temperature. The pore characteristics of concrete are mainly determined by water-cement ratio (G. G Litvan, 1973). From the test results of some mixes, it was found that concrete made with small size aggregates require more air content than concrete with larger size aggregates in order to resist frost damage (Backstrom, Burrows, Wolkodoff, & Powers, 1954).

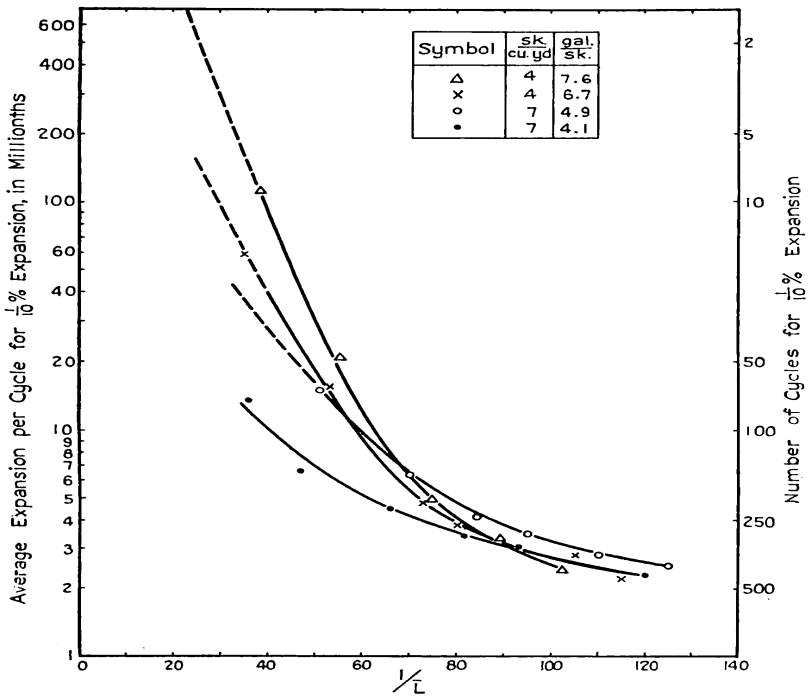

Figure 3: Relationship between frost resistance and spacing factor

Source: (Backstrom et al., 1954)

Figure 3 shows the relationship between relative frost resistance and the computed spacing factor 1/L. All concrete mixes were made with about the same water-cement ratio. Each curve represents a concrete mix with a different amount of air-entraining agent, starting from zero. The inset in Figure 3 is the water-cement ratios of the mixes. It can be easily observed that when the pores are relatively far apart, there is only a small reduction of expansion, but when the spacing factor is around 0.01 in (1/L=100), the expansion rate of all mixes was reduced to the same level despite of the different amounts of freezable water (Backstrom et al., 1954).

1.1.2.2 Pore Solution

In general, freeze-thaw damage is closely related to the pore characteristics in cement paste. In addition, pore solution is also an important factor concerning degree of saturation, concentration and freezable water. Therefore, pore characteristics (which determine the freezing point and hydraulic pressure magnitude) with pore solution reflect the durability of concrete subjected to freeze-thaw damage (Cai & Liu, 1998). The effect of pore solution can be broken down to two aspects: degree of saturation and degree of concentration.

Based on Powers' hydraulic pressure theory, the underlying mechanism of concrete frost damage is the 9% volume change of phase change from water to ice. It has also been established that concrete is safe from frost damage if capillary pores are not filled with water, even when it is non air-entrained. This means that partially saturated concrete, if it is 91.7 % or less of the fully saturated state, might be free from freeze-thaw damage (POWERS, 1975). Even though the importance of degree of saturation is evident, reducing water content of concrete to below critical saturation degree is not a practical method. The thickness of the structure is the reason it takes an unpractically long time to dry below the critical limit and the subsequent cracking and arrested hydration are even more undesirable (BAŽANT, CHERN, Rosenberg, & Gaidis, 1988).

The cooling of evaporable water progresses as the temperature is lowered. As discussed in the osmotic pressure theory, due to the existence of dissolved hydroxides, the freezing point of evaporable water will be lower than 0 °C. Furthermore, as freezing starts, the pure ice separates from the solution, thus the solution becomes more concentrated and has an even lower freezing point (Powers & Brownyard, 1946). However, it was discovered that the effect of dissolved alkali on lowering the freezing point is not as great as the effect of the small dimension of pores (POWERS, 1975).

1.1.2.3 Properties of Cementitious Materials, Aggregates and Admixtures

The durability of concrete is greatly affected by its constituent cementitious materials and aggregates, as well as admixtures. The resistance of concrete against frost damage will be significantly improved when it is well designed with high performance cement, aggregates of low porosity, and appropriate admixtures.

The product of the cement and water reaction is called the hydration product, which provides the binding effect of the aggregates and has an influence on the pore size distribution of concrete. Cement type, or more specifically cement particle size, influences the size distribution of capillary pores. Cementing materials with finer particles produce concrete with smaller capillary pores. And, as discussed above, smaller capillary pores have lower freezing points and less freezable water. In addition, fine particles, silica fume for example, will act as microfillers in concrete and further reduce pore sizes. Finer particles also promote the hydration process, thus resulting in more compact concrete (Bentz, Garboczi, Haecker, & Jensen, 1999). Thus, cement properties are of great importance to freeze-thaw resistance and finer cement particle size is beneficial to the concrete hydration process and in reducing capillary pore size, which produces more free-thaw resistant concrete.

Aggregates, including fine and coarse aggregates, normally make up 60% to 75% of the total concrete volume (70% to 85% by mass). By the total volume it takes up in concrete, aggregates are not to be neglected when considering freeze-thaw damage. It is suggested that cement paste and aggregates ought to be considered separately when designing and preparing concrete if frost damage is involved. (POWERS, 1975) Coarse aggregates can affect durability of concrete upon freezing and thawing in two ways: 1) sound aggregates may expel water and causes damage in adjacent paste and aggregates; 2) unsound aggregates can deteriorate when subjected to repeated freeze-thaw cycles (Patel, 2009). Fine aggregates are usually not considered in frost damage due to their smaller size compared to coarse aggregates.

Hydraulic pressure will develop in saturated aggregates, which leads to cracking if pressure is not relieved. This can cause damage to the aggregates themselves and the surrounding paste. A popout may happen if the particle is close to the surface (POWERS, 1975). A critical dimension of aggregate is required for frost resistance, beyond which hydraulic pressure will exceed its tensile capacity. Local scaling is often found close to the surface of the structure if aggregates exceeding the critical size, as a result of the higher water content and higher number of freeze-thaw cycles at this location (Leger & Tinawi, 1995).

Apart from cementitious materials and aggregates, various admixtures also play an important role in freeze-thaw resistance of concrete. Air-entraining agents, water-reducing agents, superplasticizers, silica fume, and metakaolin have all been found to be able to improve the performance of fresh and hardened concrete. The improved properties of the concrete yield higher strength and overall enhanced durability, including better resistance against freeze-thaw damage. Due to the complexity and the variety of supplemental materials, the effect of admixtures on the resistance of concrete against freeze-thaw damage is not further discussed in this work.

1.1.2.4 External Conditions

External conditions include cooling rate, freezing temperature, presence of de-icing salts, chemical attacks, etc.

The magnitude or severity of hydraulic pressure is determined by the rate of water transport, that is to say, the cooling rate. Therefore, the higher the cooling rate, the more destructive the effect during freezing. External conditions affect the cooling rate of concrete specimens and it is not the same throughout all parts of the specimen. To some extent, the cooling rate at a certain point in the concrete specimen should depend on its distance from the surface. The greater the distance, the lower the cooling rate. Thus, the damage due to

rapid cooling rate would be less severe in the core of the specimen. Furthermore, the size of the specimen also affects the test results, as specimens of larger size will have less internal damage (POWERS, 1945). Therefore, concrete structures with thin and thick cross sections will have very different freezing rates due to heat conduction.

From the results of different mixes, it has been observed that the freezing rate has a turning point at about -10 °C. Pore solution freezes more slowly below -10 °C. According to Powers' hydraulic pressure theory, freezing rate is closely related to the magnitude of hydraulic pressure, and concrete is subjected to higher hydraulic pressure if there is a higher freezing rate. Therefore, if only freezing rate is considered, concrete will be subjected to more frost damage between 0 °C and -10 °C, for both ordinary and high-strength concrete. A possible reason behind this phenomenon is that a significant amount of the total pores are of certain pore sizes and their pore solution freezes above -10 °C. The solution in smaller pores starts to freeze below -10 °C, which induces less damage to concrete due to their relatively limited pore number (Cai & Liu, 1998).

At this point, it is known from the above that freeze-thaw damage is not only closely related to the cooling rate upon freezing, but also to the freezing temperature. The higher the cooling rate, the higher the hydraulic pressure that is generated. Plus, more damage occurs in certain temperature ranges in concrete upon freezing. In order not to cause severe frost damage in concrete, the combined effect of rapid cooling between 0° C and -10 °C should be avoided.

In cold regions, salt scaling is very common since de-icing salt is used on roadways very often to lower the freezing point. Salt scaling is a superficial damage of concrete mainly due to the use of de-icing salt, which leads to scaling and exposure of coarse aggregates. Salt scaling alone will not have a severe effect on the service life of a structure, but the chloride in it is detrimental to the reinforcing steel. The presence of chloride will cause deterioration of reinforcing steel and subsequent expansion, which leads to cracking, making the concrete even more susceptible to freeze-thaw damage. Salt scaling will also

promote a higher degree of saturation in concrete and it provides a base for further frost damage (JValenza & Scherer, 2006).

Chemical attacks are also related to the resistance of concrete against freeze-thaw deterioration. Sulfate attack is detrimental to the durability and service life of concrete. However, when it is combined with freeze-thaw cycles, sulfate solution is considered to have both positive and negative effects on concrete. The positive side is that the freezing point of the pore solution drops and sulfate attack is restrained due to the low temperature. The negative side is that accelerated cracking and damage occur due to the formation of expansive chemical products from sulfate attack (Jiang, Niu, Yuan, & Fei, 2015).

As the possible factors were discussed above, it can be easily concluded that all these factors do not act on their own, but instead, they act as factors influencing each other or act together. The resistance of concrete against frost damage is usually not determined by a single factor, but multiple factors and combined factors. For example, cyclic loading combined with the effect of de-icing salt has been found to accelerate freeze-thaw damage (Kosior-Kazberuk, 2012). If dry weather conditions are relatively common during freeze-thaw cycles, frost damage might be mitigated because of the unsaturated state of the concrete pores. The durability of concrete can be further improved with supplementary admixtures such as fly ash and silica fume to produce high-performance concrete. Therefore, when designing concrete exposed to frost damage or study the possible cause of damage, the combined effects should not be neglected.

1.2. Non-Destructive Testing

1.2.1. Surface Resistivity

1.2.1.1 Overview

The idea of measuring concrete surface resistivity originated from geologists using a test probe to measure material resistivity when investigating soil strata properties (Ewins, 1990). Similarly, concrete is also a porous material, which is the underlying basis for the application of surface resistivity on concrete. Concrete surface resistivity testing is based on the assumption that the geometry of the concrete specimen is semi-infinite, compared to the probe spacing (Morris, Moreno, & Sagüés, 1996). Surface resistivity is considered effective for detecting concrete deterioration. When used to monitor electrical resistance of a concrete sample throughout its service life, surface resistivity acts as an indication of its strength and durability. Concrete freeze-thaw damage causes the microstructure of concrete to become less compact due to the occurrence of microcracking, leading to subsequent concrete strength decrease and durability issues. In addition, surface resistivity is closely related to pore structure and pore solution of concrete. Therefore, with long term monitoring, surface resistivity can be a good nondestructive method to detect concrete internal damage and avoid economic loss or even structural failure.

1.2.1.2 Apparatus Configuration

The surface resistivity testing apparatus consists of a calibrating resistance panel and a chargeable testing device. This device consists of a display screen, four contact 'Wenner' probes and an electrical system generating current. See Figure 4 for the schematic of the Wenner array probe test.

The surface electrical resistivity could be measured in several ways, among which the Wenner method is the most frequently used. Four equally spaced electrodes are in direct contact with the concrete surface in the Wenner method. The two outer electrodes generate an AC current and the resultant potential difference is measured between the two inner electrodes to acquire the resistivity (Lencioni & de Lima, 2013). This method is completely non-destructive and can be performed in the laboratory or *in situ* with

commercially available equipment made by Proceq (used in this research) and others. See Figure 5 for test instrument used for surface resistivity.

AASHTO (American Association of State Highway and Transportation Officials) has standardized the test method (*AASHTO TP 95-11*) used to measure the resistivity of concrete cylinders, nominal size: 200-mm (8-in.) by length and 100-mm (4-in.) by diameter when using of a 4-pin Wenner probe array. The Wenner array generates an alternating current (AC) flow in the concrete by the surface resistivity device at the outer pins. The resultant potential difference between the two inner pins is measured. The resistivity of the concrete is calculated using the current generated and resultant potential on the tested sample. The resistivity, in kilohms-cm, is found to be related to chloride ion penetration (AASHTO-TP-95-11). The use of alternating current (AC) is preferred over direct current (DC) in order to avoid the polarization phenomenon that occurs at the contact interface between the probe and concrete (Ewins, 1990).

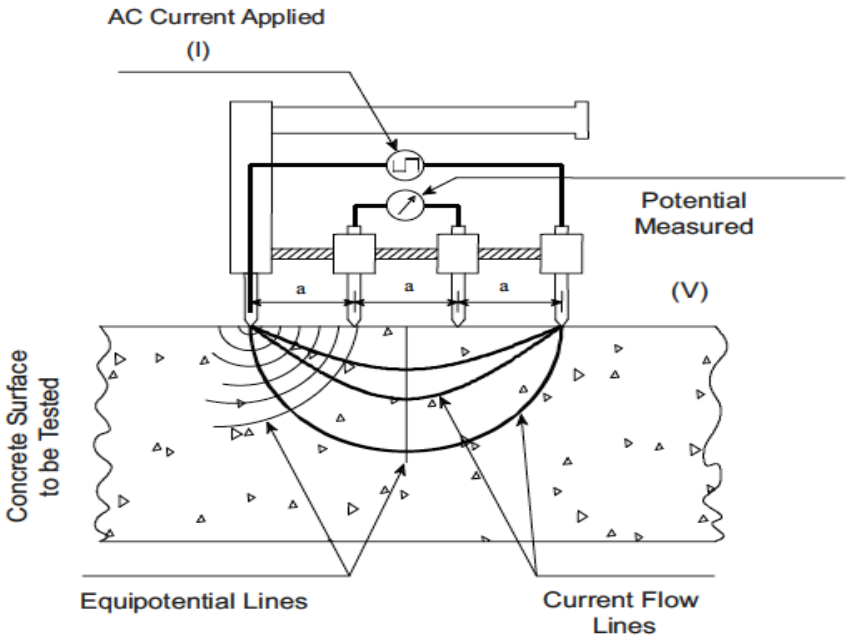

Figure 4: Four point Wenner array probe test setup

Source: (AASHTO-TP-95-11)

Figure 5: Proceq Resipod surface resistivity apparatus

The principle of this method is that chloride ions in a cylinder sample makes it more conductive, thus the test result will show a lower resistivity indicating the deterioration caused by chloride ion. Electrical resistivity can be used to evaluate microstructure of concrete because it's noninvasive and nondestructive. It is relevant to the volume fraction of the concrete pores, pore solution conductivity and can be adopted to predict the coefficients of chloride ion diffusion and water permeability (Christensen et al., 1994). The same manner can be applied to concrete cylinders subjected to freeze-thaw deterioration. Freeze-thaw cycles are known to do damage in concrete microstructures due to volume expansion of frozen water. The accompanying cracks will change the pore structure and thus have an impact on pore solution conductivity and overall conductivity. Hence, experiments were carried out in this work to further investigate the sensitivity of surface resistivity method in detecting deterioration in concrete caused by freeze-thaw damage.

1.2.1.3 Factors Affecting Surface Resistivity

Fundamentally, concrete conductivity is related to its permeability and diffusivity because of its porous nature (Whiting & Nagi, 2003). The resistivity of a saturated concrete specimen is mainly determined by the conductivity of its pore solution (Streicher &

Alexander, 1995). The main factors attributing to the surface resistivity of concrete can be summarized as the followings:

1.2.1.3.1 The Concrete Geometry

Concrete is heterogeneous by nature because concrete is composed of cement, coarse aggregates, fine aggregates, water and various admixtures. The Wenner resistivity measurement is considered valid when it is performed on a semi-infinite volume of material. If the concrete specimen has dimensions large enough, compared to the Wenner probe spacing, it can be considered as semi-infinite. Then the assumption of a semi-infinite geometry of concrete stands and will not result in significant errors. Whereas, if the dimension of the concrete specimen is relatively small, the current flow will have a different field pattern and the results are erroneous and overestimate the concrete resistivity (Gowers & Millard, 1999).

Therefore, to obtain accuracy of concrete surface resistivity measurement, the spacing of the electrode probes is critical. The materials tested are assumed to be homogeneous when using the Wenner resistivity method. However, due to its heterogeneous nature and the fact that aggregates normally have a much higher resistivity than cement paste, it is determined that the minimum probe spacing must be 1.5 times the size of the maximum aggregates. From a geometric aspect, the thickness of the measured sample also needs to be addressed. Though there is no definite depth of the penetration of the current fields, in theory 77% of the current reaches to a depth that is four times the probe spacing (Ewins, 1990; Millard & Harrison, 1989). It is recommended that the probe spacing does not exceed ¼ of the concrete section dimension. Also the distance between any contact probe and the specimen edges needs to be at least twice the probe spacing, though the proximity of the electrode probe to the end of the specimen is neglected (Lencioni & de Lima, 2013). Therefore, it can be concluded that the electric field diminishes rapidly below the surface of the concrete samples and most of the potential falls off very close to the electrodes.

1.2.1.3.2 Pore Solution

Another limitation to the application of the Wenner probe method on concrete is the pore solution. As pore solution is a determinant of concrete conductivity, if concrete is saturated with an unknown solution, the test results could yield misleading readings. One possible solution is removing the pore solution or replacing it with a known conductivity solution. However, removing pore solution in concrete requires drying the sample, which may lead to micro-cracking. Moreover, for *in situ* concrete, it is not practical to replace the pore solution (Vivas, 2007).

1.2.1.3.3 The Cement Hydration and Water Content

The electrical resistivity of concrete will increase as cement hydration progresses. The amount of evaporable water in freshly made concrete is about 60% by volume and decreases to around 20% after full hydration. With the decrease in water content, concrete resistivity also varies over time (Lencioni & de Lima, 2013). The water content of a concrete specimen is also an influencing factor on surface resistivity because conductivity changes along with the saturation state of concrete. The water content of a concrete specimen is not the same in all parts of the concrete. Near the concrete surface, the water content is most likely at or near total saturation, and is usually higher than the average water content of the concrete specimen (POWERS, 1945). Concrete will behave like an (semi-) insulator when it dries out, and no movement of ions or charges are permitted, but if water content is increased in the pore system, its resistivity will decrease significantly (Osterminski, Polder, & Schießl, 2012).

1.2.1.3.4 Aggregate Resistivities

Aggregate resistivities differ greatly depending on their sources and types. Concrete mixtures with granite aggregates have higher resistivities than those with limestone (Whiting & Nagi, 2003). But most aggregates used in structures are limited to hard, low-absorption aggregates basing on concrete specifications. Typical resistivities of these

aggregates are about 10^5 ohm-cm, while resistivities of cement paste or mortar are significantly lower, mostly in the range of 10^3 ohm-cm or less. Thus, for practical reasons, the resistivity of the aggregates could be considered as 'infinite' when compared to that of cement paste or mortar (Whiting & Nagi, 2003). The electrical resistivity of concrete will increase with an increase in the aggregate content and generally concretes containing larger aggregates has higher resistivity compared to those with smaller size. It was found that with the same aggregate volume in concrete, the resistivity of the concretes produced with crushed limestone aggregate was higher than those with gravel aggregates (Sengul, 2014).

1.2.1.3.5 Presence of Steel Reinforcement

Previous studies showed that electrical resistivity measurements give misleading results when reinforcing steel is present (Polder et al., 2000). The reinforcing steel has much better conductivity than concrete, providing a "short circuit" for the current, which leads to erroneous readings. The electrode probes should be placed at right angles to the steel instead of along them to minimize the error (Broomfield & Millard, 2002).

1.2.2. Bulk resistivity

1.2.2.1 Overview

Bulk resistivity measures the electrical resistivity of a concrete specimen over its total volume. Electrode plates replace the Wenner probes used in the surface resistivity test. The two plates are placed on the ends of the specimen to test the total bulk resistance of concrete cylinders. A potential difference is applied to the concrete specimen, producing a current flow through the cylinder. Then the bulk resistance is obtained using the potential difference and the resulting current (Ghosh & Tran, 2014). The bulk resistivity can be obtained by calculating the ratio of sample cross-section area to length. In the bulk

resistivity test, a good electrical contact between test specimen and electrode plates is necessary to ensure the accuracy of the measured value. The surface finish of the concrete cylinders should be flat to achieve good contact and the use of a conductive medium is also necessary. Similar to other electrical tests, the bulk resistivity method is influenced by the moisture content and temperature of the specimen. However, this test is rapid, easily performed and has a simple geometry factor (R. P. Spragg, Castro, Nantung, Paredes, & Weiss, 2011). It is very similar to surface resistivity in its nature and is nondestructive and noninvasive. The bulk resistivity test has the same advantages and limitations as surface resistivity test. By measuring the bulk resistivity of a saturated concrete specimen, the ability of it to resist penetration of ionic species by the diffusion mechanism is known. The curing criteria and testing specifications are same of surface resistivity test (Ghosh & Tran, 2014). However, there are also variations between these two methods, which will be illustrated later in this work with the comparison of test results.

1.2.2.2 Apparatus Configuration

The same model device was used in bulk resistivity, and in addition, two conductive plates, attached to the test device by two cables, and two conductive absorbent foams are included. The exact configuration is shown in Figure 6.

Figure 6: Proceq - Resipod bulk resistivity meter

1.2.2.3 Factors Affecting Bulk Resistivity

Bulk resistivity and surface resistivity both measure the electrical resistivity of materials, and they are subjected to the same test specifications. Thus, the factors that influence surface resistivity also influence bulk resistivity. As mentioned above, concrete geometry, degree of cement hydration, presence of reinforcing steel, as well as pore solution, aggregates and water content etc., which cause variation in concrete surface resistivity are also factors affecting bulk resistivity. Moreover, differing from surface resistivity test, the test spot does not influence the bulk resistivity as much as the surface resistivity because the measurement of overall bulk resistance eliminates the local irregularities of a concrete specimen. In addition, testing conditions are critical to avoid outliers and to measure the bulk resistivity accurately. Prior to testing, the cylinder specimen needs to be SSD (saturated-surface-dry), which is difficult to control and the absorbent foams inserted at both end of the cylinder must be saturated. The water drained out from the foams into the surface of the cylinder due to stress from the electrode plates and the cylinder. This also induces variation in measuring the bulk resistivity (Ghosh & Tran, 2014).

1.2.3. Ultrasonic Pulse Velocity

1.2.3.1 Overview

The ultrasonic pulse velocity test has been established for more than 70 years to evaluate the properties of concrete (S. R Cumming, 2004). It is based on the principle that the velocity of a compressional wave pulse through a medium depends on its elastic properties and density (Malhotra & Carino, 2003).

The ultrasonic pulse velocity (UPV) method is nondestructive and noninvasive. Mechanical waves are generated to travel through the concrete, and no damage occurs during this

process (S. R Cumming, 2004). According to *ASTM C597*, *Pulse Velocity Through Concrete*, an electro-acoustical transducer generates pulses of longitudinal stress waves, and the pulses travel through the concrete. The pulses are received after traversing the concrete, and are transferred into electrical energy by a second transducer. The measured straight-line distance and transit time are then used to calculate the velocity (ASTM-C597). The ultrasonic pulse velocity test has been used to evaluate the uniformity of concrete, detect internal cracking and voids (and their locations), perform quality control of concrete and concrete products by repeated measurements at the same locations, monitor the condition and deterioration of concrete, and determine the strength (when correlated with previous available data) (Qasrawi & Marie, 2003). The UPV method can be used to detect concrete internal damage and deterioration due to chemical invasion as well as freezing and thawing because the deterioration resulting from freeze-thaw cycles can cause cracking and changes to the pore system. The sensitivity of the UPV method in this application will be further studied in this work. It is also possible to make an estimation of the strength of concrete being tested using this method (Malhotra & Carino, 2003), provided a proper correlation between UPV and strength is available. However, the ultrasonic pulse velocity test does not provide results to be considered as a means to measure strength directly or establish the elastic modulus of field concrete (ASTM-C597).

The ultrasonic pulse velocity method can be used *in situ* and in laboratory, regardless of shape or size of the specimen as long as they are within the limitations of available pulse-generating sources (ASTM-C597). The testing device of ultrasonic pulse velocity made by Proceq is portable, easy to use and allows for rapid *in situ* or in laboratory testing.

1.2.3.2 Apparatus Configuration

The ultrasonic pulse velocity apparatus consists of a pulse generator, a transmitting transducer, a receiving transducer, an amplifier, a time-measuring circuit, a display unit

and two connecting cables (ASTM-C597). Figure 7 shows the schematic of a pulse velocity apparatus. Figure 8 shows the pulse velocity apparatus.

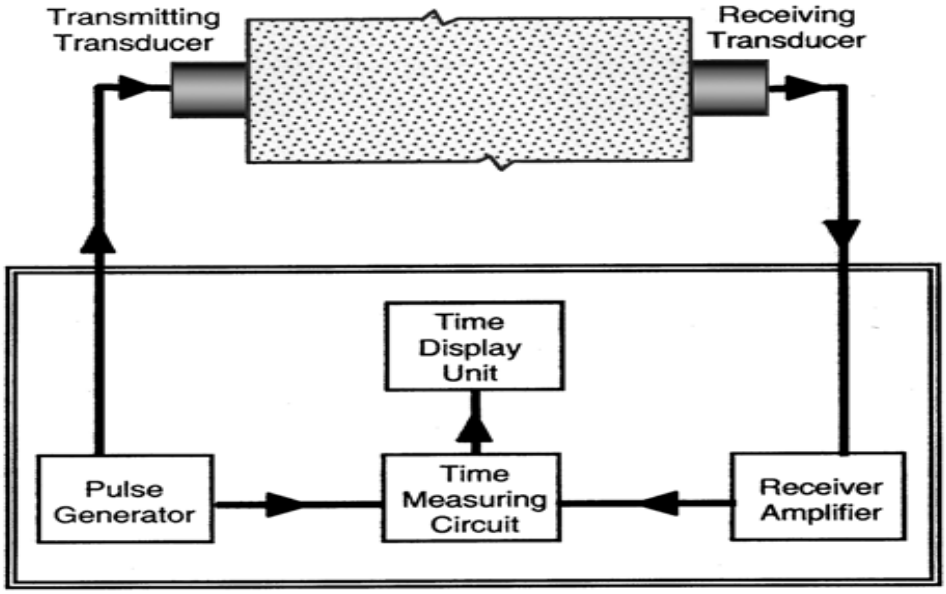

Figure 7: Schematic of pulse velocity apparatus

Source: (ASTM-C597)

Figure 8: Proceq - TICO ultrasonic pulse velocity

According to *ASTM C597*, *Pulse Velocity Through Concrete*, the pulse velocity, *V*, in concrete is related to its density and elastic properties, and this can be interpreted by the following equation (ASTM-C597):

$$v = \sqrt{\frac{E(1-\mu)}{\rho(1+\mu)(1-2\mu)}}$$

where:

E = dynamic modulus of elasticity

μ = dynamic Poisson's ratio

ρ = density

The pulse velocity provides information that can be used to estimate the strength of concrete, both *in situ* and precast concrete. However, there is no physical relation between the strength of the concrete and its velocity. The strength estimation is based on a pre-established empirical correlation between the strength and velocity. The correlation is not fixed and can be affected by many factors, such as aggregate type and size, cement type and hydration, water content, supplementary admixtures, etc. It is pointed out by many researchers that estimation of concrete compressive strength through pulse velocity is not valid unless similar relations have been studied for the type of concrete. A probabilistic model and field data combined method might be a better strategy to establish a consistent statistical quality assurance criterion (Malhotra & Carino, 2003).

The compressional pulse generated by the transducer can't be transmitted without scattering in concrete. The scattering at various aggregate-mortar boundaries transforms the pulse into multiple reflected compression waves and shear waves, The compressional waves arrive first at the receiver. The transducers must be in good contact with the concrete surface in order to transmit and receive the generated pulse. Otherwise, an air pocket between the transducer and the sample may induce an error in the transit time because limited wave energy can be transmitted through air. For concrete, the pulse velocity typically ranges from 3000 to 5000 m/s (Malhotra & Carino, 2003).

1.2.3.3 Factors Affecting Ultrasonic Pulse Velocity

The ultrasonic pulse velocity of concrete is determined by both its own properties and the external environment. Carino & Malhotra (Malhotra & Carino, 2003) summarized the factors that should be taken into account when testing concrete using ultrasonic pulse velocity:

1.2.3.3.1 Aggregates

Aggregate size, grading, type, and content in concrete are closely related to its dynamic modulus of elasticity, Poisson's ratio and density, which are the determinants for ultrasonic pulse velocity. The type and amount of aggregates affect the ultrasonic pulse velocity significantly. This can be explained by the fact that cement paste has a lower pulse velocity than aggregates and the pulse velocity varies when different types of aggregates are used in concrete. The maximum aggregate size shall be smaller than the wavelength to avoid significant reduction of wave energy. Otherwise, no clear signal may be detected at the transducer.

1.2.3.3.2 Water–Cement Ratio and Moisture Content

As the w/c increases, the corresponding pulse velocity decreases, providing no other changes are made in the composition of the concrete. The saturation degree of the concrete must be considered for UPV. The pulse velocity of saturated concrete might be up to 5% higher than that of dry concrete (ASTM-C597). Due to the difference in porosity, moisture content has less influence on the pulse velocity of high-strength concrete than that of low-strength concrete.

1.2.3.3.3 Type of Cement and Admixtures

Different types of cement and admixtures influence the pulse velocity by producing different rates of hydration. The elastic modulus increases as the degree of hydration increases, which increases the ultrasonic pulse velocity. Also worth mentioning, air entrainment appears to have no effect on the relationship between pulse velocity and compressive strength of concrete.

1.2.3.3.4 Presence of Reinforcing Steel

The presence of reinforcing steel is an important factor that influences the ultrasonic pulse velocity in concrete. The compressional pulse travels 40% to 70% faster in steel than in plain concrete. Thus, reinforcement should be avoided in the wave path. Otherwise it will result in erroneously high pulse velocity readings.

1.2.3.3.5 Other Factors

Apart from the factors mentioned above, concrete age and the curing condition of concrete affect its properties, thus influencing its pulse velocity as well. The presence of cracks or deterioration in the specimen can result in a reduction in the pulse velocity. The pulse velocity is not dependent on the dimensions of the specimen but the reflected waves from boundaries in smaller specimens can influence the time of the directly transmitted pulse. The minimum dimension of the specimen must exceed the ultrasonic pulse wavelength. Transducers should be in good contact with the surfaces of the specimen, which can be improved by applying a coupling agent (ASTM-C597). An important point to mention is that temperatures ranging between 5 and 30 °C have been found to have insignificant effect on the pulse velocity.

1.3 Destructive Testing - Pressure Tension Test

1.3.1 Overview

The pressure tension test (PT) is also known as the indirect tension or gas tension test. It was originally developed by the British Research Establishment in the UK. The pressure tension test is a test method developed for determining the tensile strength of concrete. This test method applies a much simpler technique than most other tensile strength test methods (Bremner, Boyd, Holm, & Boyd, 1998).

The pressure tension test applies an axisymmetric pressure to the outer curved surface of a concrete cylinder using pressurized gas. The ends of the concrete specimen project outside of the pressure chamber and rubber O-rings are used to seal and contain the gas pressure between the chamber and the specimen. This prevents the gas pressure from acting on the exposed ends and prevents the leakage of gas pressure. The specimens are saturated with water and pore pressure is generated by the pressurized gas acting on the water. Because the induced pressure acts in all directions while the applied pressure acts only on the curved surface of the concrete specimen inside the chamber (i.e. between the O-rings), the specimen is subjected to a net tensile pressure (Bremner et al., 1998). The pressure tension test applies a steadily increasing gas pressure onto the specimen up to the point where the specimen fails. The gas pressure at this point is taken as the ultimate tensile strength of the concrete specimen. Further discussion of the mechanism of the pressure tension test (The Diphase Concept) is developed in this part and a schematic of the pressure tension test loading mechanism is shown in Figure 9 below.

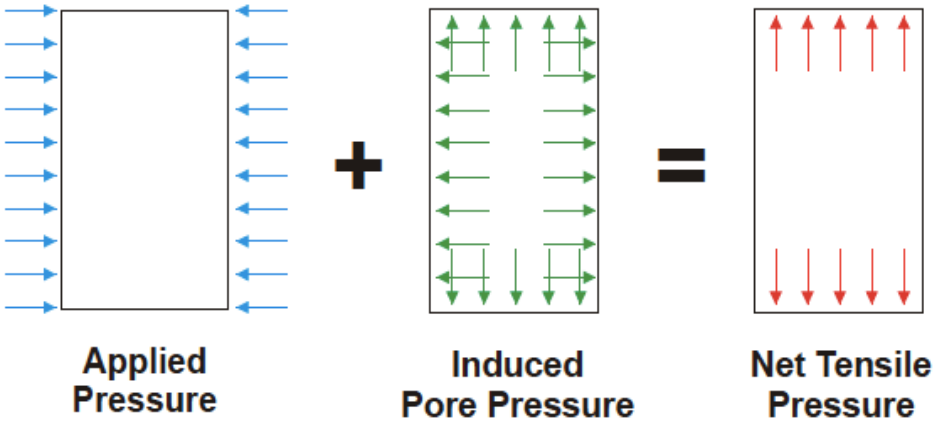

Figure 9: The mechanism of the pressure tension test

The pressure tension test method has many advantages compared to other tensile strength test methods. This test method is economical, simple to operate and the end preparation of capping or grinding required for direct tension test is not necessary (Uno, K., & Xu, 2005). It is considered to be more sensitive to internal expansive damage to the concrete because the tension generated is the outcome of an internal stress instead of an external stress. For example, sulphate attack, alkali-silicate reaction (ASR) and freeze-thaw damage are considered to cause expansive damage in concrete, thus the characteristics of the pressure tension test make it suitable for detecting these damages (Komar & Boyd, 2014). However, there is variation between the pressure tension test and other tension tests in terms of the "ultimate tensile strength". Previous research work showed that the tensile strength of concrete using this method tends to be slightly higher than the results using the direct tension test method and can be higher or lower than using the splitting tension test (S. R. Cumming, Boyd, & Ferraro, 2006).

1.3.2 The Diphase Concept

The diphase concept is used to describe the mechanism of the pressure tension test. The 'diphase' theory considers a material comprising just two phases, 'solid' and 'fluid.' The solid phase of the material consists of the particles that provide the form of the material, which are conceptualized as a finite number of particles with an indefinitely high strength and stiffness. The scale of the particles can be considered at different levels, ranging from the specimen itself to atoms and below. The fluid phase is the active constituent that applies pressure on the particles of the solid phase to hold them together. This is how the diphase model explains how a material gains its strength (Clayton & Grimer, 1979).

In the diphase model, the particles of the solid phase could be considered at different scales. For a concrete specimen, it can be differentiated in two different levels. As is shown in Figure 10, the first level differentiation comprises simply the specimen (solid phase) and its environment (fluid phase, water or air surrounding the specimen). The second level differentiation subdivides the specimen into many particles and an internal fluid. Thus, both the internal and external fluid are considered the fluid phase depending on the scale of the particles (Clayton & Grimer, 1979).

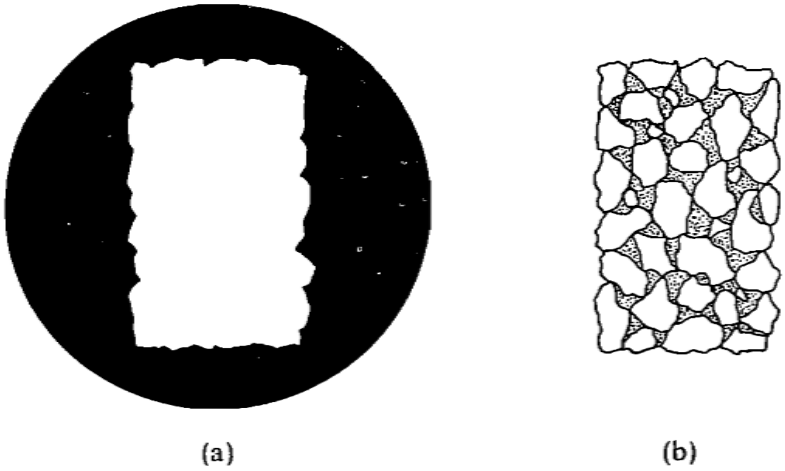

Figure 10: The diphase model (a) first order fluid and solid phase (b) second order fluid and solid phase

Source: (Clayton & Grimer, 1979)

Based on the diphase model, two points of view can be developed for a specimen under stress. First, a certain strength is assumed for the material, and fracture occurs when the external load is higher than this strength. Second, fracture can also occur when the pressure holding the particles together is removed. Therefore, fracture of the material can be realized through two general methods (Clayton & Grimer, 1979):

1. Decreasing the external stress on the solid phase
2. Increasing the internal stress on the solid phase

With the general idea of the diphase model and the occurrence of facture, the diphase concept can now be used to explain the pressure tension test mechanism. When fluid pressure is applied to the curved surface of a solid cylinder of material, internal pressure is increased on the solid. However, in the direction of the applied pressure, the change of the external fluid pressure is counteracted by a change of internal fluid pressure. While in the axial direction of the specimen, the increased internal fluid pressure reduces the pressure on the solid, and because no external fluid pressure is applied in this direction, the pressure

holding the solid together is reduced. The stress on the solid in the axial direction is further reduced as the applied fluid pressure is steadily increased. When it reaches zero, fracture occurs. The failure mode of the sample is as if it had been subjected to an applied axial "tension" (Clayton & Grimer, 1979).

1.3.3 Apparatus Configuration

The pressure tension apparatus consists a loading chamber, a loading sleeve, a gas tank, gas compressor and a computer for operation and data collection. The schematic of the pressure tension test and outlook of the system are shown in Figure 11 and Figure 12, respectively.

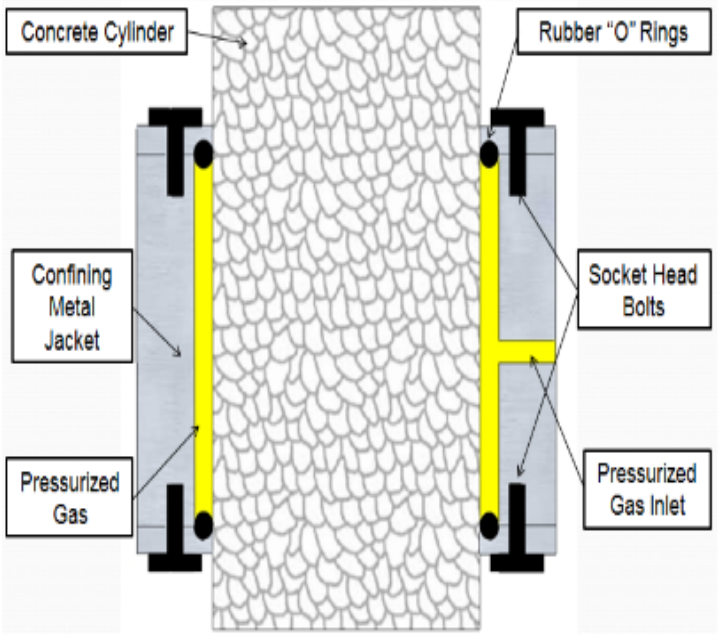

Figure 11: Schematic of pressure tension test

Source:(Komar & Boyd, 2014)

Figure 12: The outlook of the pressure tension test system

CHAPTER 2 EXPERIMENTAL PROGRAM

2.1 Materials

2.1.1 Mix Design

The concrete mix design was based on the *Handbook of Design and Control of Concrete Mixtures*, following the design example therein. Two different mixtures were designed and cast in this experiment. Mixture A was of water/cement 0.65, Mixture B was of water/cement 0.45. The large variation of W/C between the two mixes was designed to produce specimens with different pore systems (concrete with higher W/C has higher porosity), which is an important factor in terms of resistance against freeze-thaw damage.

All materials used for the experiments were commercially available. Type GU cement was used for the mix, and the air-entraining agent was Darex AEA ED. The super plasticizer was ADVA® CAST 575 produce by Grace Concrete Product. The water used for the mixes was ordinary tap water supplied by the city of Montreal. Also worth mentioning, the aggregates used for both mixes were limestone, which as mentioned above, had a lower resistivity than granite. The detailed mix design is shown in Table 1.

Table 1: Mix design of concrete Mixtures A and B

Ingredients (kg/m^3)	Mixture A (w/c 0.65)	Mixture B (w/c 0.45)
Water	227.5	193
Cement	350.0	428.89
Coarse Aggregates	894.17	894.17
Fine Aggregates	624.31	648.6
ADVA 575 Superplasticizer	1.05	1.42
Darex ED Air-Entraining Agent	0.175	0.219
Total	2097.205	2166.299

2.1.2 Concrete Specimen Preparation Procedure

Mixing procedure for concrete:

1. Prepare the coarse aggregates to be in the saturated surface-dry state; weigh all the materials separately and set them aside ready for mixing; prepare 100 mm x 200 mm cylinder moulds with form oil applied to the inside surface for later ease of demoulding.
2. Weigh the air-entraining agent and superplasticizer, and mix them separately with the to-be-added water properly; it is recommended that the air-entraining agent and superplasticizer not be combined before the mixing to avoid possible chemical interactions between them.
3. Put all dry materials into the mixer (cement, coarse aggregates and fine aggregates), and let the mixer run for around 30 seconds in order to blend the dry materials well.
4. Add water containing the admixtures and let the mixer run for three minutes, then rest for three minutes, and resume mixing for two minutes.

5. Cast freshly made concrete into the 100 mm x 200 mm previously prepared cylinder moulds, consolidate with a vibratory table, and finish their upper surfaces.

Both Mixture A and Mixture B followed the same preparation and curing procedure. After placement into the moulds, the freshly made concrete was covered by polyethylene sheets for 24 hours. Concrete samples were then removed from the moulds with pneumatic air pressure. The specimens were submerged in limewater to cure for 28 days. A concrete end grinder was used to finish the cylinder ends after the 28-day curing. The finished ends of the specimens made it easier to perform NDT tests on the samples and minimized the errors associated with rough surfaces. In addition, Type K thermocouples were embedded in two specimens from Mixture A, which were used for temperature monitoring during freeze-thaw cycles. Each thermocouple was embedded in the center of a concrete specimen. The other end of the thermocouple was connected to a data acquisition system (DAQ), which acquired the electrical potential data and converted it to temperature. The schematics of the thermocouple embedded specimens and the thermocouple monitoring process are shown in Figure 13 and Figure 14, respectively.

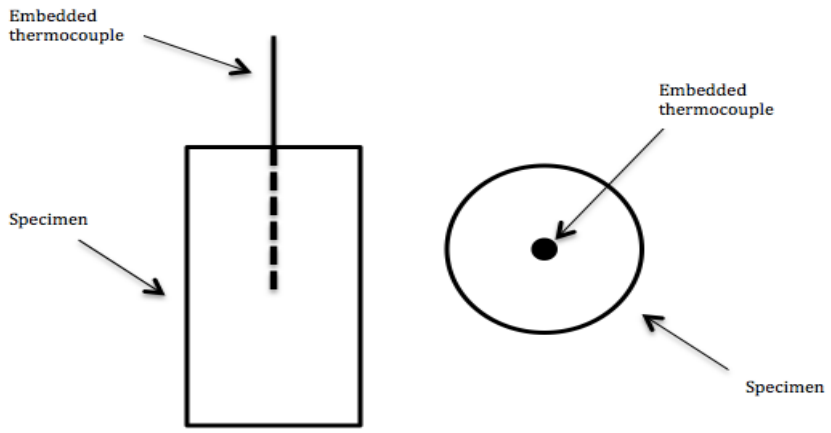

Figure 13: Schematic of specimen with thermocouple

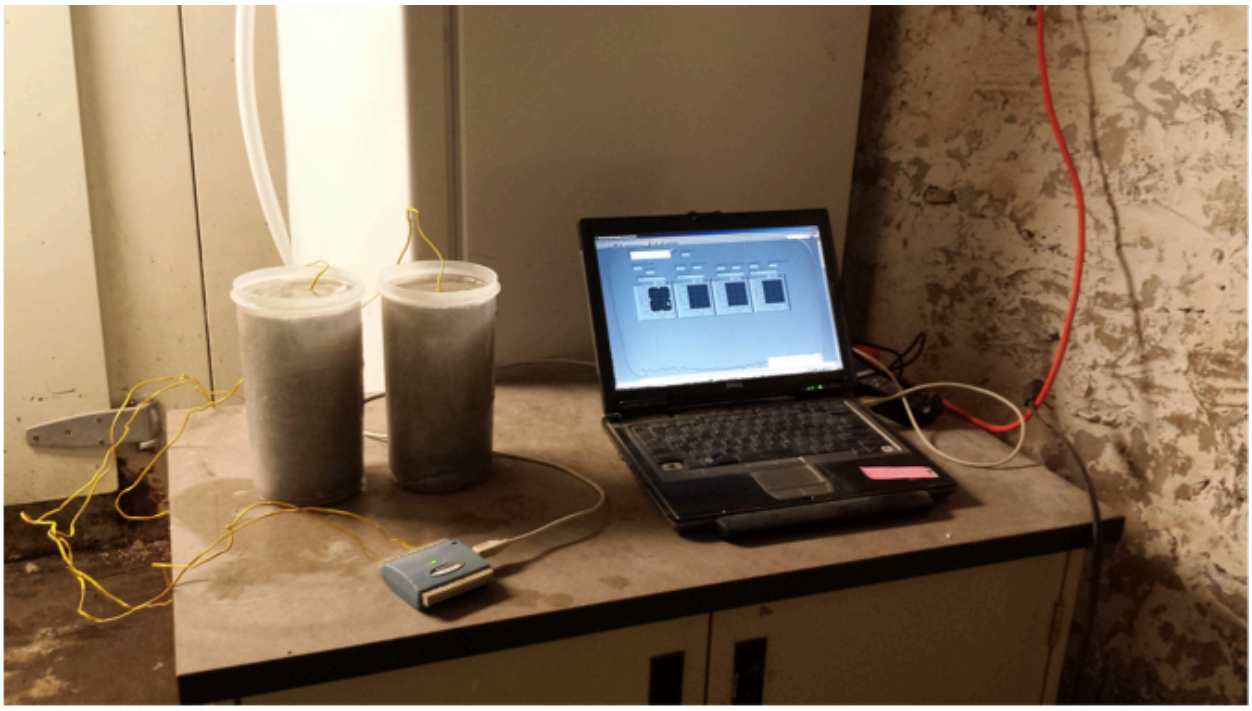

Figure 14: Monitoring temperature using thermocouples

2.2 Experimental Procedures

2.2.1 Freeze-Thaw Cycles

Immediately after 28 days of curing, samples were placed in commercially available plastic water jugs, which provided full submersion and ease of handling during freeze-thaw cycling. The concrete specimens' exposure condition followed ASTM C666 (Standard Test Method for Resistance of Concrete to Rapid Freezing and Thawing). During the freezing process, two commercially available freezers were used to bring the temperature of the concrete specimens below freezing and down to minimum of -23 ± 2 °C. During the thawing process, concrete specimens were thawed out in a custom-made water tub. This provided 100% saturation by submerging the specimens during the thawing process. A water heater was attached to the water tub to raise the temperature of water during the thawing stage, which facilitated and expedited this process. The use of a water bath during the thawing

stage conveniently ensured that all of the specimens remained at the same temperature at the same time, minimizing any temperature difference between specimens. The thawing process ended when water temperature in the water tub reached 15 ± 2 °C. After the thawing process, the specimens were placed back into the freezer to start another freeze-thaw cycle. Figure 15 and Figure 16 show the specimens undergoing the freezing process in the freezer and the water tub used for thawing, respectively.

Figure 15: Concrete specimens undergoing freezing process

Figure 16: Water tub used during thawing process

Figure 17 shows the temperature change of the specimen embedded with a thermocouple throughout a single freeze-thaw cycle. This curve shows the core temperature of the specimen. The maximum and minimum temperatures the specimen experienced during a freeze-thaw cycle were 10 °C and -24 °C, respectively.

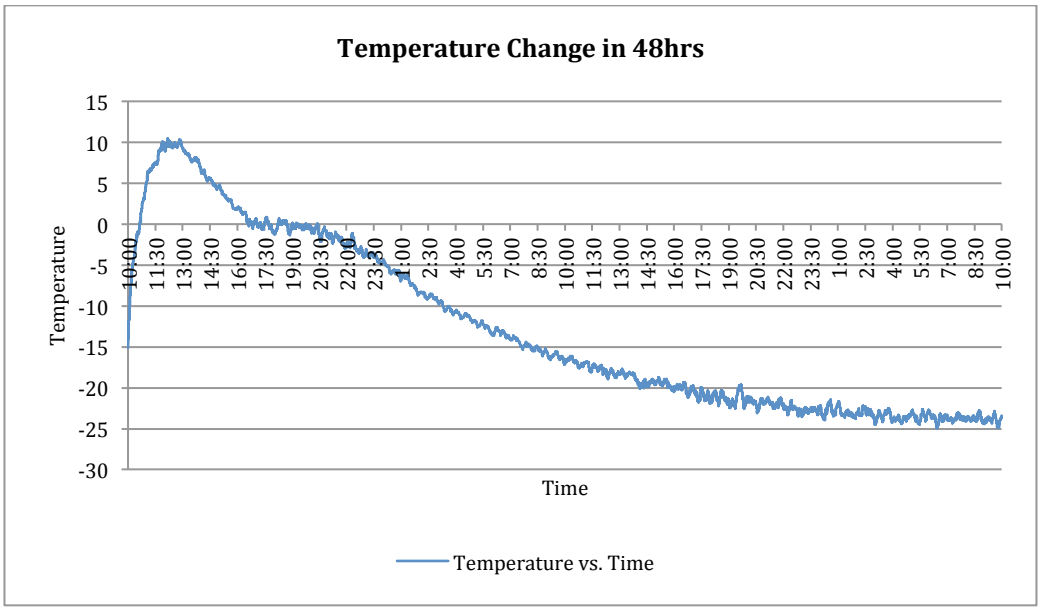

Figure 17: Temperature change in 48 hrs

After the specimens completely thawed, nondestructive testing was carried out immediately. In this experiment, three random samples were chosen from Mixture A and Mixture B, respectively, as control samples and given the identification of Control #1, 2 & 3. NDT testing (surface resistivity, bulk resistivity, ultrasonic pulse velocity) was performed on the six control samples after every freeze-thaw cycle up to 40 cycles. After 40 freeze-thaw cycles, severe deterioration was observed on concrete specimens from Mixture A (w/c 0.65) and NDT testing was terminated at cycle 40 for Mixture A. NDT testing continued for specimens of Mixture B (w/c 0.45) up to 80 cycles, though testing frequency was modified to every five freeze-thaw cycles. Pressure tension testing was performed on the specimens of Mixture A (w/c 0.65) at an interval of every five cycles up to 40 cycles. For specimens of Mixture B (w/c 0.45), pressure tension testing was carried out every five cycles up to 20 cycles and every 10 cycles from the 20th cycle to the 80th cycle.

2.2.2 Nondestructive Testing Procedures

All nondestructive testing on concrete specimens was carried out after they thawed out. The specimens were kept in the water jugs to maintain a saturated state up to the point of testing. Nondestructive testing was performed under room temperature at 22 ± 3 °C.

The detailed NDT procedure is explained as follows:

2.2.2.1 Surface Resistivity Test - Operational Procedure

This test method is nondestructive and user-friendly with the use of the Proceq surface resistivity testing device. Sample marks were made on the specimens immediately after demoulding. On the circular end face of each cylinder sample, marks were made at the 0, 90, 180 and 270 degree points of the circumference. On the longitudinal sides of the samples, 4 straight lines were drawn, aligned with the 4 marks on the end face. Marks were

made 4 cm from the end on the lines for subsequent visual reference. The marks on the samples enabled the tests to be performed on the same spots and on the center of the longitudinal sides of the samples. This was to minimize any variation resulting from geometry. Concrete specimens must not be left in the air for longer than 5 minutes, as the concrete surface may start to dry. Figure 18 shows the operational process of the surface resistivity testing.

The testing procedure followed *AASHTO TP 95-11*:

1. Ambient air temperature around the specimens must be maintained in the range of 20 °C to 25 °C through out the test.

2. Take the sample out from the water jug, blot off excess water, and place the sample on the sample holder.

3. Place the Wenner array probe on the longitudinal side of the sample with the first probe placed on the marked point. A reading is obtained within 3 seconds or when it becomes stable.

4. Rotate the sample to the next mark points, and repeat Step 2 and Step 3.

Test results are obtained from the average of the 4 measurements at the 4 different locations. (AASHTO-TP-95-11)

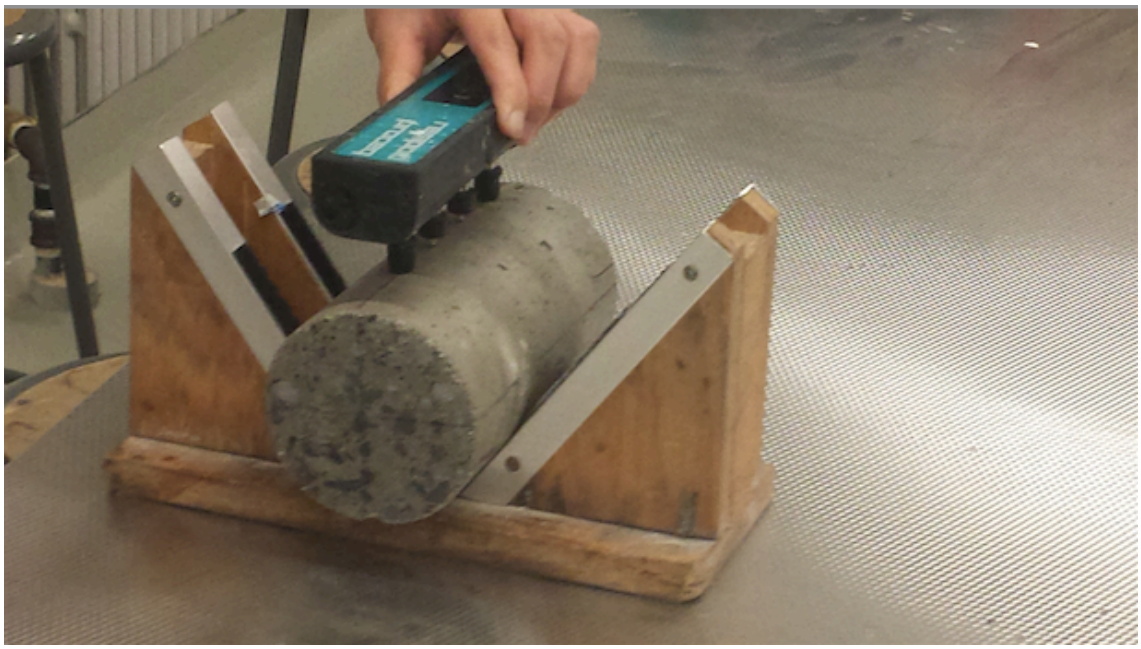

Figure 18: Testing surface resistivity using Resipod

2.2.2.2 Bulk Resistivity Testing - Operational Procedure

Bulk resistivity is a testing method designed to measure bulk electrical resistivity of saturated concrete cylinders. The same testing device described in surface resistivity testing section was used. The accessories consist of a stand, cables, measurement plates and conductive foam inserts suitable for 100 mm x 200 mm cylinders. Bulk resistivity measures the overall resistance of the samples, minimizing the variation induced from testing at local areas.

A similar method as SR testing was adopted for bulk resistivity testing:

1. Ambient air temperature around the specimens must be maintained in the range of 20 °C to 25 °C through out the test.

2. Soak the conductive foam inserts in water, and gently squeeze out excess water. Place the top and bottom foams respectively between the measurement plates to measure their

resistance. Place the concrete sample on the measurement plates while measuring the resistance of the bottom foam. This is to ensure a consistent moisture content in the conductive foams during testing.

3. Take the sample out from the water jug, blot off excess water, and place the sample between the plates with the conductive foams inserted between the plates and the sample. A test reading is obtained within 3 seconds or when it becomes stable.

In addition, because of the default set-up in surface resistivity testing, the measured value using the Proceq Resipod instrument can be corrected and calculated as follows to obtain true bulk resistivity (Proceq-Resipod):

$$R_{cylinder} = R_{measured} - R_{upper} - R_{lower}$$

$$R_{cylinder(corrected)} = R_{cylinder}/2\pi a$$

$$Bulk\ resistivity\ \rho = K \cdot R_{cylinder(corrected)}$$

$$K = A/L$$

where,

$R_{cylinder}$ *- bulk resistance*

$R_{measured}$ *– measured resistance value*

R_{upper} *– resistance of the upper insert foam*

R_{lower} *– resistance of the lower insert foam*

A - surface area

L - length of specimen

a – probe spacing, 3.8 cm in this experiment

2.2.2.3 Ultrasonic Pulse Velocity Testing - Operational Procedure

The ultrasonic testing instrument used in this work was TICO, made by Proceq. It consists of a display unit, 2 transducers of 54 kHz, 2 cables and a calibration rod (Figure 19).

The following test procedure was summarized from *ASTM C597* (ASTM-C597):

1. Ambient air temperature was maintained between 22 ± 3 °C, and the samples were tested in the fully saturated state.

2. Connect transducers and display unit with the cables; perform calibration with the calibration rod; the transit time should agree with the calibration value (20.5 μs); use coupling agent (lubricant jelly) to ensure a good connection.

3. Apply appropriate amount of coupling agent (lubricant jelly) to the transducer or to the ends of the concrete cylinder, and hold the transducers firmly against the ends of the concrete cylinder until a stable transit time is displayed.

4. Switch the two transducers to the opposite ends of the concrete cylinders and repeat Step 3.

5. Repeat Step 4

Figure 19: Operation of ultrasonic pulse velocity test

The repeated measurements were included to enhance the accuracy and minimize possible erroneous readings due to poor coupling. The transducer transmits a compressional wave into the concrete and it is received by the other transducer, at a distance L (the length of the concrete specimen). The transit time, T, is displayed on the display unit (Malhotra & Carino, 2003).

The pulse velocity is calculated as follows:

$$V = L/T$$

where:

V = pulse velocity, m/s,

L = distance between centers of transducer faces, m, and

T = transit time, s.

2.2.2.4 Pressure Tension Testing Procedures

The concrete samples tested were all kept saturated up to the time of testing. Moisture content was considered to be an important factor for the pressure tensile strength of concrete. Keeping all sample saturated eliminates this factor and minimizes the variations. In order to produce a good seal in the air pressure chamber, rubber O-rings were used. In addition, even with the rubber O-rings, leakage might be present because of defects, damage and voids on the sample surface. In this case, duct-tape was used to provide a better seal. When air pressure leakage still occurred after the usage of duct-tape, epoxy was applied to the concrete surface, filling the surface voids. The pressure chamber was designed to be slightly bigger than the standard concrete cylinder (100 mm diameter) providing a tight fit to the concrete cylinder. The concrete cylinder was placed in the chamber, ideally equally spaced in it. The O-rings were mounted on both ends, and then the end rings were bolted to the chamber. The pressure tension test machine is shown in Figure 20. The details of the specimens tested are shown in Table 2 and Table 3.

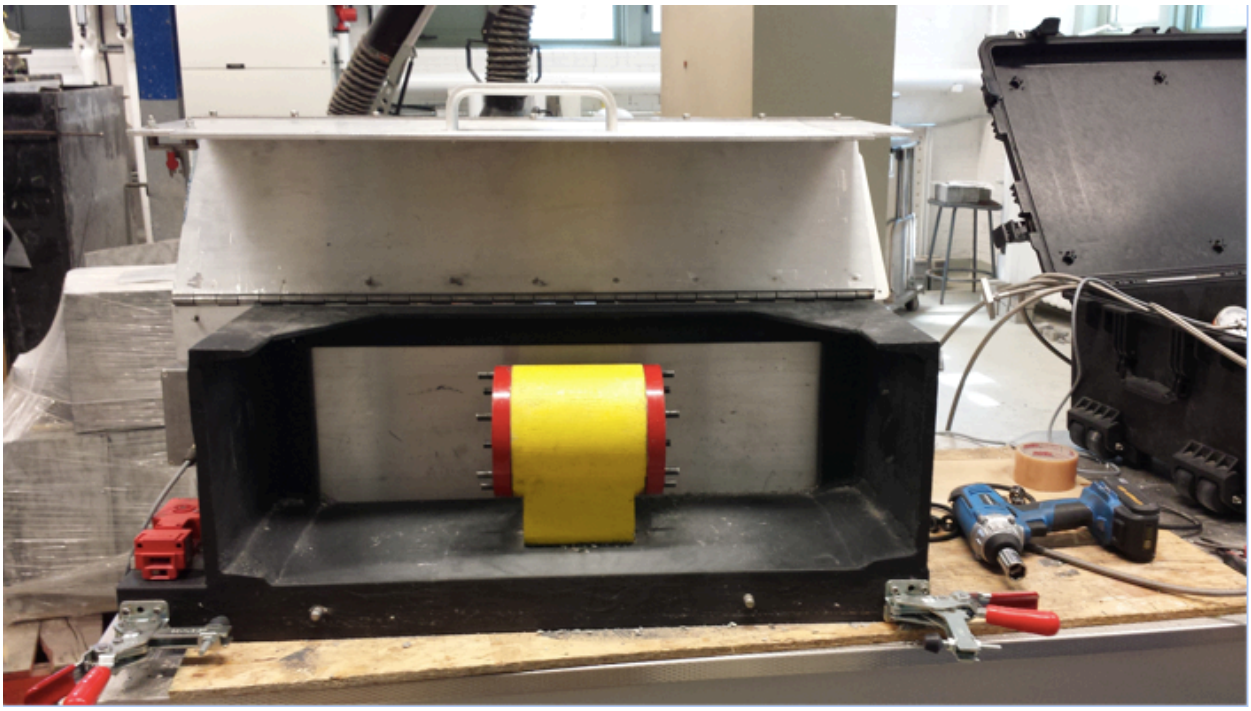

Figure 20: Pressure tension machine

Table 2: Concrete specimen identification for Mixture A

Sample #	W/C ratio	Freeze-thaw cycles	Sample #	W/C ratio	Freeze-thaw cycles	Sample #	W/C ratio	Freeze-thaw cycles
01	0.65	0	10	0.65	15	19	0.65	30
02	0.65	0	11	0.65	15	20	0.65	30
03	0.65	0	12	0.65	15	21	0.65	30
04	0.65	5	13	0.65	20	22	0.65	35
05	0.65	5	14	0.65	20	23	0.65	35
06	0.65	5	15	0.65	20	24	0.65	35
07	0.65	10	16	0.65	25	25	0.65	40
08	0.65	10	17	0.65	25	26	0.65	40
09	0.65	10	18	0.65	25	27	0.65	40

Table 3: Concrete specimen Identification for Mixture B

Sample #	W/C ratio	Freeze-thaw cycles	Sample #	W/C ratio	Freeze-thaw cycles	Sample #	W/C ratio	Freeze-thaw cycles
01	0.45	0	12	0.45	15	23	0.45	50
02	0.45	0	13	0.45	20	24	0.45	50
03	0.45	0	14	0.45	20	25	0.45	60
04	0.45	5	15	0.45	20	26	0.45	60
05	0.45	5	16	0.45	30	27	0.45	60
06	0.45	5	17	0.45	30	31	0.45	70
07	0.45	10	18	0.45	30	32	0.45	70
08	0.45	10	19	0.45	40	33	0.45	70
09	0.45	10	20	0.45	40	34	0.45	80
10	0.45	15	21	0.45	40	35	0.45	80
11	0.45	15	22	0.45	50	36	0.45	80

CHAPTER 3 RESULTS AND DISCUSSION

In this chapter, the test results are discussed in three parts: nondestructive test results, pressure tension test results and the relationships between nondestructive test and pressure tension test results.

3.1 Nondestructive testing results

3.1.1 Surface Resistivity Test Results

For specimens of Mixture A (w/c 0.65, hereafter referred as Mix 0.65), the surface resistivity test was performed on the three control samples after every freeze-thaw cycle to monitor changes in surface resistivity.

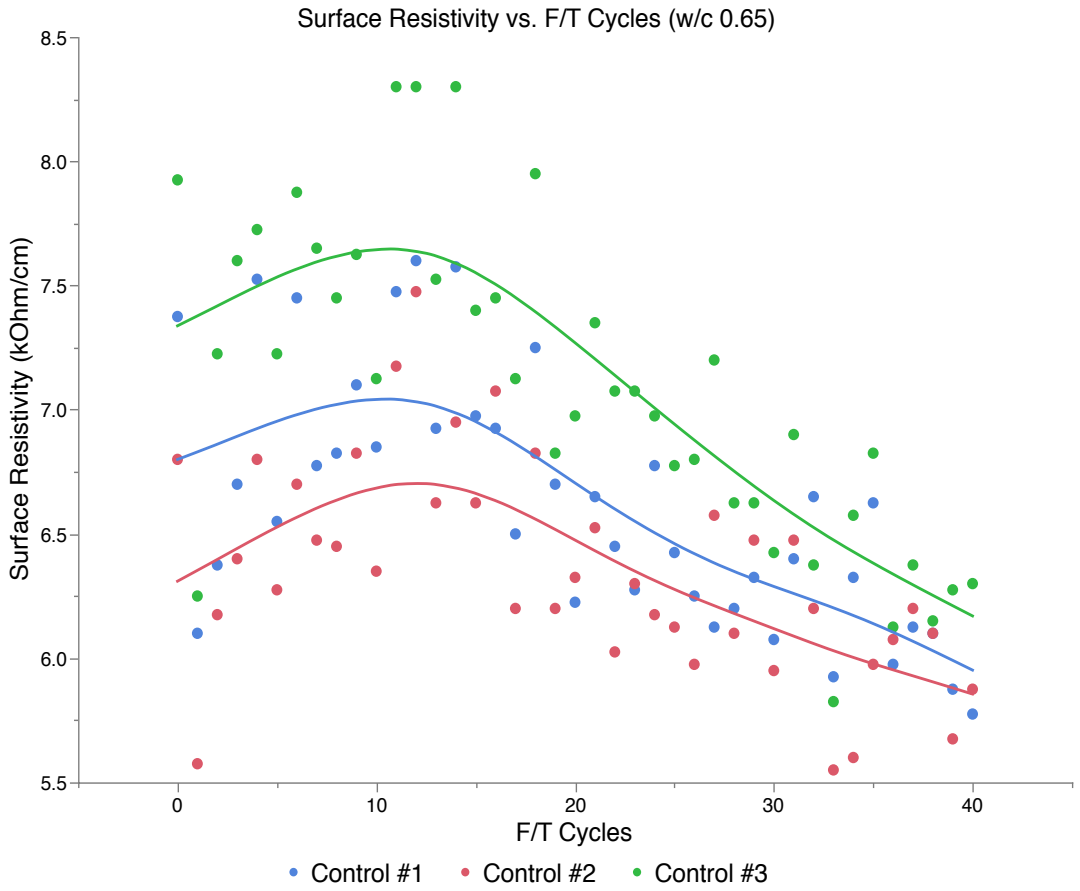

Figure 21: Relationship between surface resistivity and F/T cycles

Figure 22: Concrete sample #25 of Mix 0.65 after 40 freeze-thaw cycles

From Figure 21, it can be shown that the three specimens exhibited the same trend over successive freeze-thaw cycles. The three smoothed lines show a small increase in surface resistivity during the initial freeze-thaw cycles and reach their maximum surface resistivity at around the 12th cycle. After reaching this maximum, the surface resistivity starts to decrease and maintains this trend until the 40th cycle. Compared to its initial surface resistivity before being subjected to freeze-thaw cycling, apparent decrease was observed at the 40th cycle. The decrease of surface resistivity indicates that there was deterioration in the concrete specimens. This is consistent with the severe scaling, spalling and exposed coarse aggregates observed on the concrete samples after 40 cycles, which is shown in Figure 22. The small increase of surface resistivity at early stages can be explained by the effect of continued hydration of concrete. The surface of the specimen has a higher degree of saturation, thus continued hydration occurred at the early stages of the freeze-thaw cycles. This hydration caused a change in the pore system. The surface resistivity test, as its

name indicates, measures the resistivity of the material near the surface. The change caused by hydration was picked up by the surface resistivity test. At the 40th cycle, severe deterioration was observed on the concrete samples and freeze-thaw testing was terminated for Mix 0.65.

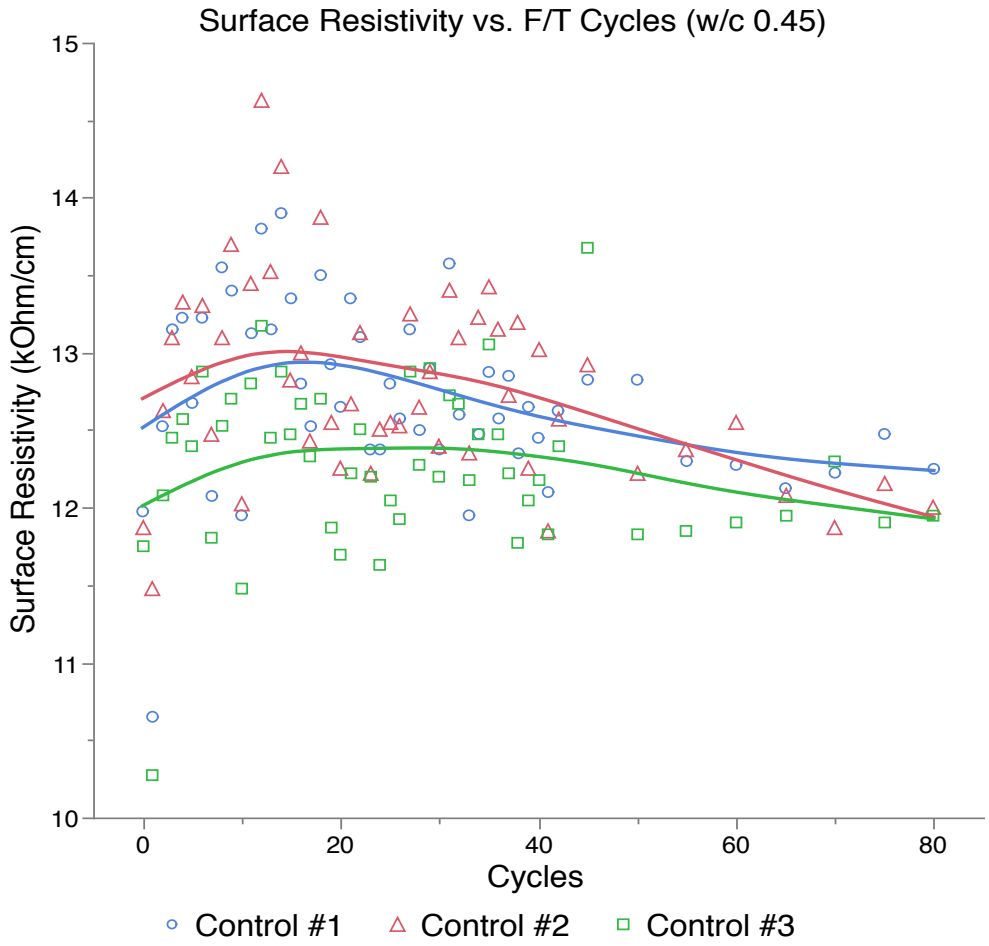

Figure 23: Surface resistivity vs. F/T cycles (w/c 0.45)

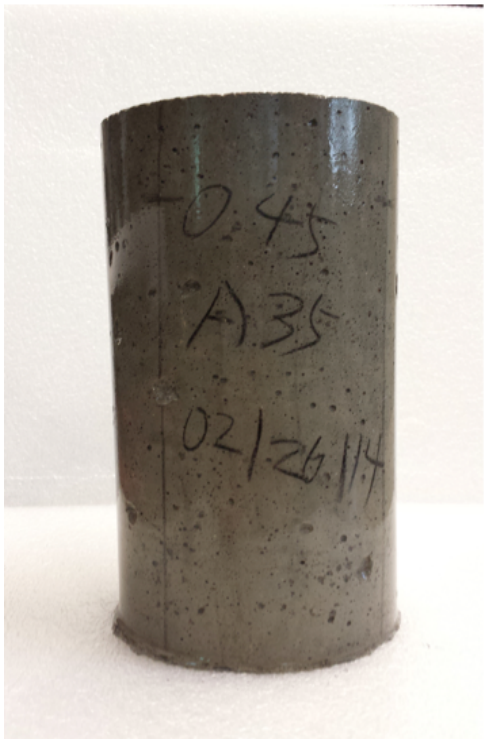

Figure 24: Specimen #35 of Mix 0.45 after subjected to 80 cycles.

As for specimens of Mixture B (w/c 0.45, hereafter referred as Mix 0.45), surface resistivity testing was performed on the three control samples after every freeze-thaw cycle for the first 40 cycles and every 5 cycles for the last 40 cycles. The test results and smoothed lines are shown in Figure 23.

The three curves show a small increase at their initial stages and reach their maximum surface resistivity at around Cycle 12. This characteristic resembles the test results of Mix 0.65. After the peak, the surface resistivity starts to decrease and this trend is consistent until the end of 80 cycles. However, compared to the obvious freeze-thaw damage of the specimens of Mix 0.65, the specimens of Mix 0.45 presented no significant visible damage after 80 freeze-thaw cycles. Figure 24 shows specimen #35 of Mix 0.45 after being subjected to 80 cycles.

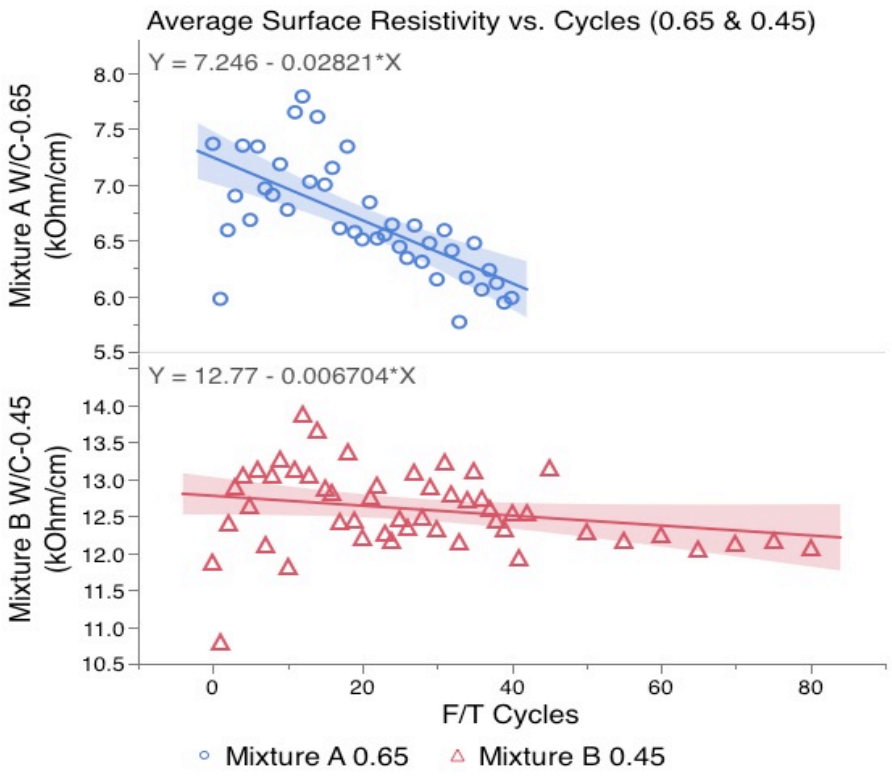

Figure 25: Average surface resistivity vs. cycles (w/c 0.65 & w/c 0.45)

From Figure 25, a comparison of the average surface resistivity between Mix 0.65 and Mix 0.45 was drawn. The surface resistivity of Mix 0.45 is much higher than that of Mix 0.65, which demonstrates that concretes with higher porosity have lower surface resistivity. Linear regression lines were used to quantify the changes of the surface resistivity over F/T cycles. The regression line for Mix 0.65 has an obvious decrease over the testing period while the regression line for 0.45 shows only a minor decrease. Mix 0.65 presents an obvious drop compared to its initial surface resistivity whereas only a small decrease was observed in Mix 0.45. This difference can also be found in the specimens, where the Mix 0.65 samples exhibited severe damage while Mix 0.45 samples were almost intact. The surface resistivity of Mix 0.65 showed a 23.2% decrease at cycle 40 compared to its maximum surface resistivity at Cycle 12. As for Mix 0.45, it showed a 13% decrease at Cycle 80 compared to its maximum value at Cycle 12. This comparison is more straightforward

when the slopes of the linear trendlines are considered. The slope of trendline of Mix 0.65 is 0.02821 while the slope of Mix 0.45 is 0.006704.

3.1.2 Bulk Resistivity Results

The results of the bulk resistivity test are shown in Figure 26 and Figure 27. The bulk resistivity results of Mix 0.65 are very similar to its surface resistivity results. The three curves of the control samples show a small increase of the bulk resistivity during the initial freeze-thaw cycles and start to decrease after until Cycle 40. This is consistent with the results of surface resistivity. However, for Mix 0.45, the three curves of the control samples show a different trend. The bulk resistivity of Mix 0.45 increases with the increase of freeze-thaw cycles and this increase is not linear. Continued hydration may have happened in the specimens of Mix 0.45 during the thawing process. The bulk resistivity test measures the overall resistance of the concrete specimen and the change caused by the continued hydration seemed to be detected by the test. The increment of the bulk resistivity compared to its initial is around 40%, which suggests that the pore system of the concrete specimen may have changed significantly.

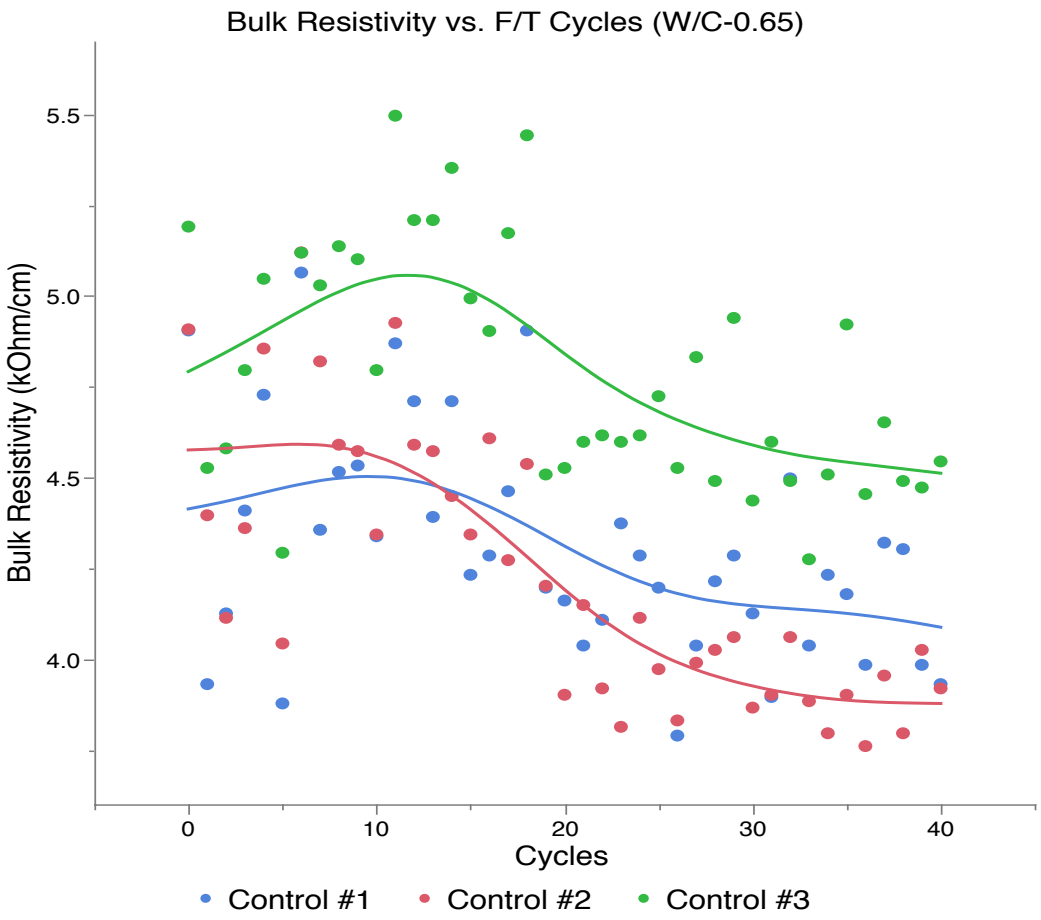

Figure 26: Bulk resistivity vs. F/T cycle (w/c 0.65)

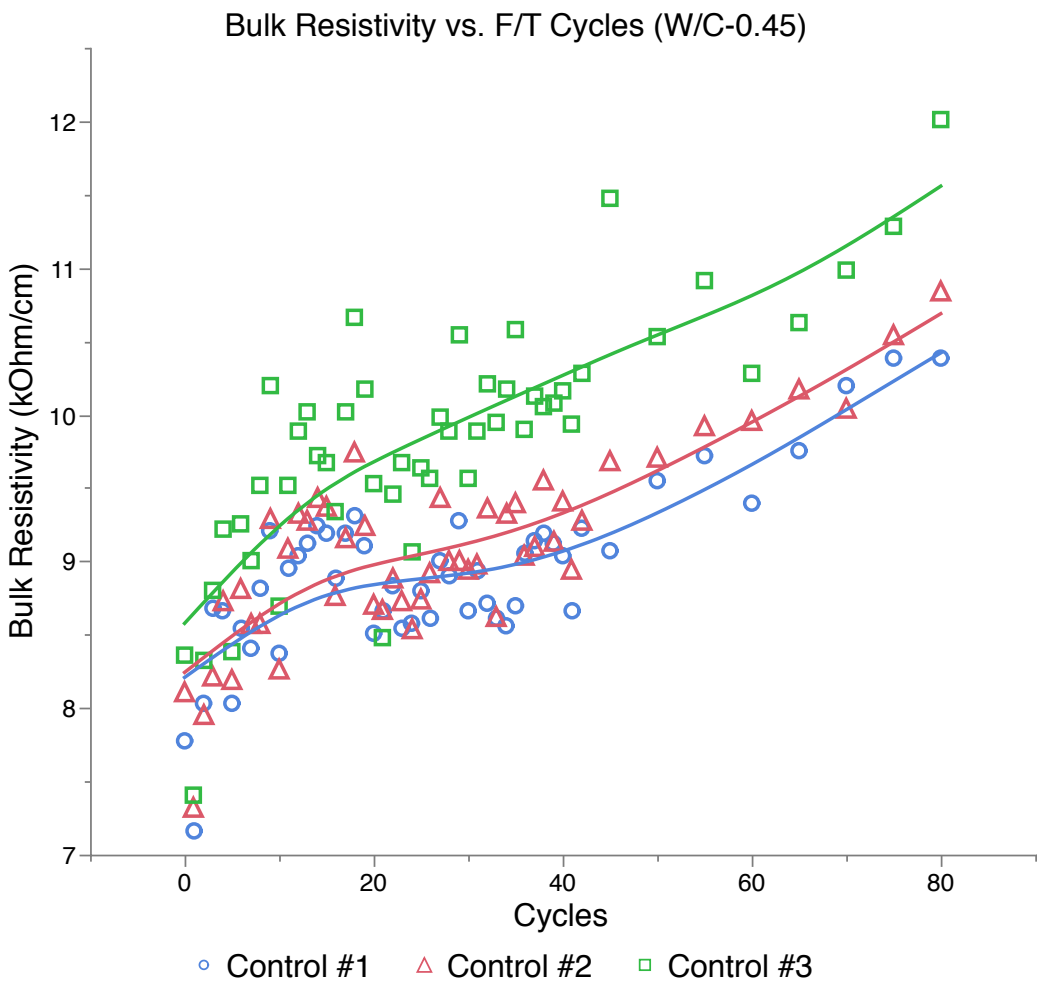

Figure 27: Bulk resistivity vs. F/T cycles (w/c 0.45)

A comparison of the bulk resistivity change over F/T cycles was drawn between Mix 0.65 and Mix 0.45 in Figure 28. The scatter points were fitted with linear trendlines and the equations are shown in Figure 28 as well. The bulk resistivity of these two mixes with different water/cement present opposite changes with the increase of F/T cycles. From Figure 28, the trendline for Mix 0.65 shows a 0.01632 negative slope while the trendline for Mix 0.45 shows a 0.02781 positive slope. The variation between high and low water/cement on freeze-thaw resistance apparently shows in these two curves. With higher w/c, concrete specimens display more severe visual F/T damage. This is consistent with the bulk resistivity test results. Lower water/cement ratio and air-entrainment

provide concrete with higher endurance against freeze-thaw damage. The bulk resistivity results of Mix 0.45 did not show a decrease, but an increase, over the freeze-thaw cycles.

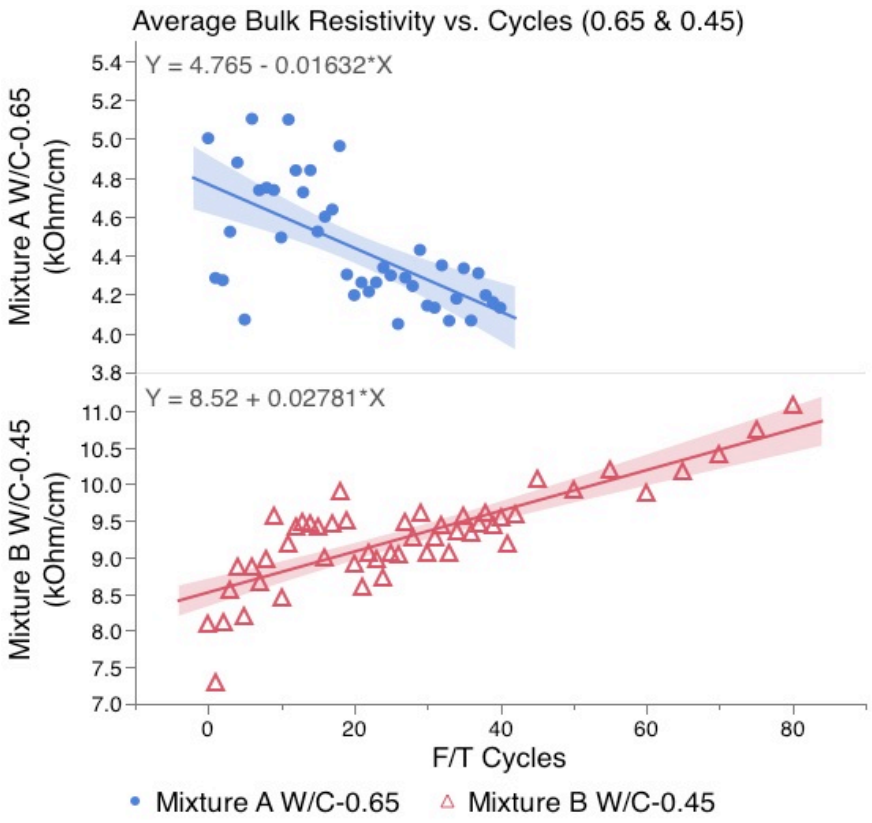

Figure 28: Average bulk resistivity vs. cycles (w/c 0.65 & w/c 0.45)

3.1.3 Ultrasonic Pulse Velocity Results

For concrete, the pulse velocity typically ranges from 3000 to 5000 m/s (Malhotra & Carino, 2003). The test results were consistent with this range. From Figure 29, Mix 0.65 showed an immediate decrease in its pulse velocity as soon as the freeze-thaw cycles began. The results of the three control samples show the same decreasing trend. The UPV of the specimens decreased faster at later freeze-thaw cycles. This is shown from the slope of the curves in Figure 29. The decrease in UPV is considered to be an indication of

deterioration in concrete. These test results are consistent with the severe deterioration observed on the specimens.

However, the UPV of Mix 0.45 showed much different results. From Figure 30, it is clear that the UPV increased over the freeze-thaw cycles, until the end of the testing period (Cycle 80). This is consistent across the three controls samples. Overall, the pulse velocity increased over the freeze-thaw cycles but there was obvious fluctuation. Mix 0.45 had a low water/cement, so the increase in UPV may be related to continued hydration of the unhydrated cement in the specimens.

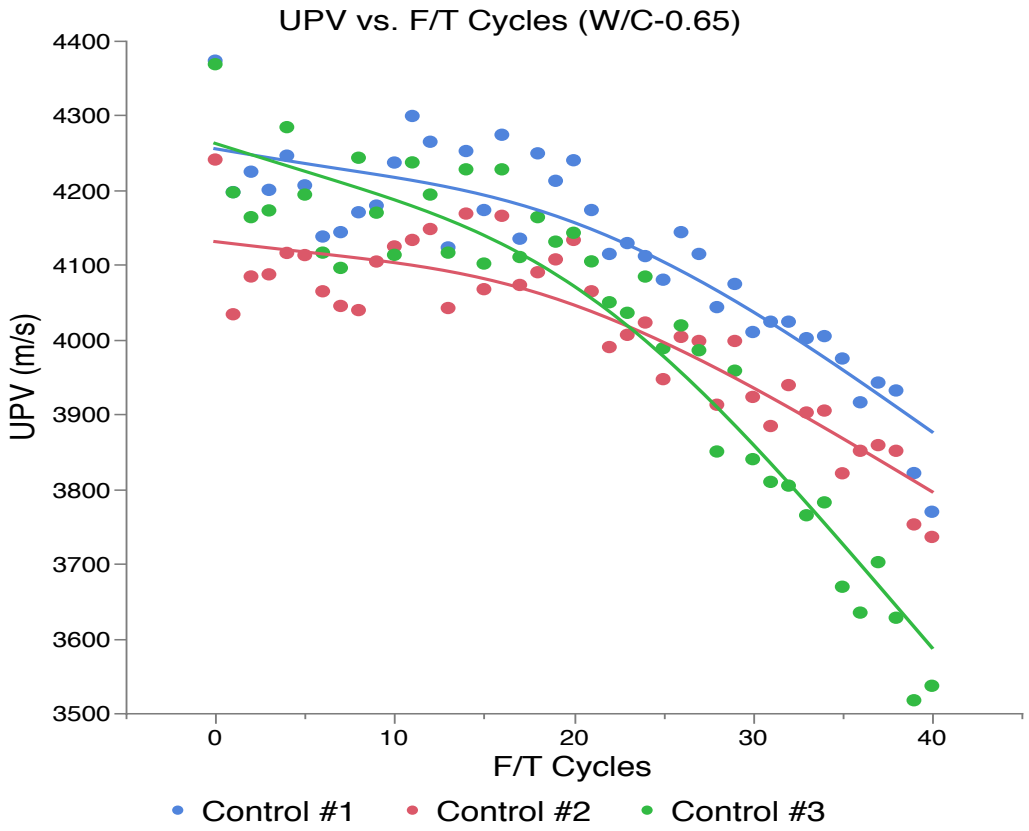

Figure 29: UPV vs. F/T cycles (w/c 0.65)

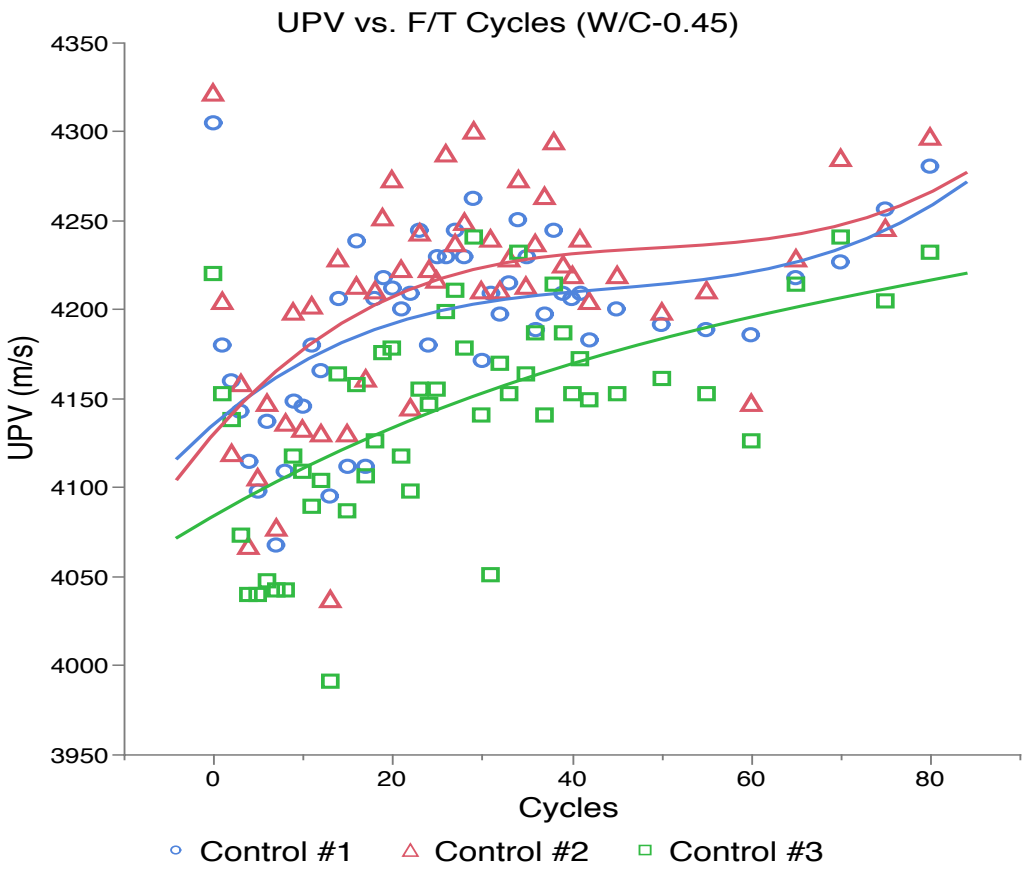

Figure 30: UPV vs. F/T cycles (w/c -0.45)

From Figure 31, a comparison was developed between test results of Mix 0.65 and Mix 0.45. As shown in Figure 31, the two linear regression lines have different slopes. For Mix 0.65, an apparent decrease was observed and the decrease rate (slope) was -11.41 over the freeze-thaw cycles. However, an opposite trend was exhibited by the results of Mix 0.45. Over the freeze-thaw cycles, the UPV displayed an increase instead of a decrease. This may indicate that the concrete specimens had less porosity over the ongoing freeze-thaw cycles, at least along the wave path of the ultrasonic pulse. This likely means that the concrete at the core was not subjected to freeze-thaw damage even after 80 cycles, and the continued hydration reduced porosity, creating a more compact structure. Because the transducers generate and receive pulses at the center of the ends of the specimens, the UPV showed an increase over the freeze-thaw cycles.

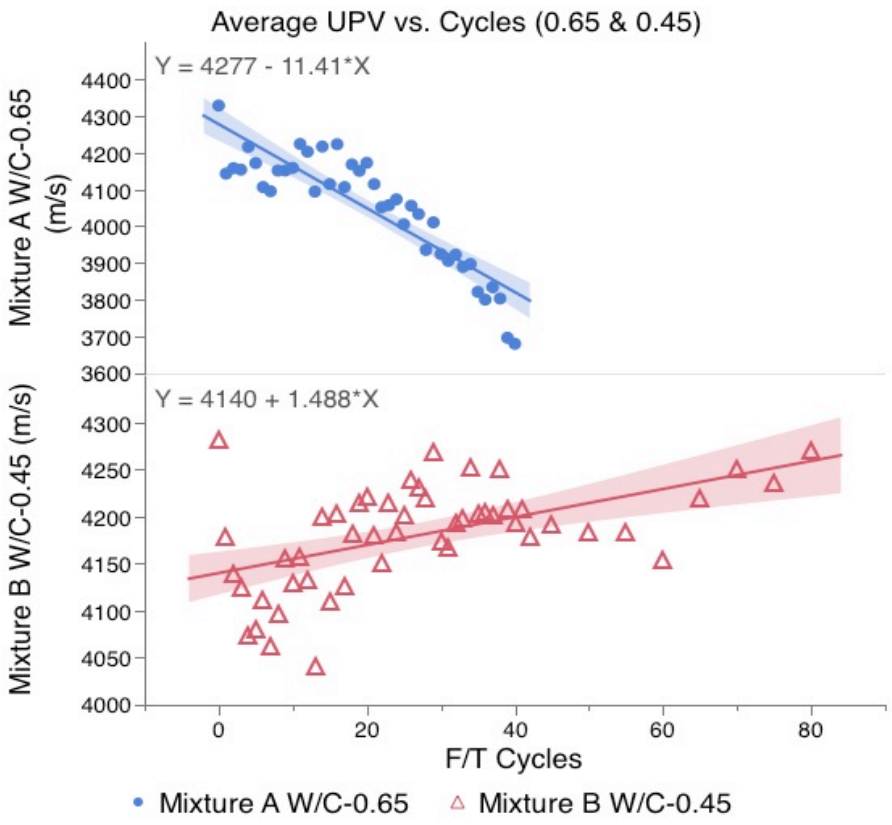

Figure 31: Average UPV vs. cycles (w/c 0.65 & w/c 0.45)

In conclusion, the visual observations and test results were consistent for specimens of Mix 0.65. The specimens showed severe deterioration over freeze-thaw cycles and the NDT results all showed an obvious decrease, which were considered to be an indication of the deterioration in the concrete specimens. However, the NDT results for Mix 0.45 were not consistent. Surface resistivity results showed a small decrease over the freeze-thaw cycles while the results of bulk resistivity and ultrasonic pulse velocity showed an increase. This difference may have been caused by the continued hydration of the specimens, the sensitivities of the test methods, and the mechanism of the test methods in detecting freeze-thaw damage.

3.2 Pressure Tension Test Results

The test results of the pressure tension test for Mix 0.65 over the freeze-thaw cycling are shown in Figure 32. The results indicate that the pressure tensile strength began decreasing as soon as the freeze-thaw cycles started. The pressure tensile strength of the specimens of Mix 0.65 decreased with the increase of freeze-thaw cycles. The results also indicated that the drop in tensile strength was more rapid over the first 20 cycles and slowed when the tensile strength reached around 1 Mpa.

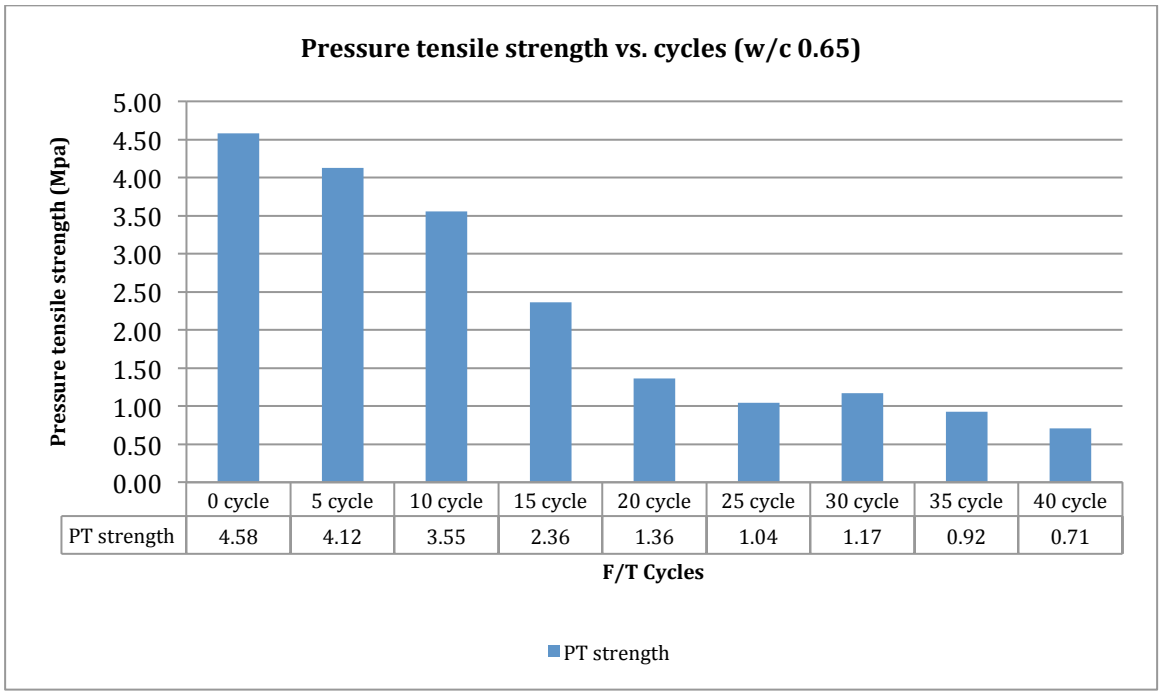

Figure 32: Pressure tensile strength vs. cycles (w/c 0.65)

Figure 33: Specimen #15 of Mix 0.65 after 20 cycles

Figure 34: Specimen #25 of Mix 0.65 after 40 cycles

Figure 33 and Figure 34 show specimens after Cycle 20 and Cycle 40, respectively. Some minor scaling was observed at the bottom of the specimen at Cycle 20 while severe deterioration was observed at Cycle 40. Across the failure surface of the specimen, it was observed that a large proportion of the failure was through the ITZ (Interfacial Transition Zone). The ITZ has higher porosity and is more susceptible to freeze-thaw damage. This

indicates that the pressure tension test is sensitive in detecting the internal expansive damage due to freeze-thaw cycling in concrete.

Figure 35 shows the pressure tension test results for Mix 0.45. Overall, the change in pressure tensile strength cannot be simply described as an increase or a decrease throughout freeze-thaw cycles. The specimens at Cycle 0 had a pressure tensile (PT) strength of 4.18 MPa. Over the freeze-thaw cycles, the PT strength increased until Cycle 60, with the maximum PT strength recorded at Cycle 60. An obvious drop in PT strength occurred after 70 and 80 cycles of freezing and thawing.

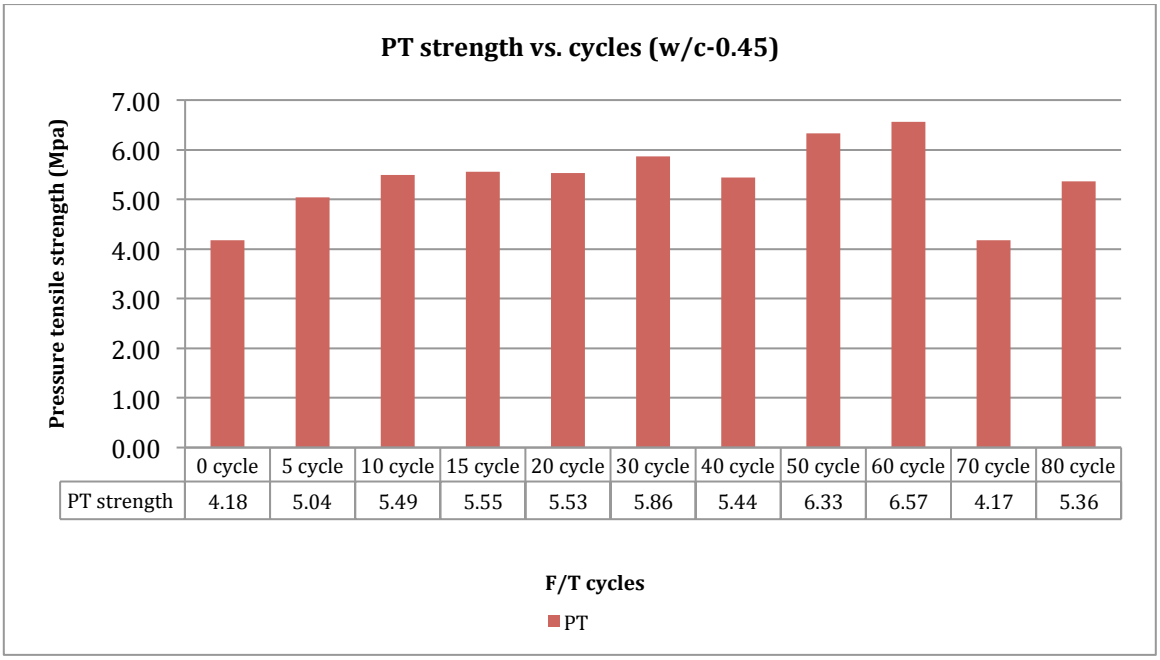

Figure 35: PT strength vs. cycles (w/c 0.45)

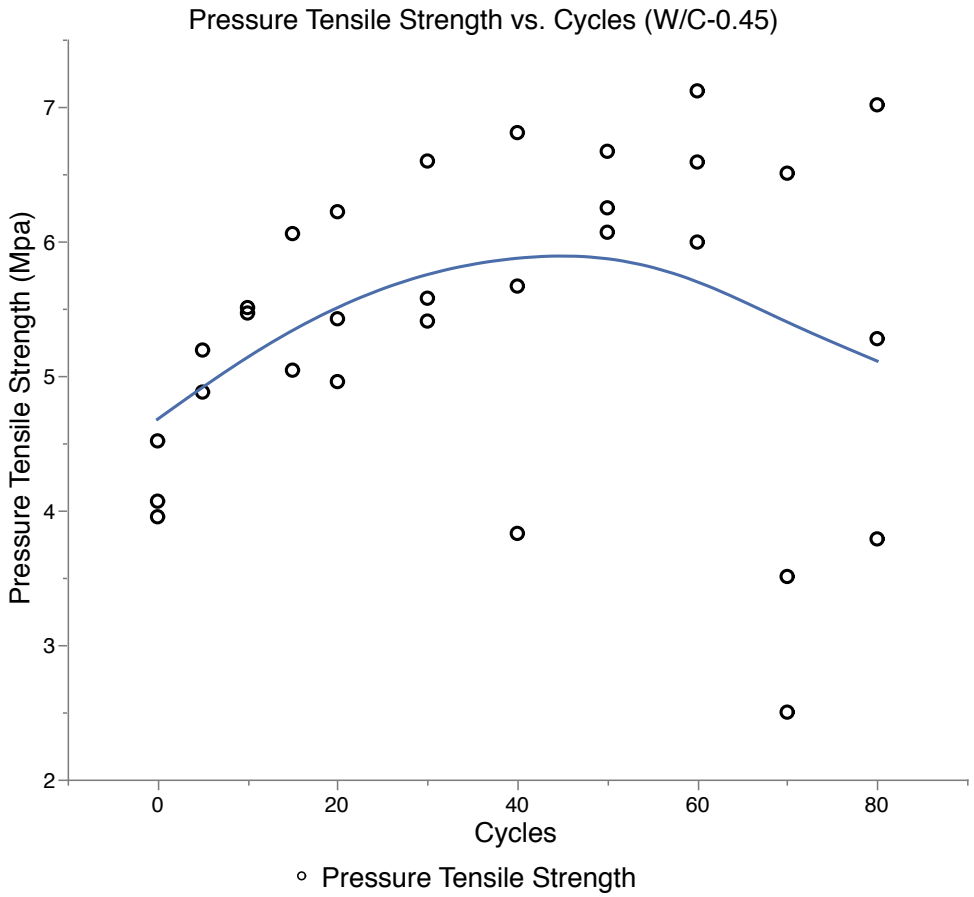

Figure 36: PT strength vs. cycles (w/c 0.45, scatter plot)

The change in PT strength is more apparent when it is plotted with scatter points and smoothed line, as in Figure 36. It can be seen from Figure 36 that the PT strength first experiences an increase and then starts to decrease over the freeze-thaw cycles. The initial increase in PT strength is consistent with the test results from the research of Al-Assadi (2011), who observed improved mechanical properties and lower porosity of the concrete specimens after the freeze-thaw test. In Al-Assadi's research, the w/c of the specimens were 0.4 and 0.5. He concluded that the cement hydration process continued during the freeze-thaw test, which densified the concrete pore structure (Al‐Assadi et al., 2011).

The increase in PT strength may be related to the continued hydration of the concrete. The specimens became more compact through the continued hydration over the freeze-thaw cycles and gained higher strength. The low water/cement and the continuing hydration of

the concrete acted together to provide the specimens with higher endurance against freeze-thaw damage. This was shown by the increase in PT strength up to 60 cycles. After 60 cycles, freeze-thaw damage became the dominant factor, and started to cause a decrease in PT strength. The deterioration of the specimens after 70 and 80 freeze-thaw cycles can also be demonstrated by the larger variation of the PT strength between the specimens. A large variation in strength between specimens is a typical result of rapid deterioration mechanisms.

Figure 37: Specimen #35 of Mix 0.65 after 80 cycles

From Figure 37, the specimen of Mix 0.45 displays no significant visible damage due to cyclic freezing and thawing.

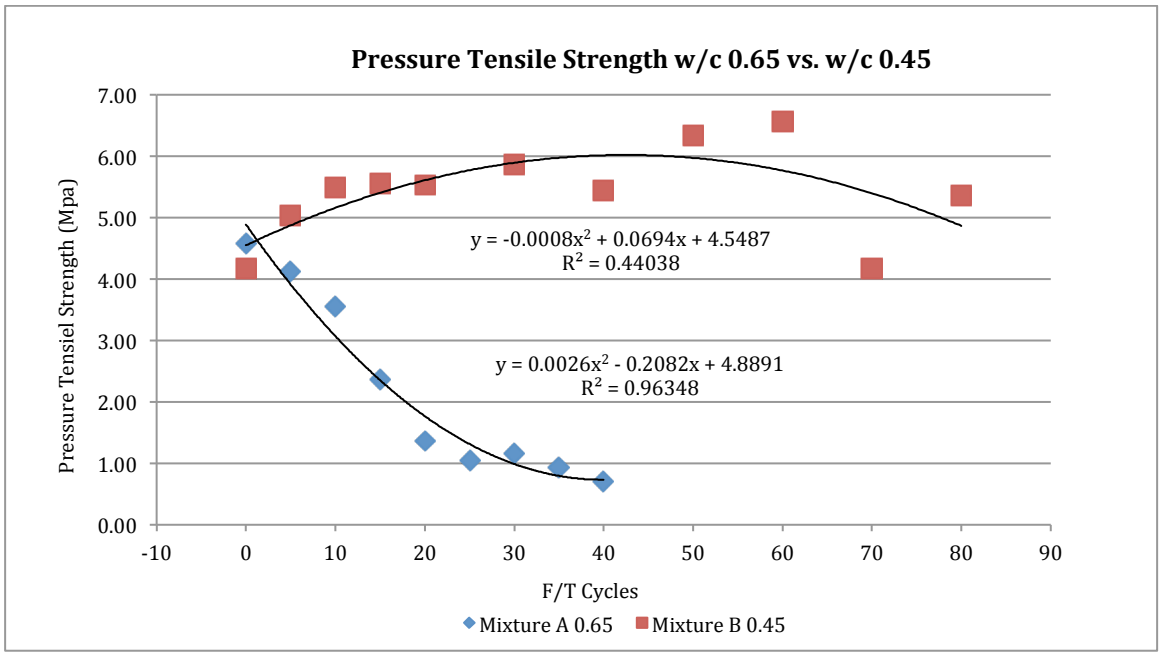

Figure 38: PT strength vs. cycles (w/c 0.65 & w/c 0.45)

In Figure 38, two regression trendlines were drawn to show the change in pressure tensile strength of Mix 0.65 and Mix 0.45. The scatter points were fitted with quadratic equations, and their R^2 values are shown in Fig. 39 to describe how well the lines fit the data. The R^2 value of Mix 0.65 was 0.96348, which indicates a close fit. The regression line for Mix 0.65 showed a moderate fit with an R^2 value of 0.44038. This is due to the larger variation between the test results. Clearly, Mix 0.65 presents more rapid change over freeze-thaw cycles. After 80 freeze-thaw cycles, the PT strength of Mix 0.45 showed a small decrease. An interesting point worth noticing; at the age of 28 days, before the initiation of freeze-thaw cycling, Mix 0.65 had a higher pressure tensile strength (4.58 MPa) than Mix 0.45 (4.18 MPa). It must be clarified here that this is a tensile strength phenomenon, which does not necessarily increase at the same rate as compressive strength, nor does it maintain a constant proportion with compressive strength. This phenomenon is probably due to the higher hydration degree of Mix 0.65 and insufficient hydration of Mix 0.45. This also supports the theory that the subsequent increase of the tensile strength of Mix 0.45 is due to continued hydration because there was insufficient hydration at the beginning. A high degree of hydration reduces the capillary porosity of the concrete and, therefore, affects the

concrete freeze-thaw resistance. (Al‐Assadi et al., 2011) This increase in resistance is shown by the increase in PT strength of Mix 0.45.

3.3 Relationships Between Nondestructive and Pressure Tension Test Results

This work was designed to investigate the sensitivity of nondestructive testing (NDT) in detecting freeze-thaw damage in concrete and pressure tension test (PT) was used to quantify their sensitivities. A series of comparison of the test results between NDT (SR, BR and UPV) and PT are shown below.

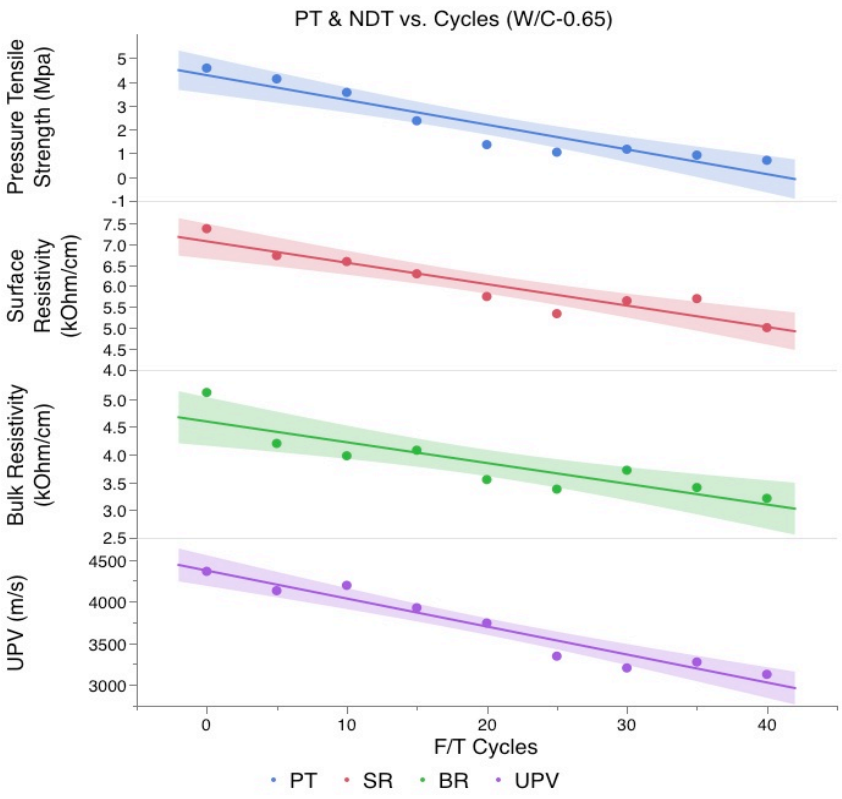

Figure 39: PT & NDT vs. cycles (w/c 0.65)

Figure 39 shows the comparison of the test results of the four tests (PT, SR, BR and UPV). In general, the test results of the four tests for Mix 0.65 all showed an obvious decrease over

the freeze-thaw cycles. These decreasing trends were almost linear and consistent in all the four tests results, which indicates that the three NDT techniques (SR, BR and UPV) are capable of detecting freeze-thaw damage in concrete when there is apparent deterioration, albeit the three NDT vary in testing mechanism and testing location with respect to the specimen. The changes in results are consistent with the results of the pressure tension test.

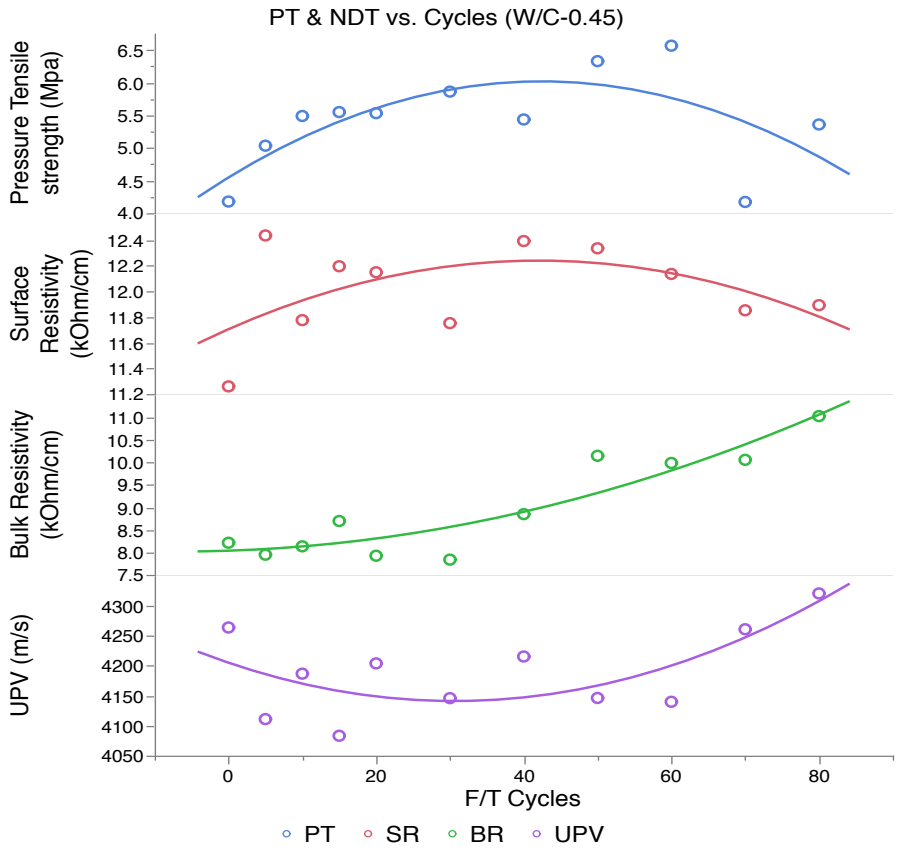

Figure 40: PT & NDT vs. cycle (w/c 0.45)

A comparison was also drawn for the results of the specimens from Mix 0.45. As seen from Figure 40, the four sets of test results showed different behaviors over the range of freeze-thaw cycles. PT test results and SR results present an overall synchronous change over the 80 freeze-thaw cycles, as expected, while the BR results and UPV results both show a completely different, increasing trend. This increase, as discussed above, could be linked to

the continued hydration and reduced porosity of concrete specimens. Of the three NDT tests, only the surface resistivity indicated there might be damage occurring in the concrete specimens after 80 freeze-thaw cycles. This implication is consistent with the decrease in pressure tensile strength after 80 cycles. Therefore, when freeze-thaw damage is not severe (i.e. at early stages) or not easily observable, surface resistivity is more capable in detecting freeze-thaw damage than the other two nondestructive test methods. Bulk resistivity and UPV did not show such sensitivity and may even give a false indication of the freeze-thaw damage in concrete.

The reason for the surface resistivity test being more sensitive in detecting concrete freeze-thaw damage can be explained as follows: the specimen surface is considered more saturated because it has been in contact with the water for some time. Thus, the water to ice phase transition will start from the surface. And the water in bigger capillary pores near the surface will freeze first. As this continues, the unfrozen water will be propelled into the less saturated pores, causing hydraulic pressure in concrete (Powers, 1945). Moreover, the surface of the specimen experiences a faster cooling rate, so there is more severe damage near the surface. Therefore, the damage due to rapid cooling rate would be less severe in the core of the specimen, so the freeze-thaw damage starts from the surface of the specimen. Surface resistivity, as its name suggests, measures the resistivity in the near–surface region, which makes it more sensitive to this damage.

Nevertheless, even though the BR and UPV test results are inconclusive, this should not exclude the capabilities of these two methods in detecting freeze-thaw damage in concrete. This is because the freeze-thaw cycles were relatively short in this experiment compared to the standard 300 cycles according to *ASTM C666*. An extended testing period ought to be carried out to further investigate the sensitivity of the nondestructive testing techniques at more severe levels of damage. Such work is beyond the scope of this project, whose intent was to evaluate sensitivity to early age deterioration.

In order to find out how sensitive the NDT techniques are in detecting frost damage in concrete, curve fitting software was used to develop the relationships between PT results and NDT results. Linear models were developed to find these relationships.

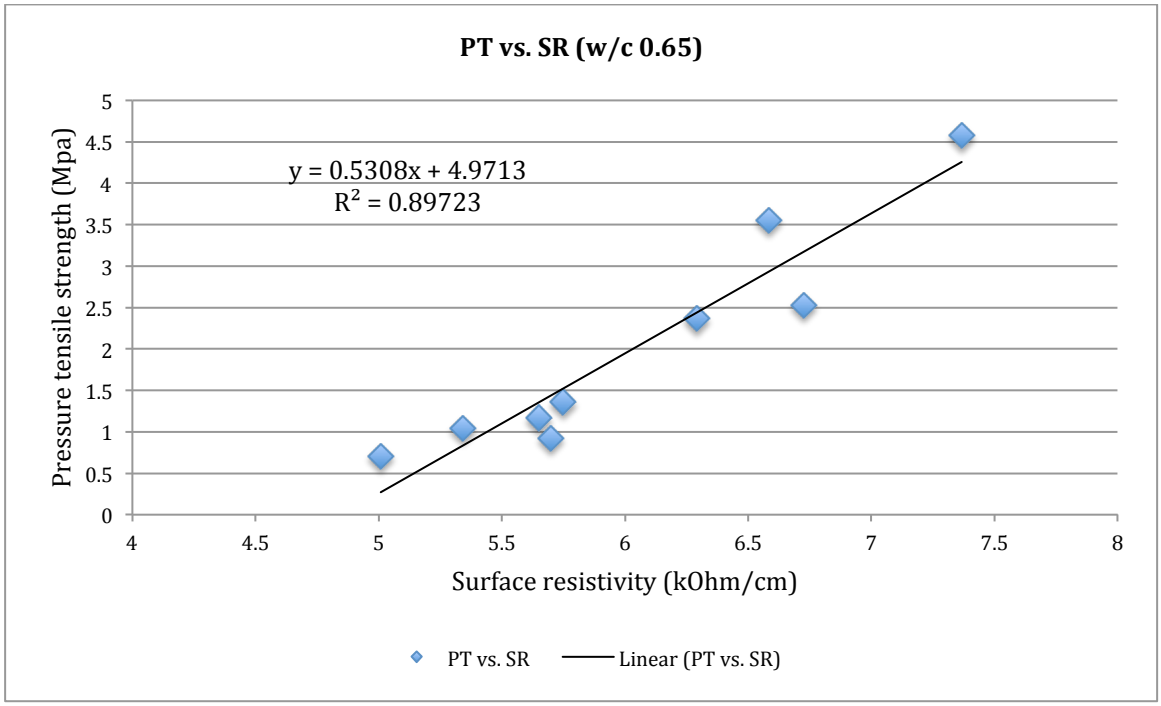

Figure 41: PT vs. SR (w/c 0.65)

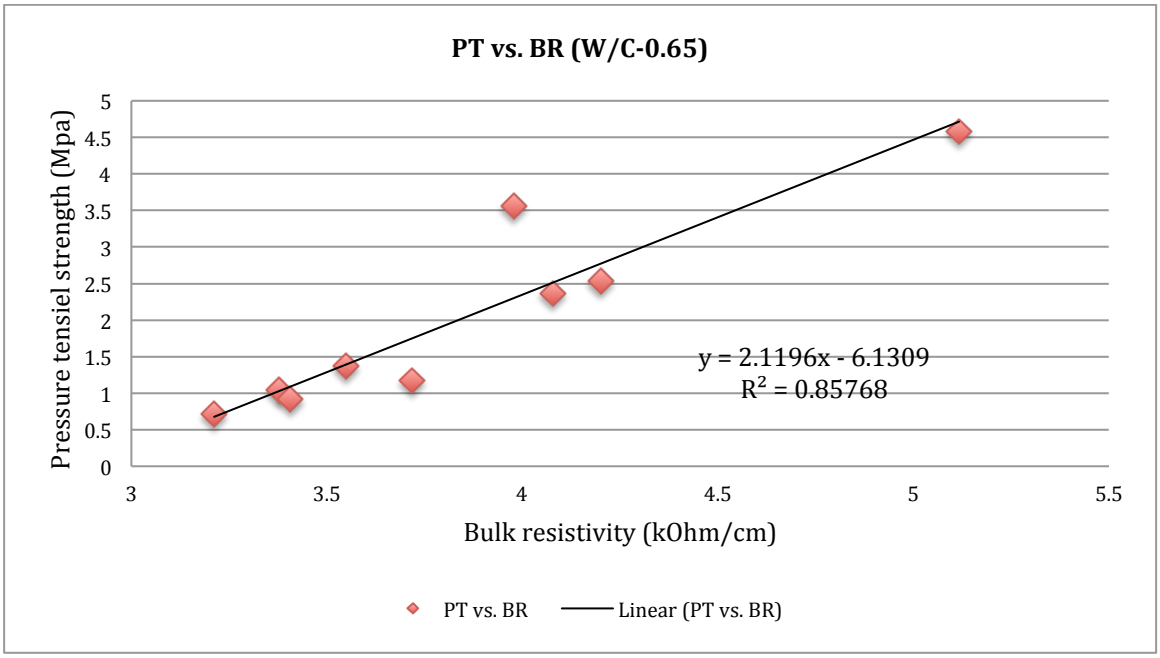

Figure 42: PT vs. BR (w/c 0.65)

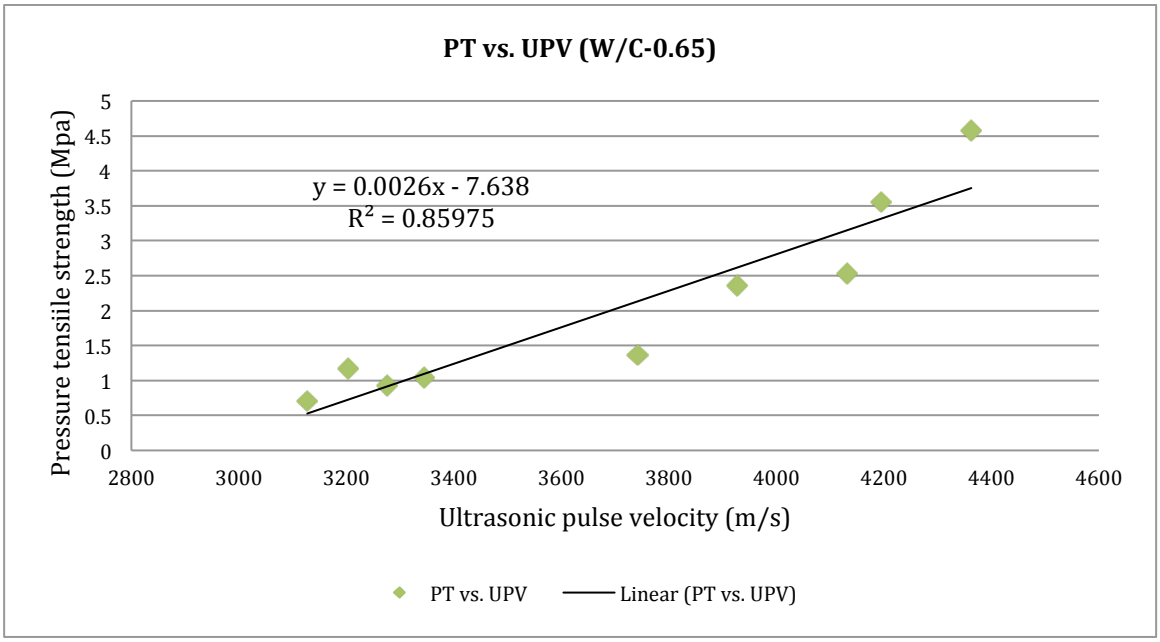

Figure 43: PT vs. UPV (w/c 0.65)

From Figure 41, Figure 42 and Figure 43, the three linear models yield good correlations between their test results and the corresponding tensile strength. The three best-fit lines

all had an R^2 value over 0.85, indicating the regression lines fit the data well. These well-fitted regression lines show that the three NDT methods are capable of indicating the pressure tensile strength or even predicting it. The pressure tension and surface resistivity results give the highest R^2 value of 0.89723, which may indicate that surface resistivity test is more sensitive in detecting the freeze-thaw damage in the concrete specimens.

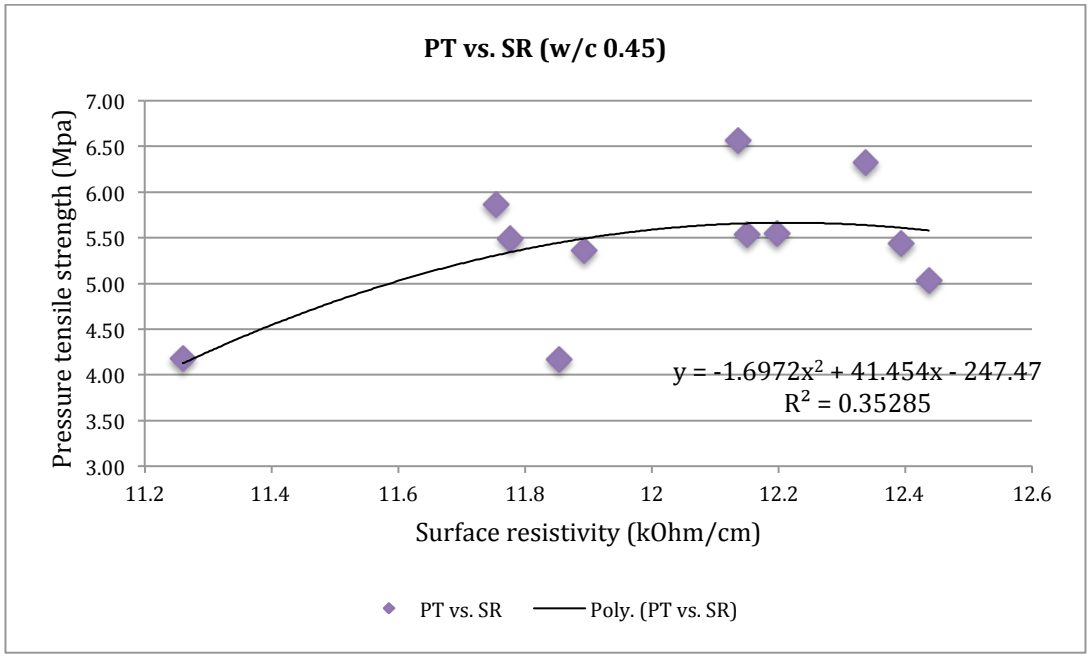

Figure 44: PT vs. SR (w/c 0.45)

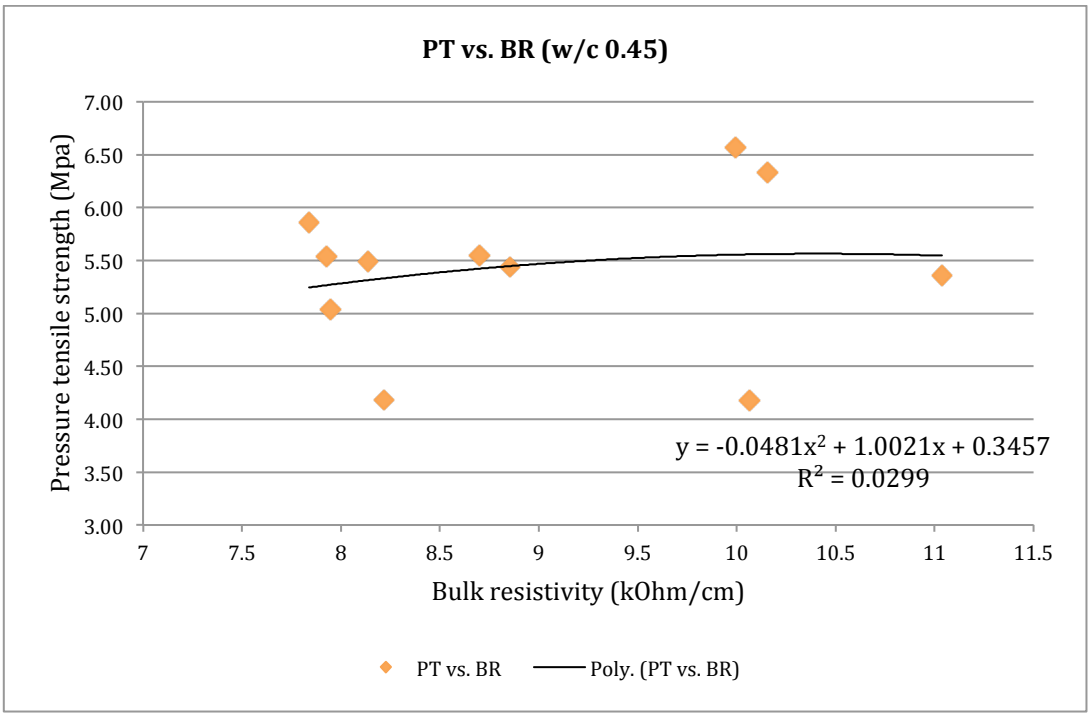

Figure 45: PT vs. BR (w/c 0.45)

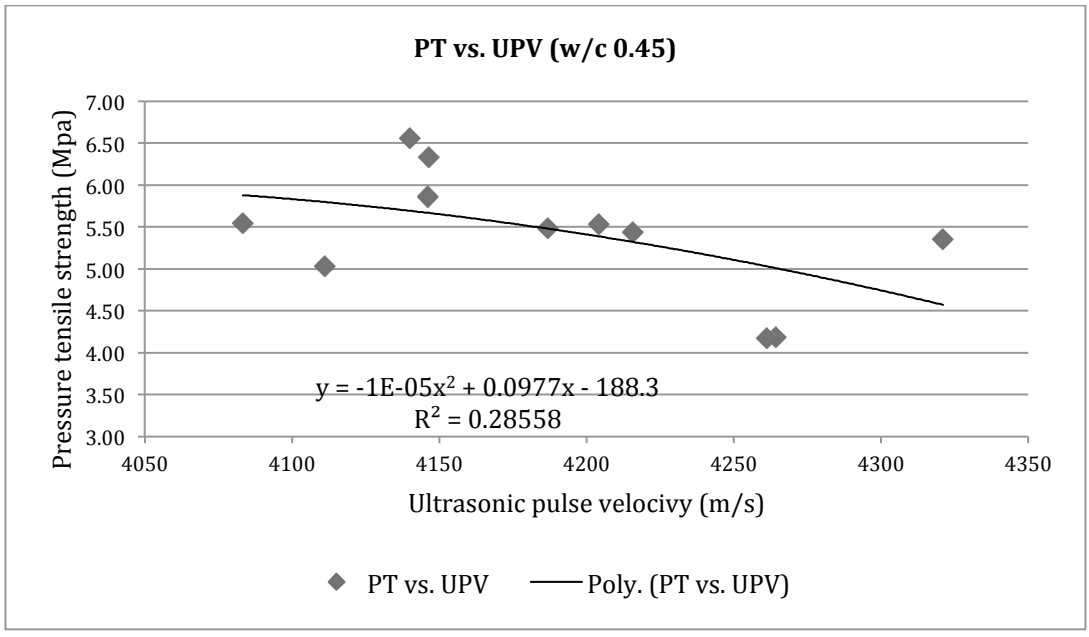

Figure 46: PT vs. UPV (w/c 0.45)

Quadratic fitting curves were used to describe and quantify the relationships between PT test results and NDT results of Mix 0.45. From Figure 44, Figure 45 and Figure 46, it can be

seen that the three fitting curves demonstrate there are certain relationships between the two variables. However, the R^2 values are relatively low compared to those of Mix 0.65. While the regression lines of PT vs. SR and PT vs. UPV yield R^2 values of 0.35285 and 0.28558, respectively, PT vs. BR presents an R^2 of 0.0299. This means that the fitting line for PT vs. BR poorly indicates the relationships between the two variables (the pressure tensile strength and the bulk resistivity). From the regression lines of PT vs. SR and PT vs. UPV, the former has a higher R^2 value, which may indicate a better capability in predicting the pressure tensile strength of the specimens. The overall relatively low R^2 values of the three regression lines may have something to do with the limited variation of the test results. The change in pressure tensile strength and the NDT results after 80 F/T cycles are not significant. Thus extended freeze-thaw cycles should be considered in the future to better develop the relationships between these variables. Moreover, the limited amount of specimens included in this experiment may have also led to difficulty in developing better relationships between the NDT and the PT.

CHAPTER 4 SURFACE RESISTIVITY – TEMPERATURE RELATIONSHIPS

4.1 Introduction

Over the course of the carrying out surface resistivity tests on the concrete specimens, it was observed that surface resistivity was very sensitive to the change of temperature of the concrete during the thawing process. Previous research done by Spragg (2013) to investigate the influence of temperature showed that the resistivity of mortar and paste samples could differ by as much as 80 % when the temperature of the sample ranged from 10 °C to 45 °C (R. P Spragg, 2013).

The effect of temperature on the resistivity of concrete samples was also investigated by Sengul (2014). Ordinary Portland concrete specimens with water-cement ratio of 0.45 were tested at the temperature of 5°C, 10°C and 35°C. Temperature was found to affect the resistivity significantly, which is shown in Figure 47 (Sengul, 2014).

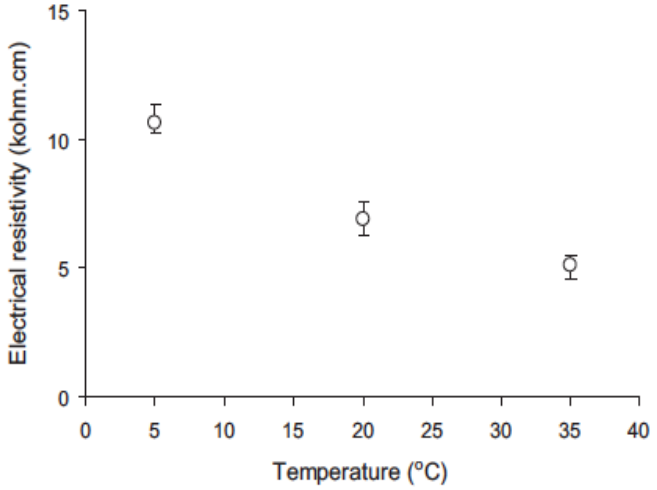

Figure 47: Effect of temperature on electrical resistivity

Source: (Sengul, 2014)

The surface resistivity test generates a current in the concrete specimen and the resistivity is obtained by calculating the measured potential and the generated current. Temperature can affect the resistivity of a material significantly by influencing the mobility of the ions of the material. An increase in temperature accelerates the mobility of the ions dissolved in the pore liquid and increases its conductivity (Osterminski et al., 2012). The porosity and continuity of the pore system of concrete, the composition, concentration and the mobility of the ions in the pore fluid determine the amount of current passed through the concrete, thus determining the resistivity of concrete. In addition, most of the current (i.e. electron flow) must move through the pore fluid in concrete (Julio-Betancourt & Hooton, 2004). Therefore, an increase in temperature will promote the mobility of the ions in the pore fluid of concrete, thus resulting in an increased conductivity and a decreased resistivity. And importantly, concrete is similar to a semi-conductor in terms of the influence of temperature on its resistivity, where the resistivity decreases as the temperature increases (Julio-Betancourt & Hooton, 2004).

A significant influence of temperature on the electrical resistivity of concrete was found in previous research and it was observed in this work that surface resistivity was very sensitive to temperature changes. Therefore, an experimental program was carried out to investigate the relationships between surface resistivity and temperature. A section of discussion and conclusion are also presented in this chapter.

4.2 Experimental Program

4.2.1 Materials

In order to study the influence of temperature on surface resistivity, eight concrete mixtures were cast. Mixtures 1-4 were of water/cement 0.65; Mixtures 5-8 were of water/cement 0.45. Mixtures 1-8 adopted the same mix design as Mixture A and B as

described in Chapter 2, but different types of aggregates were used and the inclusion of air-entraining agent (AEA) varied. The mix designs of the eight mixtures are shown in Table 3 and Table 4, and each mixture produced 2 concrete specimens. The reason for preparing specimens with different types of aggregates and the inclusion of air-entraining agent was to investigate how the relationships between temperature and surface resistivity change in different concrete specimens.

Table 4: Specimen identification for Mixtures 1-8

Mix 1	Mix 2	Mix 3	Mix 4	Mix 5	Mix 6	Mix 7	Mix 8
0.65ALT	0.65AGT	0.65NLT	0.65NGT	0.45ALT	0.45AGT	0.45NLT	0.45NGT

Where,

0.65, 0.45 specify the respective water/cement

A – air-entrained, N – non air-entrained

L – limestone, G – granite

T – sample prepared for study of surface resistivity – temperature relationship

Table 5: Mix design for Mixture 1-4

Ingredients (kg/m^3)	0.65ALT	0.65AGT	0.65NLT	0.65NGT
Water	227.5	227.5	227.5	227.5
Cement	350.0	350.0	350.0	350.0
Coarse Aggregates	894.17	894.17	894.17	894.17
Fine Aggregates	624.31	624.31	624.31	624.31
ADVA 575 Superplasticizer	1.05	1.05	1.05	1.05
Darex ED Air-Entraining Agent	0.175	0.175	/	/

Total	2097.205	2097.205	2097.03	2097.03

Table 6: Mix design for Mixture 5-8

Ingredients (kg/m^3)	0.45ALT	0.45AGT	0.45NLT	0.45NGT
Water	193	193	193	193
Cement	428.89	428.89	428.89	428.89
Coarse Aggregates	894.17	894.17	894.17	894.17
Fine Aggregates	648.6	648.6	648.6	648.6
ADVA 575 Superplasticizer	1.42	1.42	1.42	1.42
Darex ED Air-Entraining Agent	0.219	0.219	/	/
Total	2166.299	2166.299	2166.08	2166.08

Figure 48: Marked specimens after demoulding

All the specimens were of nominal size 100 mm x 200 mm. The mixing procedures were the same as described in Chapter 2. After demoulding, the specimens were submerged in limewater to cure for 14 days. All specimens followed the marking method on the specimens as described in Chapter 2, Surface Resistivity Test - Operational Procedure (Figure 48).

4.2.2 Test Methods

The objective of this experiment was to study how temperature in the range of 0 °C to 30 °C would affect the surface resistivity. After curing for 14 days in limewater, the specimens were placed in the freezer to lower the temperature down to freezing. This was done right after the curing process of the concrete samples.

The second part included continuous temperature monitoring while performing surface resistivity tests on the concrete specimens. A water bath affixed with a heating rod was used to raise the temperature of the specimens. An infrared thermometer (Figure 49) and an ordinary thermometer were used to monitor the temperature of the specimen and the water, respectively. Concrete specimens were first thawed out in the water bath, and ice cubes were used to slow down the thawing speed. Ice in the specimen must be completely thawed before resistivity testing because ice is considered to be a nonconductor and will cause erroneous high surface resistivities of the concrete specimen. When the specimen was completely thawed, which was when its surface temperature reached 3 ± 1 °C, surface resistivity testing was carried out on the specimens. The heater attached to the container was turned on to raise the temperature of the specimen by raising the temperature of the water bath. The same operational procedure was adopted as described in Chapter 2, Surface Resistivity Test-Operational Procedure. The infrared thermometer was used to record the surface temperature of the specimen at 4 different marked spots on the concrete specimen. The surface resistivity test and temperature recording were then carried out on the same specimen at intervals of 10 minutes. This continuous test was continued until the surface temperature of the specimen reached 30 ± 2 °C. Figure 50 shows the testing process.

This test is straightforward and relatively easy to operate. Using the water bath to raise the temperature of the specimen ensured that it was fully saturated without drying out due to the increase of temperature.

Figure 49: Infrared thermometer Fluke 568

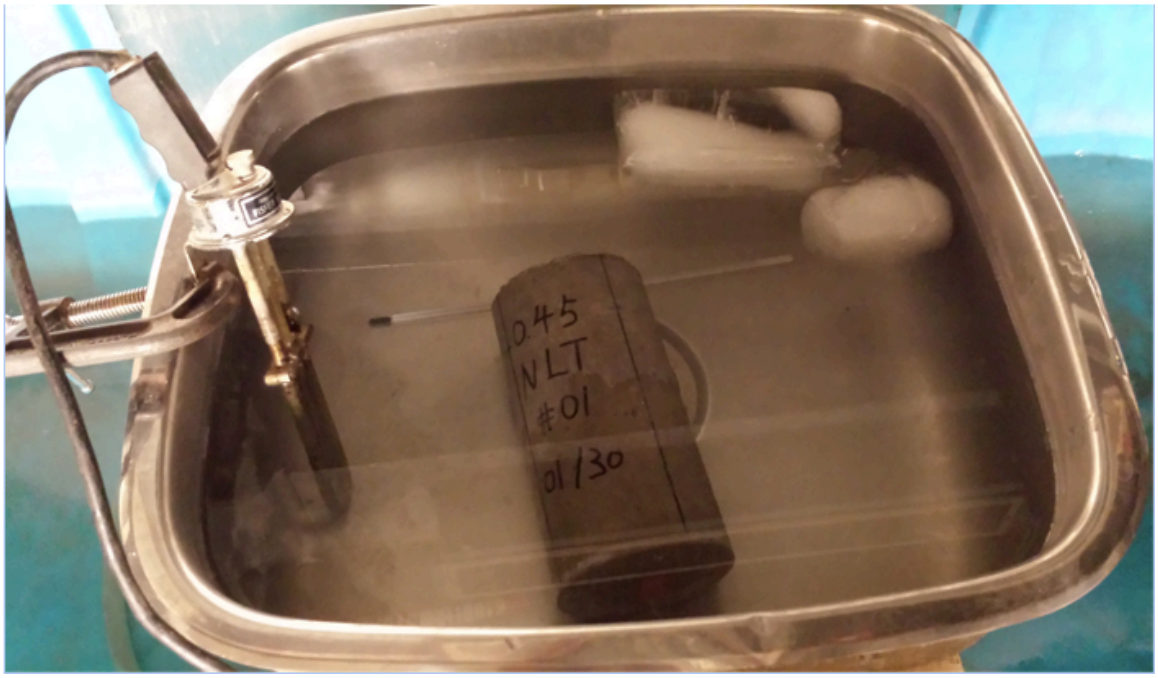

Figure 50: The outlook of testing process

4.3 Results and Discussion

The test results are discussed in three aspects to investigate how these factors affect the relationships between surface resistivity and temperature: The effect of water/cement, the effect of aggregate types and the effect of air entrainment.

4.3.1 The Effect of Water/Cement

The eight mixtures had the same amount of coarse aggregates and close amount of fine aggregates (Mixtures 1-4 have 3.7% less fine aggregates than Mixtures 5-8). Thus the different water/cement would be the only considerable variation between the specimens of Mixtures 1-4 (w/c0.65) and Mixtures 5-8 (w/c 0.45).

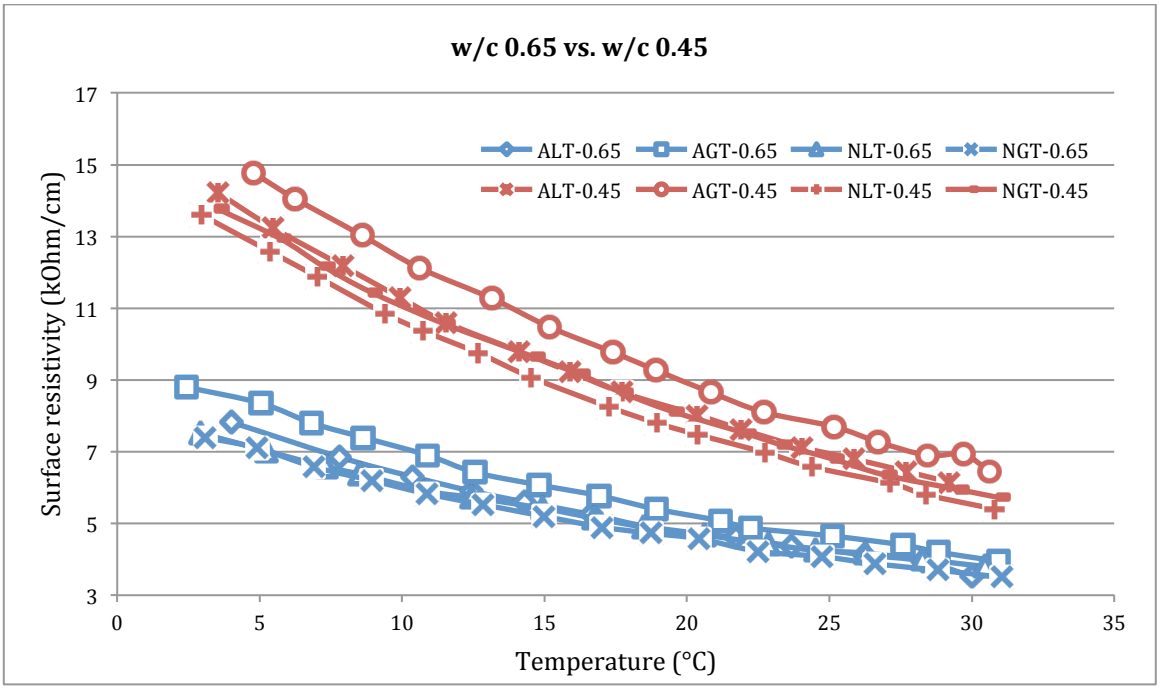

Figure 51: Test result Mixtures 1-8

As is seen clearly in Figure 51, specimens with a w/c 0.45 showed a higher surface resistivity than those of w/c 0.65 under the same temperature. This trend is consistent with the increase of temperature. It shows that water/cement ratio has a larger influence

on the surface resistivity of concrete than the effect of aggregate types and the inclusion of air-entrainment. The essential reason for this is that higher w/c creates higher porosity in concrete, and thus more pore fluid in the specimen when it is saturated. The lower surface resistivity of Mixtures 5-8 (w/c 0.65) is the combined result of higher porosity and higher amount of pore fluid.

The surface resistivity of the specimens decreases as temperature increases. This is consistent with the theory that increased temperature increases the mobility of the ions in pore solution and thus results in reduced resistivity of the concrete specimen. And as the temperature gets higher, the decrease in surface resistivity tends to slow down and eventually plateaus. The surface resistivity tested at 3 °C is as much as 2.5 times that tested at 30 °C. A quadratic regression model was found to fit the relationships between temperature change and surface resistivity the best. The fitting regression line of ALT-0.65 and ALT-0.45 are shown in Figure 52. Both the regression lines have very high R^2 values (0.99957 and 0.99535 respectively). These regression lines have a profound implication in predicting the surface resistivity of concrete specimens at a given temperature or, more importantly. Adjusting surface resistivity readings to account for concrete surface temperature under field conditions.

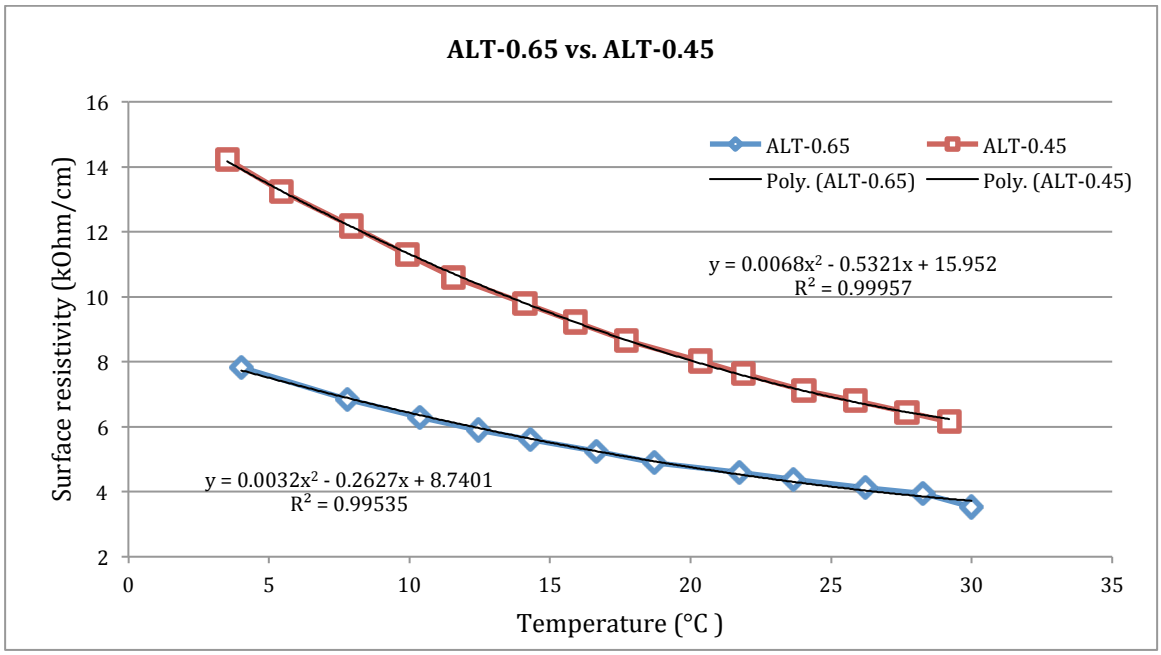

Figure 52: Regression models of ALT-0.65 and ALT-0.45

4.3.2 The Effect of Aggregate Type

Aggregate resistivities differ greatly depending on their sources and types. Concrete mixtures with granite aggregates have higher resistivity than those with limestone (Whiting & Nagi, 2003). But most aggregates used in structures are limited to hard, low-absorption aggregates basing on concrete specifications. Typical resistivities of these aggregates are about 10^5 ohm/cm, while resistivities of cement paste or mortar are significantly lower, mostly in the range of 10^3 ohm/cm or less (Whiting & Nagi, 2003).

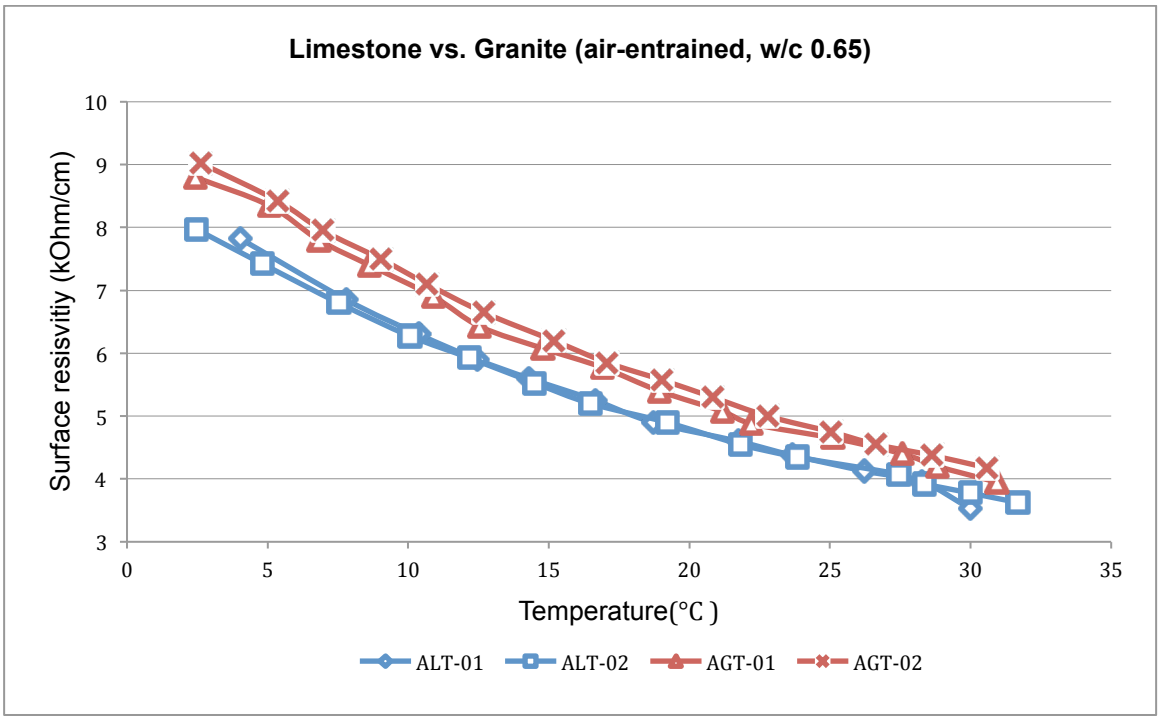

Figure 53: Limestone vs. granite (air-entrained, w/c 0.65)

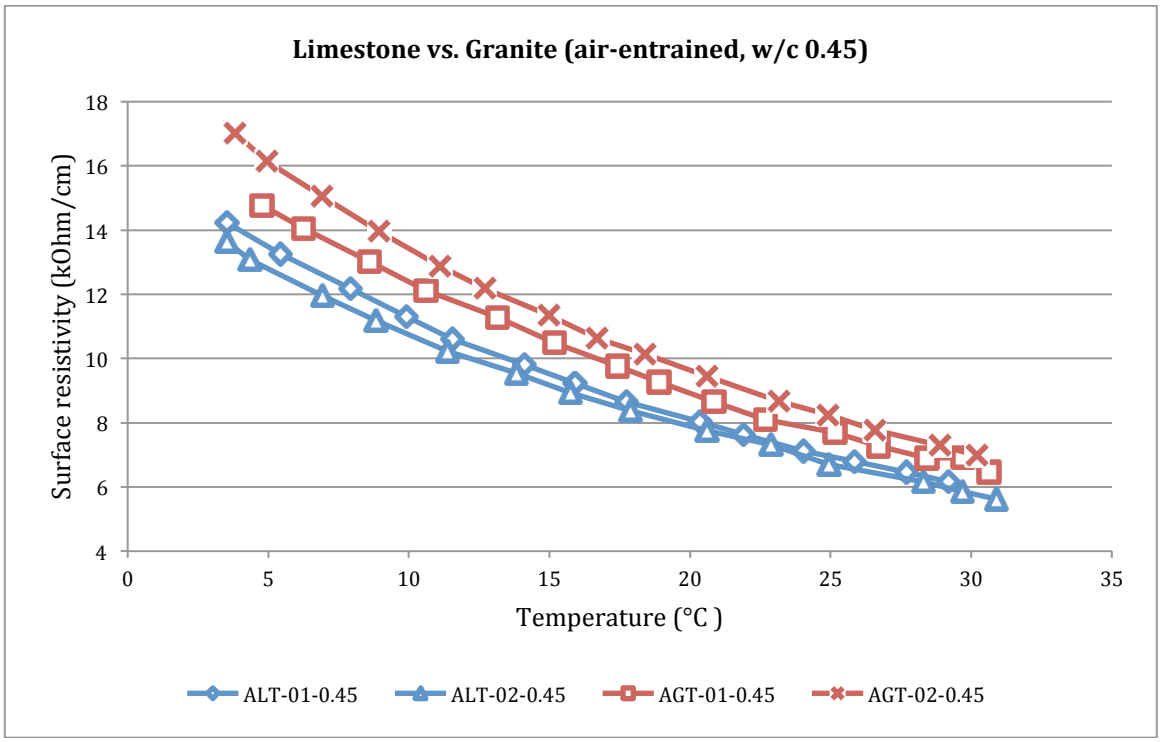

Figure 54: Limestone vs. granite (air-entrained, w/c 0.45)

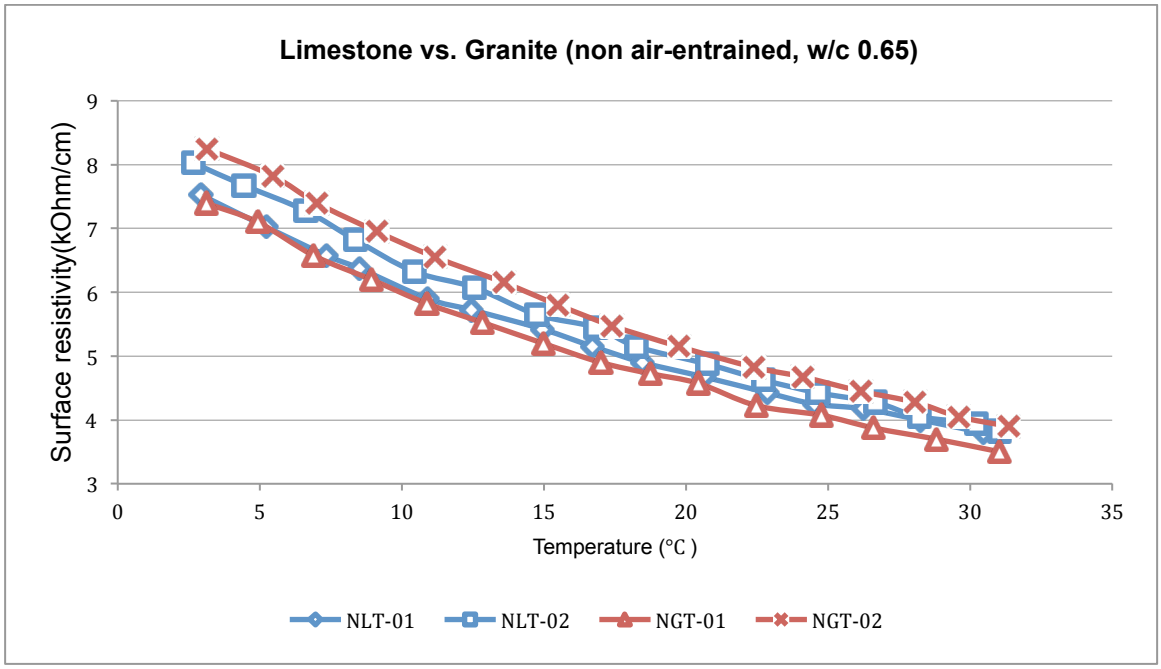

Figure 55: Limestone vs. granite (non air-entrained, w/c 0.65)

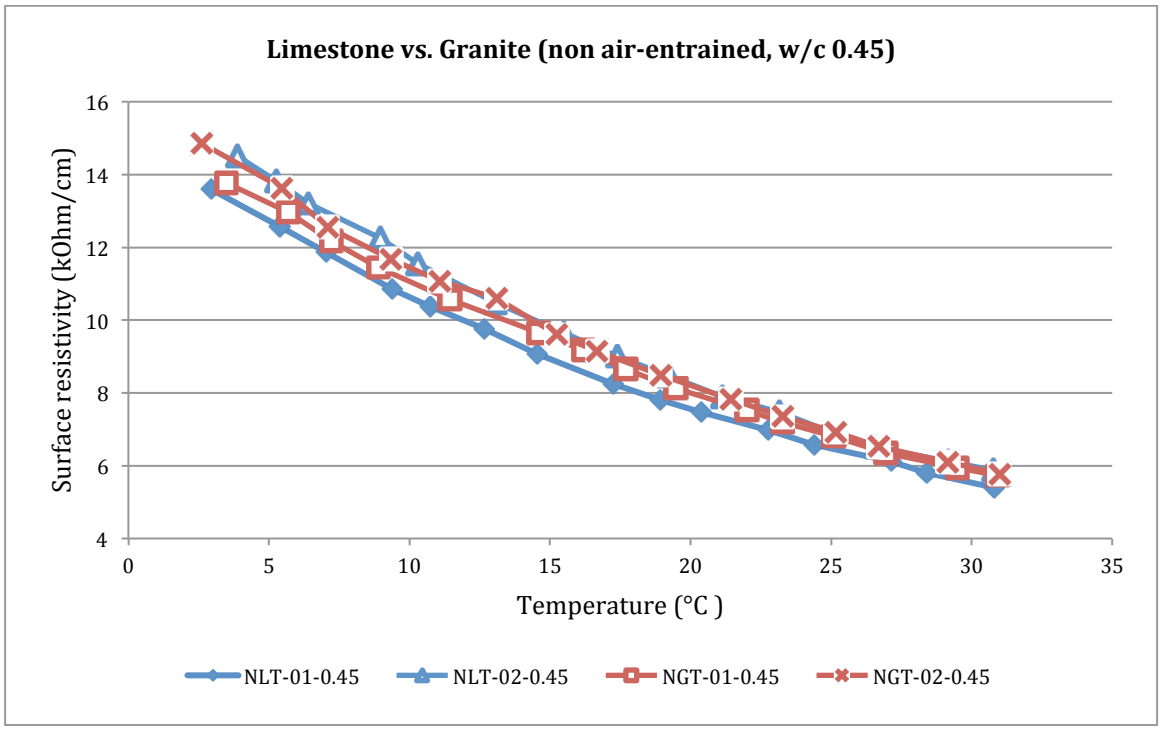

Figure 56: Limestone vs. Granite (non air-entrained, w/c 0.45)

From Figure 53 and Figure 54, it is shown that the specimens with granite had higher surface resistivity than those of limestone under the same temperature if an air-entraining agent was used. The temperature-surface resistivity relationships display obvious differences when different types of aggregates were used in air-entrained concrete. However, this conclusion did not apply to the specimens without air-entrainment. As seen in Figure 55 and Figure 56, without air-entrainment, the specimens with granite did not show higher surface resistivity than those of limestone. The type of aggregates seems to have a much less obvious change on the surface resistivity of the specimens when air-entrainment was not used.

4.3.3 The Effect of Air-Entrainment

Air-entrainment in concrete is believed to affect its surface resistivity because air-entrainment creates higher porosity in concrete, and this higher porosity will lead to higher resistivity of concrete because these added pores are not connected.

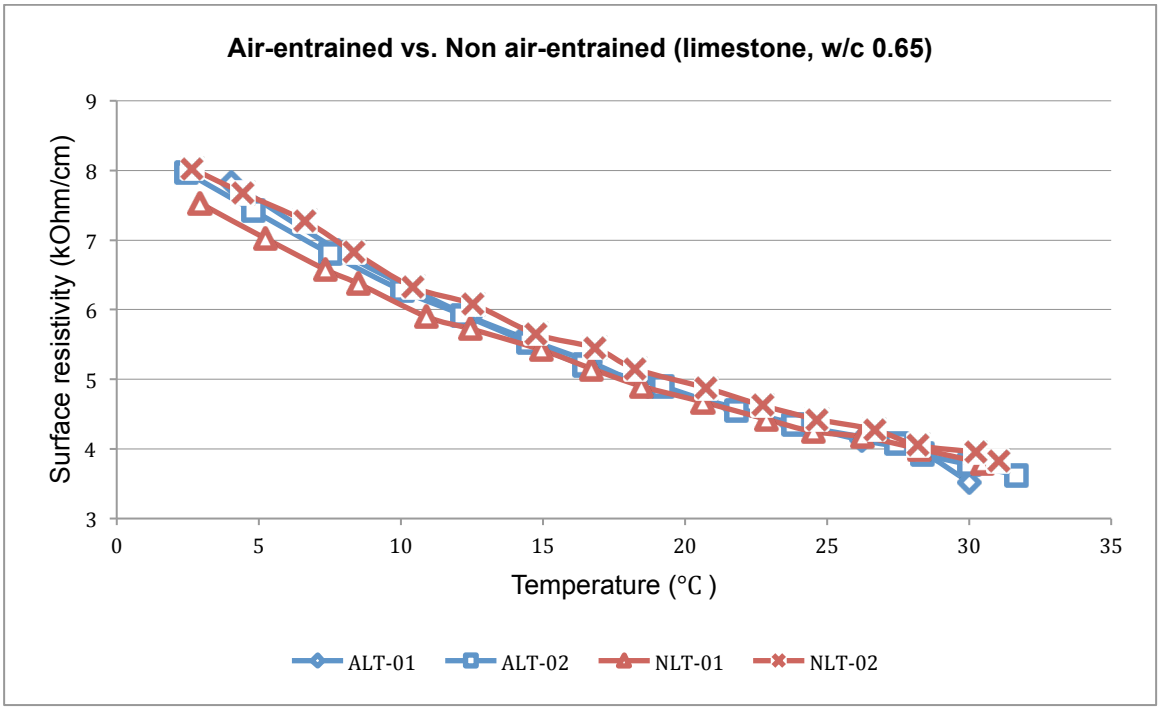

Figure 57: Air-entrained vs. non air-entrained (limestone, w/c 0.65)

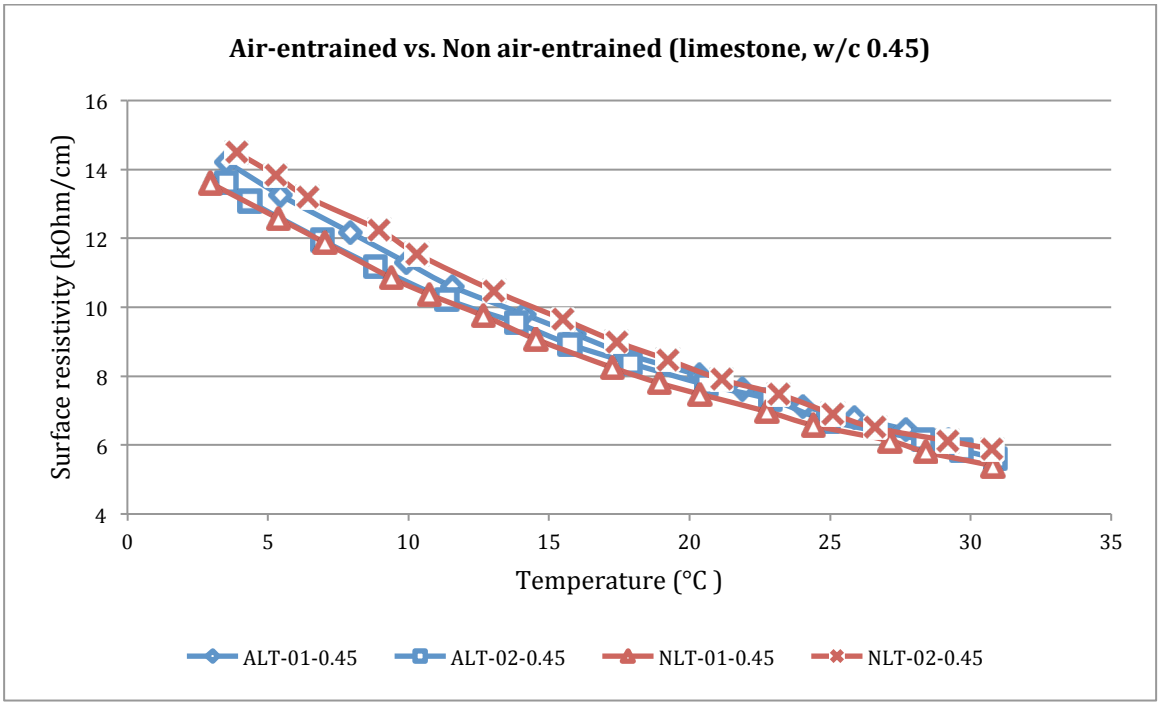

Figure 58: Air-entrained vs. non air-entrained (limestone, w/c 0.45)

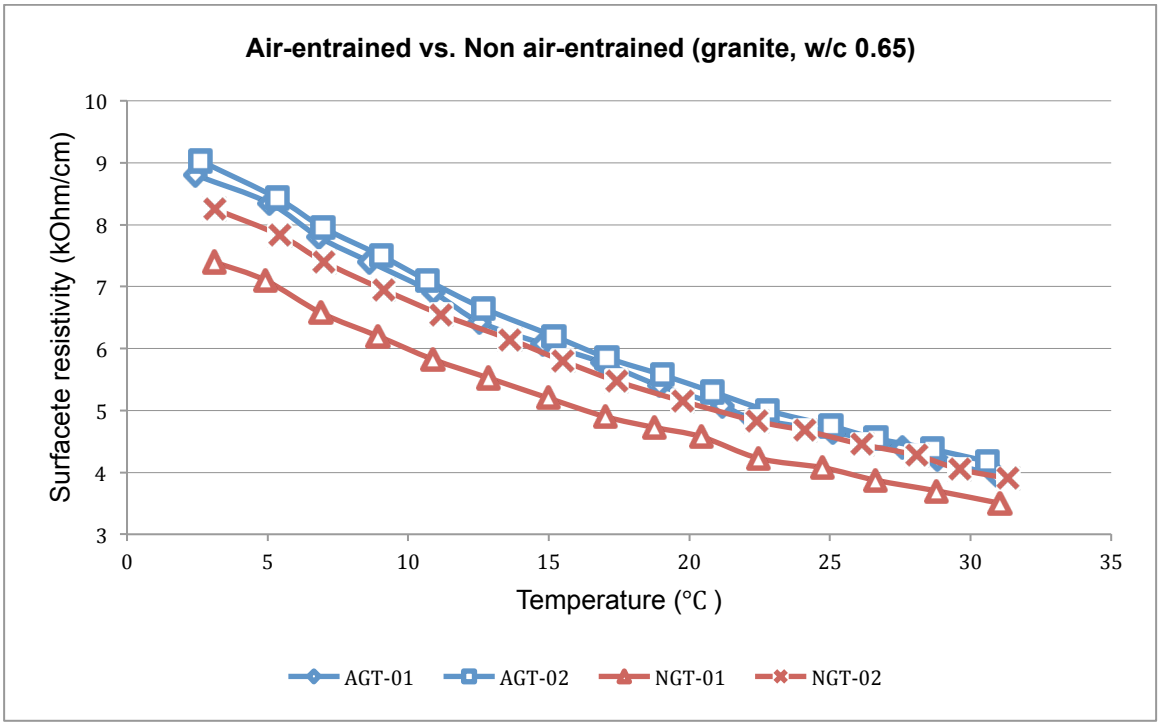

Figure 59: Air-entrained vs. non air-entrained (granite, w/c 0.65)

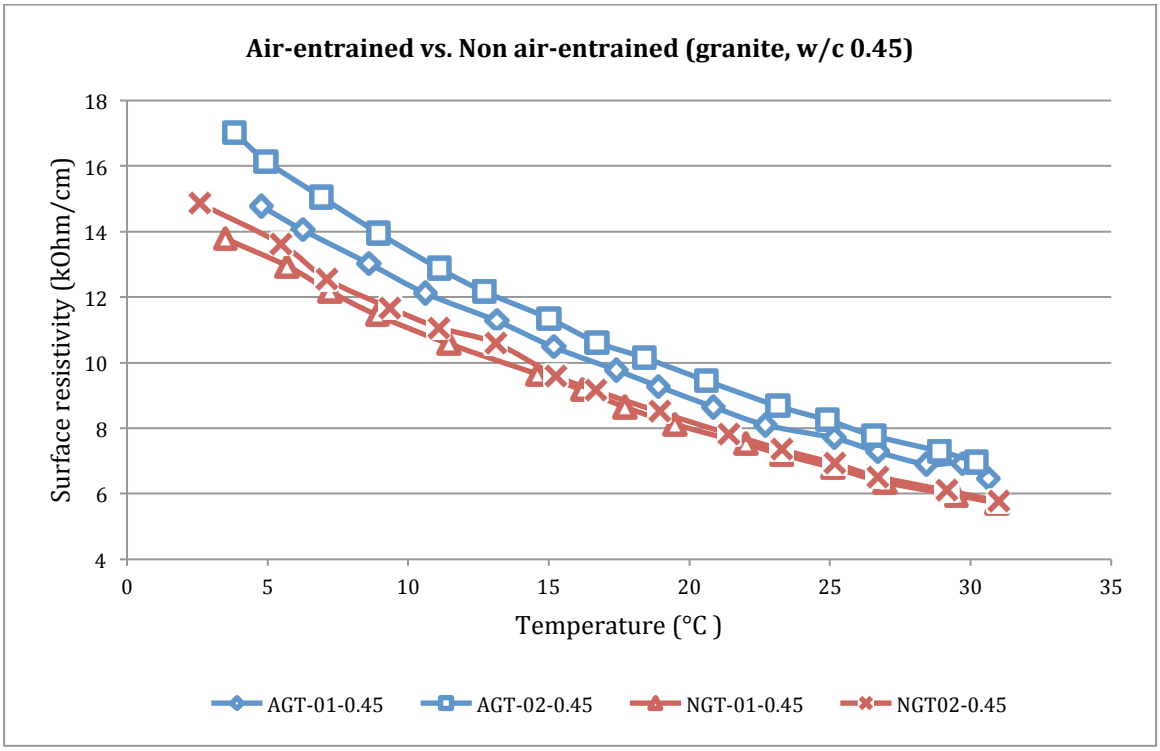

Figure 60: Air-entrained vs. non air-entrained (granite, w/c 0.45)

However, from Figure 57 and Figure 58, such an assumption cannot be confirmed from the results of samples made with limestone. No obvious contrast was observed between the specimens with air-entrainment and the specimens without air-entrainment. This means that the inclusion of air-entrainment does not affect the relationship between temperature and surface resistivity for the specimens made with limestone. This was consistent for specimens with water/cement 0.65 and 0.45.

As for the specimens made with granite, an apparent difference was observed in the specimens, albeit quite small. From Figure 59 and Figure 60, concrete specimens with air-entrainment presented higher resistivity than those without air-entrainment for specimens made with granite. This remained consistent as the temperature increased. These results are consistent with the theory that air-entrained concrete has higher surface resistivity than non air-entrained concrete.

4.4 Conclusion

Eight mixtures (ALT-0.65, AGT-0.65, NLT-0.65, NGT-0.65, ALT-0.45, AGT-0.45, NLT-0.45, NGT-0.45) were used to investigate the relationship between temperature and surface resistivity (SR). The effects of water/cement, aggregate types and inclusion of air-entrainment on this relationship was also studied.

The surface resistivity of all the eight mixtures decreased as temperature increased. The increased temperature facilitates the movement of ions, which results in increased conductivity and decreased resistivity. This is consistent for all the mixtures with different w/c, aggregate types and inclusion of air-entrainment. A quadratic regression model was found to best describe the relationship between temperature and SR.

Water/cement plays an important role in the relationships between temperature and SR. Specimens with w/c 0.45 had higher resistivity than those of w/c 0.65 under the same temperature. It was shown that water/cement had a much larger influence on the surface resistivity of concrete than the effect of aggregate type and the inclusion of air-entrainment. The essential reason for this is a higher w/c creates higher porosity and when the specimens are saturated, they show much lower resistivity.

It is shown in the results that specimens made with granite had slightly higher surface resistivity than those of limestone under the same temperature if an air-entraining agent was used. However, without air-entrainment, no obvious influence was observed. The inclusion of air-entrainment did not affect the relationship between temperature and SR for the specimens made with limestone. Concrete specimens with air-entrainment presented higher resistivity than those without air-entrainment for specimens made with granite. These results are consistent with the theory that air-entrained concrete has higher surface resistivity than non air-entrained concrete. The above conclusions apply to both the specimens of water/cement 0.65 and 0.45.

CONCLUSIONS

In order to investigate the sensitivity of nondestructive testing in detecting freeze-thaw damage in concrete, two mixtures were prepared in this work: Mix 0.65 (w/c 0.65) and Mix 0.45 (w/c 0.45). The specimens of Mix 0.65 were subjected to 40 freeze-thaw cycles and those of Mix 0.45 were subjected to 80 cycles. Nondestructive testing techniques: surface resistivity (SR), bulk resistivity (BR) and ultrasonic pulse velocity (UPV) were utilized to monitor changes over freeze-thaw cycles. The pressure tension test is considered sensitive to internal damage in concrete and was used to quantify the freeze-thaw damage and determine the sensitivities of NDT in detecting the damage. In addition, the relationship between temperature and surface resistivity was also studied.

After the freeze-thaw test, specimens of Mix 0.65 showed much more severe and obvious damage than those of Mix 0.65. This is consistent with the visual observation and the test results of pressure tension test. The NDT results of Mix 0.65 displayed apparent decreases after the freeze-thaw test, which was caused by the freeze-thaw damage in the specimens. This indicates that the three NDT methods are all capable of detecting the freeze-thaw damage in the specimens of Mix 0.65. From studying the relationships between NDT and PT, surface resistivity test was considered to be more sensitive than bulk resistivity test and the ultrasonic pulse velocity test.

However, the NDT results of Mix 0.45 were inconclusive. PT and SR results indicated that there is freeze-thaw damage after 80 cycles while BR and UPV did not show damage in the concrete specimens. In fact, the test results of BR and UPV showed an increase after the freeze-thaw test. This can be due to the continued hydration of the concrete, which reduced its porosity. The reason for the surface resistivity test being more sensitive is that freeze-thaw damage happens first at the surface where it is more saturated and has a higher cooling rate. Thus, this led to freeze-thaw damage occurring first near the surface, which was detected by the surface resistivity test. Therefore, it can be concluded that SR is very

sensitive in detecting early age freeze-thaw damage, while BR and UPV are only capable of detecting freeze-thaw damage when the damage is more severe.

The study of the relationship between temperature and SR indicated that SR was very sensitive to change in surface temperature of the concrete. As surface temperature increases, SR decreases significantly due to the higher mobility of ions. The relationship between temperature and SR is not linear and quadratic regression models were found to best correlate these relationships. The effect of w/c on influencing these relationships was apparent while the effect of aggregate type and the effect of the inclusion of air-entrainment were inconclusive.

This investigation's findings have significant implication on the capability and limitations of nondestructive testing, and provide insight for its application in the future.

References

AASHTO-TP-95-11. Standard Method of Test for Surface Resistivity Indication of Concrete's Ability to Resist Chloride Ion Penetration.

Al‐Assadi, G., Casati, M. J., Fernández, J., & Gálvez, J. C. (2011). Effect of the curing conditions of concrete on the behaviour under freeze–thaw cycles*. *Fatigue & Fracture of Engineering Materials & Structures, 34*(7), 461-469.

ASTM-C597. Standard Test Method for Pulse Velocity Through Concrete. *ASTM International*.

B., C. E. (1989). Durable Concrete Structures CEB Design Guide. *CEB Design Guide, Bulletin d'information*(182).

Backstrom, J. E., Burrows, R. W., Wolkodoff, V. E., & Powers, T. C. (1954). Void spacing as a basis for producing air-entrained concrete. *ACI Journ., 4*, 760-761.

BAŽANT, Z. P., CHERN, J. C., Rosenberg, A. M., & Gaidis, J. M. (1988). Mathematical model for freeze‐thaw durability of concrete. *Journal of the American Ceramic Society, 71*(9), 776-783.

Bentz, D. P., Garboczi, E. J., Haecker, C. J., & Jensen, O. M. (1999). Effects of cement particle size distribution on performance properties of Portland cement-based materials. *Cement and Concrete Research, 29*(10), 1663-1671.

Bremner, T. W., Boyd, A. J., Holm, T. A., & Boyd, S. R. (1998). Tensile testing to evaluate the effect of alkali-aggregate reaction in concrete. *Proceedings of Alkali-Aggregate Reactions in Concrete, CANMET/ACI, Dartmouth, NS, Canada, CANMET/NRC, Ottawa*, 311-326.

Broomfield, J., & Millard, S. (2002). Measuring concrete resistivity to assess corrosion rates. *Concrete, 36*(2).

Cai, H., & Liu, X. (1998). Freeze-thaw durability of concrete: ice formation process in pores. *Cement and Concrete Research, 28*(9), 1281-1287.

Chini, A. R., Muszynski, L. C., & Hicks, J. K. (2003). Determination of acceptance permeability characteristics for performance-related specifications for Portland cement concrete (No. Final Report).

Christensen, B. J., Coverdale, T., Olson, R. A., Ford, S. J., Garboczi, E. J., Jennings, H. M., & Mason, T. O. (1994). Impedance Spectroscopy of Hydrating Cement‐Based Materials: Measurement, Interpretation, and Application. *Journal of the American Ceramic Society, 77*(11), 2789-2804.

Clayton, N., & Grimer, F. J. (1979). The diphase concept, with particular reference to concrete. *Building research establishmen, building research station, Watford, UK*.

Cordon, W. A. (1966). Freezing and thawing of concrete-mechanisms and control.

Cumming, S. R. (2004). Nondestructive testing to monitor concrete deterioration caused by sulfate attack (Doctoral dissertation, University of Florida).

Cumming, S. R., Boyd, A. J., & Ferraro, C. C. (2006). Tensile strength prediction in concrete using nondestructive testing techniques. *Research in Nondestructive Evaluation, 17*(4), 205-222.

Ewins, A. J. (1990). Resistivity measurements in concrete. *British Journal of Non-Destructive Testing, 32*(3), 120-126.

Ghosh, P., & Tran, Q. (2014). Correlation Between Bulk and Surface Resistivity of Concrete. *International Journal of Concrete Structures and Materials, 9*(1), 119-132.

Gowers, K. R., & Millard, S. G. (1999). Measurement of concrete resistivity for assessment of corrosion severity of steel using Wenner technique. *ACI Materials Journal, 96*(5).

Jiang, L., Niu, D., Yuan, L., & Fei, Q. (2015). Durability of concrete under sulfate attack exposed to freeze–thaw cycles. *Cold Regions Science and Technology, 112*, 112-117.

Julio-Betancourt, G. A., & Hooton, R. D. (2004). Study of the Joule effect on rapid chloride permeability values and evaluation of related electrical properties of concretes. *Cement and Concrete Research, 34*(6), 1007-1015.

JValenza, J. J., & Scherer, G. W. (2006). Mechanism for salt scaling. *Journal of the American Ceramic Society, 89*(4), 1161-1179.

Komar, A. J. K., & Boyd, A. (2014). Pressure-Tension Testing in the Evaluation of Freeze-Thaw Deterioration. *10th fib International PhD Symposium in Civil Engineering*.

Kosior-Kazberuk, M. (2012). Effects of Interaction of Static Load and Frost on Damage Mechanism of Concrete Elements. *JOURNAL OF SUSTAINABLE ARCHITECTURE AND CIVIL ENGINEERING, 1*(1), 40-45.

Leger, P., Cote, M.,, & Tinawi, R. (1995). Thermal protection of concrete dams subjected to freeze-thaw cycles. *Canadian Journal of Civil Engineering, 22*(3), 588-602.

Lencioni, J. W., & de Lima, M. G. (2013). A study of the parameters that affect the measurements of superficial electrical resistivity of concrete. *Nondestructive Testing of Materials and Structures*, 271-276.

Litvan, G. G. (1973). Frost action in cement paste. *Materials and structures, 34*, 1-8.

Litvan, G. G. (1980). Freeze-thaw durability of porous building materials. *ASTM special technical publication, 691*, 455-463.

Malhotra, V. M., & Carino, N. J. (2003). andbook on Nondestructive Testing of Concrete Second Edition. *CRC press*.

Mertz, E. (2015). Edmonton researches how different asphalt mixes withstand freeze/thaw cycles.

Millard, S. G., & Harrison, J. (1989). Measurement of the electrical resistivity of reinforced concrete structures for the assessment of corrosion risk. *Brit. J. Nondestructive Testing, 31*(11), 617-621.

Mindess, S., Young, J. F., & Darwin, D. (1981). Concrete, Prentice Hall. *Englewood Cliffs, NJ*, 481.

Morris, W., Moreno, E. I., & Sagüés, A. A. (1996). Practical evaluation of resistivity of concrete in test cylinders using a Wenner array probe. *Cement and Concrete Research, 26*(12), 1779-1787.

Osterminski, K., Polder, R. B., & Schießl, P. (2012). Long term behaviour of the resistivity of concrete. *Heron, 57*(3), 211-230.

Patel, V. N. (2009). SORPTIVITY TESTING TO ASSESS DURABILITY OF CONCRETE AGAINST FREEZE-THAW CYCLING.

Polder, R., Andrade, C., Elsener, B., Vennesland, O., Gulikers, J., Weidert, R., & Raupach, M. (2000). RILEM TC 154-EMC: electrochemical techniques for measuring metallic corrosion. *Materials and structures, 33*, 603-611.

POWERS, T. C. (1945). A working hypothesis for further studies of frost resistance of concrete. *ACI journal Proceedings, 41*(1).

POWERS, T. C. (1975). Freezing effects in concrete. *ACI Special Publication, 47*.

Powers, T. C., & Brownyard, T. L. (1946). Studies of the physical properties of hardened Portland cement paste. *ACI journal Proceedings, 43*(9).

Powers, T. C., & Helmuth, R. A. (1953). *Theory of volume changes in hardened portland-cement paste during freezing.* Paper presented at the Highway research board proceedings.

Powers, T. C., & Willis, T. F. (1950). *The air requirement of frost resistant concrete.* Paper presented at the Highway Research Board Proceedings.

Proceq-Resipod. Proceq Resipod Operating Instructions.

Qasrawi, H. Y., & Marie, I. A. (2003). The use of USPV to anticipate failure in concrete under compression. *Cement and Concrete Research, 33*(12), 2017-2021.

Sengul, O. (2014). Use of electrical resistivity as an indicator for durability. Construction and Building Materials. *Construction and Building Materials, 73*, 434-441.

Spragg, R. P. (2013). The rapid assessment of transport properties of cementitious materials using electrical methods (Doctoral dissertation, PURDUE UNIVERSITY).

Spragg, R. P., Castro, J., Nantung, T. E., Paredes, M., & Weiss, W. J. (2011). Variability analysis of the bulk resistivity measured using concrete cylinders.

Streicher, P. E., & Alexander, M. G. (1995). A chloride conduction test for concrete. *Cement and Concrete Research, 25*(6), 1284-1294.

Uno, T., Fujikake,, K., M., S.,, & Xu, H. (2005). CONCRETE FAILURE MECHANISM IN THE NITROGEN GAS TENSION TEST.

Vivas, E. A. (2007). Allowable limits for conductivity test methods and diffusion coefficient prediction of concrete structures exposed to marine environments (Doctoral dissertation, University of Florida).

Ward, M. A., & Langan, B. W. (1990). Effect of concrete specifications and inspection practices on freeze-thaw resistance: a field study. *Canadian Journal of Civil Engineering, 17*(2), 271-276.

Whiting, D. A., & Nagi, M. A. (2003). Electrical resistivity of concrete-a literature review. R&D Serial, (2457).

Appendix A - Surface Resistivity Results – w/c 0.65, Sample #1-#27

Surface resistivity – w/c 0.65 (kOhm/cm)						
Sample #	Cycles	0°	90°	270°	360°	Average
#1	0 cycle	7.9	7	7.4	7.2	7.375
#2		6.8	6.5	7	6.9	6.8
#3		7.8	8.1	8	7.8	7.925
#4	5 cycle	7.1	6.7	7.3	6.8	6.975
#5		6.2	6.4	7.2	6.6	6.6
#6		6.1	6.5	6.8	7	6.6
#7	10 cycle	5.7	5.8	5.8	5.7	5.75
#8		7.1	6.4	7.5	7	7
#9		7	7	6.9	7.1	7
#10	15 cycle	6.4	6.2	7	6.7	6.575
#11		6.1	6.4	6.1	6.2	6.2
#12		6.1	6.1	6.1	6.1	6.1
#13	20 cycle	6.2	5.5	5.8	6.1	5.9
#14		6.2	6.2	6.8	5.4	6.15
#15		5.1	5.3	5.2	5.2	5.2
#16	25 cycle	5.1	4.7	5.1	5.5	5.1
#17		5.5	5.6	4.9	5.2	5.3
#18		5.5	5.5	5.9	5.6	5.625
#19	30 cycle	6.3	6.1	6.2	5.6	6.05
#20		5.9	6.1	5.9	6.2	6.025
#21		4.9	4.8	4.9	4.9	4.875
#22	35 cycle	5.2	4.8	4.8	5.1	4.975
#23		6.8	6.7	6.6	6.8	6.725
#24		5.4	5.4	4.9	5.9	5.4
#25	40 cycle	5	5.3	4.8	4.9	5
#26		5.5	5.9	6.2	5.7	5.825
#27		4	4.3	4	4.5	4.2

Appendix B - Surface Resistivity Results – w/c 0.65, Control Samples

Surface resistivity – w/c 0.65 (kOhm/cm)						
	Sample #	0°	90°	270°	360°	Average
Cycle 0	Control #1	7.9	7	7.4	7.2	7.375
	Control #2	6.8	6.5	7	6.9	6.8
	Control #3	7.8	8.1	8	7.8	7.925
Cycle 01	Control #1	6.5	5.9	6.1	5.9	6.1
	Control #2	5.4	5.6	5.8	5.5	5.575
	Control #3	6.1	6.4	6.4	6.1	6.25
Cycle 02	Control #1	7	5.8	6.6	6.1	6.375
	Control #2	6.4	5.6	6.5	6.2	6.175
	Control #3	7.2	7.1	7.2	7.4	7.225
Cycle 03	Control #1	7.2	6.6	6	7	6.7
	Control #2	6	6.7	6.3	6.6	6.4
	Control #3	7.4	7.5	7.8	7.7	7.6
Cycle 04	Control #1	7.4	7.6	7.3	7.8	7.525
	Control #2	7	6.5	7.1	6.6	6.8
	Control #3	7.9	7.8	7.8	7.4	7.725
Cycle 05	Control #1	6.4	6.4	6.4	7	6.55
	Control #2	6.4	6.2	6.3	6.2	6.275
	Control #3	7.2	7.4	7.2	7.1	7.225
Cycle 06	Control #1	7.5	7	7.9	7.4	7.45
	Control #2	6.7	6.9	6.5	6.7	6.7
	Control #3	8.1	7.8	7.8	7.8	7.875
Cycle 07	Control #1	7.2	6.7	6.8	6.4	6.775
	Control #2	6.5	6.6	6.1	6.7	6.475
	Control #3	8.2	7.5	7.4	7.5	7.65
Cycle 08	Control #1	7	6.6	6.9	6.8	6.825
	Control #2	6.2	6.8	6.1	6.7	6.45
	Control #3	7.4	7.6	7.8	7	7.45
Cycle 09	Control #1	7.4	7.1	7.3	6.6	7.1
	Control #2	6.6	7	6.7	7	6.825
	Control #3	7.8	7.7	7.4	7.6	7.625
Cycle 10	Control #1	7.3	6.7	6.7	6.7	6.85
	Control #2	6.6	6	6.7	6.1	6.35
	Control #3	7.4	6.9	7.2	7	7.125
Cycle 11	Control #1	7.6	7.4	7.6	7.3	7.475
	Control #2	6.9	7.4	7	7.4	7.175
	Control #3	8.4	8.6	8.1	8.1	8.3

Cycle 12	Control #1	8.1	7.6	6.4	8.3	7.6
	Control #2	7.4	7.5	7.4	7.6	7.475
	Control #3	8	8.3	8.7	8.2	8.3
Cycle 13	Control #1	6.5	7.4	7.1	6.7	6.925
	Control #2	6.7	6.4	6.7	6.7	6.625
	Control #3	7.7	7.4	7.6	7.4	7.525
Cycle 14	Control #1	7.3	7.8	7.4	7.8	7.575
	Control #2	7	7.1	6.7	7	6.95
	Control #3	8.6	8.2	8.4	8	8.3
Cycle 15	Control #1	7.4	6.9	7.4	6.2	6.975
	Control #2	6.7	6.4	7	6.4	6.625
	Control #3	7.4	7.4	7.4	7.4	7.4
Cycle 16	Control #1	6.8	7	6.8	7.1	6.925
	Control #2	7.3	6.7	7.4	6.9	7.075
	Control #3	7	7.4	7.5	7.9	7.45
Cycle 17	Control #1	6.2	6.7	6.6	6.5	6.5
	Control #2	6.4	5.7	6.6	6.1	6.2
	Control #3	7.1	7.4	7	7	7.125
Cycle 18	Control #1	6.9	7	7.7	7.4	7.25
	Control #2	6.7	6.9	7	6.7	6.825
	Control #3	8	7.9	8.1	7.8	7.95
Cycle 19	Control #1	7.1	6.3	6.5	6.9	6.7
	Control #2	5.8	6.4	6	6.6	6.2
	Control #3	6.7	6.8	7	6.8	6.825
Cycle 20	Control #1	5.9	6.2	6	6.8	6.225
	Control #2	6.4	6.2	6.4	6.3	6.325
	Control #3	7	6.7	7	7.2	6.975
Cycle 21	Control #1	6.2	7	6.7	6.7	6.65
	Control #2	6.9	6.7	7	5.5	6.525
	Control #3	7.4	7.6	7.3	7.1	7.35
Cycle 22	Control #1	5.7	6.7	6.5	6.9	6.45
	Control #2	5.3	6.3	6.4	6.1	6.025
	Control #3	7	7	7	7.3	7.075
Cycle 23	Control #1	6.8	6.7	6.3	5.3	6.275
	Control #2	7	5.9	6.4	5.9	6.3
	Control #3	7.1	7.4	7.1	6.7	7.075
Cycle 24	Control #1	6.8	6.8	6.9	6.6	6.775
	Control #2	6.7	6.2	5.7	6.1	6.175
	Control #3	7	7.3	7	6.6	6.975
Cycle 25	Control #1	6.1	6.5	6.7	6.4	6.425
	Control #2	6.1	6	6.3	6.1	6.125

	Control #3	6.8	6.5	6.8	7	6.775
	Control #1	6.1	6.4	6.4	6.1	6.25
Cycle 26	Control #2	6.1	5.2	6.1	6.5	5.975
	Control #3	6.9	6.7	6.8	6.8	6.8
	Control #1	6.3	6.1	6.4	5.7	6.125
Cycle 27	Control #2	6.7	6.5	6.7	6.4	6.575
	Control #3	7	7.3	7.3	7.2	7.2
	Control #1	6.2	6	6.4	6.2	6.2
Cycle 28	Control #2	6.4	5.8	6.1	6.1	6.1
	Control #3	6.6	6.6	6.6	6.7	6.625
	Control #1	6.1	6.4	6.5	6.3	6.325
Cycle 29	Control #2	6.4	6.7	6.2	6.6	6.475
	Control #3	6.6	6.4	6.6	6.9	6.625
	Control #1	6.3	6	6.1	5.9	6.075
Cycle 30	Control #2	6	5.6	6.1	6.1	5.95
	Control #3	6	6.6	6.6	6.5	6.425
	Control #1	6.5	6.4	6.3	6.4	6.4
Cycle 31	Control #2	6.6	6.5	6.8	6	6.475
	Control #3	7.1	6.7	7	6.8	6.9
	Control #1	6.7	6.5	6.7	6.7	6.65
Cycle 32	Control #2	6.4	6	6.4	6	6.2
	Control #3	6.3	6.2	6.4	6.6	6.375
	Control #1	5.7	6	5.9	6.1	5.925
Cycle 33	Control #2	5.7	5.3	5.7	5.5	5.55
	Control #3	5.4	6	6.2	5.7	5.825
	Control #1	6.4	6.5	6.1	6.3	6.325
Cycle 34	Control #2	5.8	5.3	5.9	5.4	5.6
	Control #3	6.4	6.7	6.6	6.6	6.575
	Control #1	6.4	6.7	6.7	6.7	6.625
Cycle 35	Control #2	5.3	6.4	6.4	5.8	5.975
	Control #3	7	7.3	6.2	6.8	6.825
	Control #1	6.1	6	5.8	6	5.975
Cycle 36	Control #2	6.1	6.2	5.7	6.3	6.075
	Control #3	6.4	5.8	6.4	5.9	6.125
	Control #1	6.7	6.3	6.1	5.4	6.125
Cycle 37	Control #2	6.1	6.3	6	6.4	6.2
	Control #3	6.5	6.5	6.4	6.1	6.375
	Control #1	6.2	6.2	5.9	6.1	6.1
Cycle 38	Control #2	6.4	6.1	6.1	5.8	6.1
	Control #3	6	6.3	6.1	6.2	6.15
Cycle 39	Control #1	6.1	5.9	5.9	5.6	5.875

	Control #2	5.4	5.1	6	6.2	5.675
	Control #3	6.4	6.4	6.2	6.1	6.275
Cycle 40	Control #1	5.8	6.2	5.7	5.4	5.775
	Control #2	6.1	5.7	5.8	5.9	5.875
	Control #3	6.1	6.4	6.4	6.3	6.3

Appendix C - Surface Resistivity Results – w/c 0.45, Sample #1-#27, #31-#36

Surface resistivity – w/c 0.45 (kOhm/cm)						
	Sample #	0°	90°	270°	360°	Average
Cycle 0	#01	10	10.2	11	11.2	10.6
	#02	10.7	12	11.1	11.8	11.4
	#03	11.4	11.4	12	12.3	11.775
Cycle 05	#04	12.8	13.5	12.5	12.1	12.725
	#05	13.3	13.1	12	12.3	12.675
	#06	11.6	12	11.4	12.6	11.9
Cycle 10	#07	12	11.4	11.7	12.9	12
	#08	11.3	11	12.5	11.5	11.575
	#09	11.7	12.3	11.7	11.3	11.75
Cycle 15	#10	11.2	11.8	12.5	11.4	11.725
	#11	12.1	11.7	11.8	11.7	11.825
	#12	13.5	13.1	12.7	12.8	13.025
Cycle 20	#13	12.2	13	12.3	12.7	12.55
	#14	12.2	13	12.3	13.3	12.7
	#15	11.8	11.4	10.6	11	11.2
Cycle 30	#16	12.8	12.2	11.8	11.8	12.15
	#17	12.5	12.4	11.4	11	11.825
	#18	12	10.3	11.4	11.4	11.275
Cycle 40	#19	13.1	13.5	12.2	11.8	12.65
	#20	12.2	13.1	12.6	11.5	12.35
	#21	12.1	12.3	12.6	11.7	12.175
Cycle 50	#22	12.9	11.5	12.7	13	12.525
	#23	12.7	11.6	10.9	11.8	11.75
	#24	12.4	13.2	11.9	13.4	12.725
Cycle 60	#25	10.8	12	11.9	11.9	11.65
	#26	12.1	13.7	13.1	12	12.725
	#27	12	12.3	11.4	12.4	12.025
Cycle 70	#31	11.7	12.2	11.5	11.3	11.675
	#32	12.4	12	13.1	12	12.375
	#33	11.7	11.3	11.6	11.4	11.5
Cycle 80	#34	11.4	12.2	12.9	12	12.125
	#35	12.7	11.6	11.2	11.7	11.8
	#36	12.4	11.3	11.6	11.7	11.75

Appendix D - Surface Resistivity Results – w/c 0.45, Control Samples

Surface resistivity – w/c 0.45 (kOhm/cm)						
	Sample #	0	90	270	360	Average
Cycle 0	Control #1	12.6	11.3	11.6	12.4	11.975
	Control #2	11.4	10.7	13.1	12.3	11.875
	Control #3	12	10.9	11.8	12.3	11.75
Cycle 01	Control #1	11.2	10	10.5	10.9	10.65
	Control #2	12	11.5	10.6	11.8	11.475
	Control #3	10.3	9.6	10.3	10.9	10.275
Cycle 02	Control #1	11.9	12.3	13	12.9	12.525
	Control #2	12	11.4	14	13.1	12.625
	Control #3	11.3	12.3	12.6	12.1	12.075
Cycle 03	Control #1	13.6	13.6	13	12.4	13.15
	Control #2	13.8	12.7	11.9	14	13.1
	Control #3	12.7	11.8	12.6	12.7	12.45
Cycle 04	Control #1	14	12.6	12.7	13.6	13.225
	Control #2	13	12	14.7	13.6	13.325
	Control #3	12.7	12.9	12.7	12	12.575
Cycle 05	Control #1	12.4	12.9	13.2	12.2	12.675
	Control #2	12.5	11.7	13.9	13.3	12.85
	Control #3	12.4	13.1	12.5	11.6	12.4
Cycle 06	Control #1	13.6	13.9	12.7	12.7	13.225
	Control #2	11.7	14.5	14	13	13.3
	Control #3	13.1	13.5	13.4	11.5	12.875
Cycle 07	Control #1	11.8	12.8	11.6	12.1	12.075
	Control #2	12	11.4	13.6	12.9	12.475
	Control #3	11.4	12.3	11.4	12.1	11.8
Cycle 08	Control #1	14.5	12.8	13	13.9	13.55
	Control #2	13.8	12.6	11.7	14.3	13.1
	Control #3	11.7	12.7	13	12.7	12.525
Cycle 09	Control #1	13.8	14.1	12.9	12.8	13.4
	Control #2	15.1	14.2	13.3	12.2	13.7
	Control #3	11.4	12.9	13.5	13	12.7
Cycle 10	Control #1	12.3	12.5	11.5	11.5	11.95
	Control #2	11.6	10.8	13.2	12.5	12.025
	Control #3	10.6	11.7	11.9	11.7	11.475
Cycle 11	Control #1	13.6	13.8	12.3	12.8	13.125
	Control #2	13.1	12	14.4	14.3	13.45
	Control #3	13.1	12.3	12.7	13.1	12.8

Cycle 12	Control #1	14.1	14.3	12.9	13.9	13.8
	Control #2	15.9	15.3	14	13.3	14.625
	Control #3	12.4	13.1	13.6	13.6	13.175
Cycle 13	Control #1	13.6	13.9	12.4	12.7	13.15
	Control #2	12.5	14.7	13.9	13	13.525
	Control #3	12	12.5	12.7	12.6	12.45
Cycle 14	Control #1	13	13.7	14.3	14.6	13.9
	Control #2	12.7	15.4	15.1	13.6	14.2
	Control #3	13.3	13.1	12.3	12.8	12.875
Cycle 15	Control #1	13	13.8	13.6	13	13.35
	Control #2	13.3	12.3	11.5	14.2	12.825
	Control #3	11.7	12.7	12.9	12.6	12.475
Cycle 16	Control #1	13.3	12	12.6	13.3	12.8
	Control #2	14	13.5	12.8	11.7	13
	Control #3	13.2	13.1	12.7	11.7	12.675
Cycle 17	Control #1	13	12	12.1	13	12.525
	Control #2	11.1	13.6	13	12	12.425
	Control #3	11.4	12.5	13	12.4	12.325
Cycle 18	Control #1	14	14.4	12.4	13.2	13.5
	Control #2	12.6	15.3	14.3	13.3	13.875
	Control #3	12	12.7	13.2	12.9	12.7
Cycle 19	Control #1	12.3	13.4	13.5	12.5	12.925
	Control #2	12.3	11.4	13.5	13	12.55
	Control #3	12	12.1	11.2	12.2	11.875
Cycle 20	Control #1	13	12	12.7	12.9	12.65
	Control #2	13.4	12.8	11.7	11.1	12.25
	Control #3	11	11.9	12	11.9	11.7
Cycle 21	Control #1	13	13.8	13.9	12.7	13.35
	Control #2	13.9	13	12.3	11.5	12.675
	Control #3	12.6	11.5	12.2	12.6	12.225
Cycle 22	Control #1	12.7	13.6	13.7	12.4	13.1
	Control #2	11.7	14.4	13.7	12.7	13.125
	Control #3	12.8	12.8	12.7	11.7	12.5
Cycle 23	Control #1	11.7	12.1	12.7	13	12.375
	Control #2	11.8	11	13.4	12.7	12.225
	Control #3	12.7	12.3	11.5	12.3	12.2
Cycle 24	Control #1	12.7	13	11.7	12.1	12.375
	Control #2	13.8	13.3	11.6	11.3	12.5
	Control #3	11.9	12	11.7	10.9	11.625
Cycle 25	Control #1	13.5	12.2	12.3	13.2	12.8
	Control #2	11.2	13.8	13.1	12.1	12.55

	Control #3	12.3	11.2	12.1	12.6	12.05
Cycle 26	Control #1	12.3	12.7	13.2	12.1	12.575
	Control #2	12.2	11.2	13.7	13	12.525
	Control #3	12.3	12.2	11.1	12.1	11.925
Cycle 27	Control #1	12.8	13.5	13.8	12.5	13.15
	Control #2	14.9	13.5	12.7	11.9	13.25
	Control #3	12	13.2	13.3	13	12.875
Cycle 28	Control #1	13.2	11.8	12	13	12.5
	Control #2	13.6	13.3	12.3	11.4	12.65
	Control #3	12.3	11.4	12.7	12.7	12.275
Cycle 29	Control #1	12.1	12.7	13.2	13.6	12.9
	Control #2	12.7	11.5	14.1	13.2	12.875
	Control #3	11.9	13	13.6	13.1	12.9
Cycle 30	Control #1	13	11.7	12.1	12.7	12.375
	Control #2	13	12	11	13.6	12.4
	Control #3	12.3	11.4	12.3	12.8	12.2
Cycle 31	Control #1	13.3	14.1	14	12.9	13.575
	Control #2	12.9	12	14.8	13.9	13.4
	Control #3	13	11.4	13	13.5	12.725
Cycle 32	Control #1	12.1	12.3	12.9	13.1	12.6
	Control #2	14.6	13.6	12.5	11.7	13.1
	Control #3	13.1	12.8	11.9	12.9	12.675
Cycle 33	Control #1	12.6	11.4	11.7	12.1	11.95
	Control #2	11.1	13.6	12.8	11.9	12.35
	Control #3	11.5	12.3	12.7	12.2	12.175
Cycle 34	Control #1	12.1	12.8	13	12	12.475
	Control #2	12.9	11.7	14.4	13.9	13.225
	Control #3	12.8	12.7	12.6	11.8	12.475
Cycle 35	Control #1	12.5	13.3	13.4	12.3	12.875
	Control #2	12.3	14.6	13.9	12.9	13.425
	Control #3	13.2	13.6	13.1	12.3	13.05
Cycle 36	Control #1	11.9	12.2	13	13.2	12.575
	Control #2	11.8	14.5	13.6	12.7	13.15
	Control #3	12	12.8	12.3	12.8	12.475
Cycle 37	Control #1	12.2	12.4	13.2	13.6	12.85
	Control #2	13.3	12.3	11.4	13.9	12.725
	Control #3	12.3	12.8	12.4	11.4	12.225
Cycle 38	Control #1	12.7	12.9	11.8	12	12.35
	Control #2	12.1	14.3	13.6	12.8	13.2
	Control #3	11	11.9	12.2	12	11.775
Cycle 39	Control #1	12.3	13	13.3	12	12.65

	Control #2	11	13.4	12.8	11.8	12.25
	Control #3	12.5	12.3	11.3	12.1	12.05
Cycle 40	Control #1	12.1	12	12.7	13	12.45
	Control #2	12.8	11.7	14.3	13.3	13.025
	Control #3	12.3	12.6	12.4	11.4	12.175
Cycle 45	Control #1	13.4	12.2	12.4	13.3	12.825
	Control #2	13.9	13.4	12.7	11.7	12.925
	Control #3	14.1	13.3	13.3	14	13.675
Cycle 50	Control #1	13.4	12.2	12.4	13.3	12.825
	Control #2	13.3	12.9	11.7	11	12.225
	Control #3	11.9	11.1	12	12.3	11.825
Cycle 55	Control #1	12	12.7	12.8	11.7	12.3
	Control #2	11	13.6	12.9	12	12.375
	Control #3	12.3	11.4	12.1	11.6	11.85
Cycle 60	Control #1	11.8	11.9	12.7	12.7	12.275
	Control #2	12.1	11.3	13.7	13.1	12.55
	Control #3	11.5	12.2	11.6	12.3	11.9
Cycle 65	Control #1	12.9	11.6	11.7	12.3	12.125
	Control #2	11.4	10.9	13.4	12.6	12.075
	Control #3	11.4	12	12.3	12.1	11.95
Cycle 70	Control #1	11.9	12.8	12.5	11.7	12.225
	Control #2	10.6	13.2	12.3	11.4	11.875
	Control #3	11.7	12.7	12.5	12.3	12.3
Cycle 75	Control #1	12.5	12.9	12.2	12.3	12.475
	Control #2	10.9	13.1	13	11.6	12.15
	Control #3	11.2	12.3	12.2	11.9	11.9
Cycle 80	Control #1	11.9	12.7	12.7	11.7	12.25
	Control #2	11.7	10.9	13.1	12.3	12
	Control #3	11.8	11.1	12.5	12.4	11.95

Appendix E - Bulk Resistivity Results – w/c 0.65, Control Samples

Bulk resistivity – w/c 0.65 (kOhm/cm)						
Cycle#	Control#1 Measured	Control#2 Measured	Control#3 Measured	Control#1 Calculated	Control#2 Calculated	Control#3 Calculated
0	27.7	27.8	28.9	4.90	4.91	5.19
1	22.2	24.9	25.2	3.93	4.40	4.53
2	23.3	23.3	25.5	4.13	4.11	4.58
3	24.9	24.7	26.7	4.41	4.36	4.80
4	26.7	27.5	28.1	4.73	4.85	5.05
5	21.9	22.9	23.9	3.88	4.04	4.29
6	28.6	29	28.5	5.06	5.12	5.12
7	24.6	27.3	28	4.36	4.82	5.03
8	25.5	26	28.6	4.52	4.59	5.14
9	25.6	25.9	28.4	4.53	4.57	5.10
10	24.5	24.6	26.7	4.34	4.34	4.80
11	27.5	27.9	30.6	4.87	4.93	5.50
12	26.6	26	29	4.71	4.59	5.21
13	24.8	25.9	29	4.39	4.57	5.21
14	26.6	25.2	29.8	4.71	4.45	5.35
15	23.9	24.6	27.8	4.23	4.34	4.99
16	24.2	26.1	27.3	4.28	4.61	4.90
17	25.2	24.2	28.8	4.46	4.27	5.17
18	27.7	25.7	30.3	4.90	4.54	5.44
19	23.7	23.8	25.1	4.20	4.20	4.51
20	23.5	22.1	25.2	4.16	3.90	4.53
21	22.8	23.5	25.6	4.04	4.15	4.60
22	23.2	22.2	25.7	4.11	3.92	4.62
23	24.7	21.6	25.6	4.37	3.81	4.60
24	24.2	23.3	25.7	4.28	4.11	4.62
25	23.7	22.5	26.3	4.20	3.97	4.72
26	21.4	21.7	25.2	3.79	3.83	4.53
27	22.8	22.6	26.9	4.04	3.99	4.83
28	23.8	22.8	25	4.21	4.03	4.49
29	24.2	23	27.5	4.28	4.06	4.94
30	23.3	21.9	24.7	4.13	3.87	4.44
31	22	22.1	25.6	3.90	3.90	4.60
32	25.4	23	25	4.50	4.06	4.49
33	22.8	22	23.8	4.04	3.88	4.27
34	23.9	21.5	25.1	4.23	3.80	4.51
35	23.6	22.1	27.4	4.18	3.90	4.92

36	22.5	21.3	24.8	3.98	3.76	4.45
37	24.4	22.4	25.9	4.32	3.95	4.65
38	24.3	21.5	25	4.30	3.80	4.49
39	22.5	22.8	24.9	3.98	4.03	4.47
40	22.2	22.2	25.3	3.93	3.92	4.54

Appendix F - Bulk Resistivity Results – w/c 0.65, Sample #1-#27

Bulk resistivity – w/c 0.65 (kOhm/cm)						
	Sample #	Upper foan	Lower foam and cylinder	Cylinder & foams	NET	Calculated
Cycle 0	#01	4.4	1.5	34.8	28.9	5.17
	#02	4.6	1.8	34.2	27.8	4.99
	#03	5.8	1.5	36.2	28.9	5.19
Cycle 05	#04	4.9	1.3	30.3	24.1	4.53
	#05	4.5	1.2	27.6	21.9	3.87
	#06	5.1	1.3	30.6	24.2	4.20
Cycle 10	#07	4.5	1.3	27.7	21.9	3.86
	#08	4.3	1.6	32.2	26.3	4.53
	#09	5.1	1.4	27	20.5	3.54
Cycle 15	#10	5.3	1.6	31.3	24.4	4.18
	#11	5	1.2	29.1	22.9	4.05
	#12	4.6	1.3	28.3	22.4	4.00
Cycle 20	#13	5.2	1	26	19.8	3.52
	#14	4.2	1.5	30	24.3	4.31
	#15	4.8	1.4	22	15.8	2.81
Cycle 25	#16	3.8	1.5	22.5	17.2	2.95
	#17	3.3	1.3	23.2	18.6	3.19
	#18	4.8	1.3	29.6	23.5	3.99
Cycle 30	#19	4.2	1.6	24.7	18.9	3.24
	#20	4.1	1.4	30.6	25.1	4.25
	#21	4.7	1.7	25.4	19	3.66
Cycle 35	#22	3.2	1	19	14.8	2.70
	#23	4.3	1.4	30	24.3	4.52
	#24	3.8	1.4	22.1	16.9	3.00
Cycle 40	#25	3.1	1.4	24.6	20.1	3.52
	#26	2.6	1.2	24.9	21.1	3.79
	#27	2.3	1.1	16.1	12.7	2.32

Appendix G - Bulk Resistivity Results – w/c 0.45, Control Samples

Bulk resistivity – w/c 0.45 (kOhm/cm)						
Cycle#	Control#1 Measured	Control#2 Measured	Control#3 Measured	Control#1 Calculated	Control#2 Calculated	Control#3 Calculated
0	45.6	47.3	47.9	7.78	8.11	8.36
1	42	42.7	42.4	7.16	7.32	7.40
2	47.1	46.4	47.7	8.03	7.96	8.33
3	50.9	47.9	50.4	8.68	8.21	8.80
4	50.8	50.9	52.8	8.66	8.73	9.22
5	47.1	47.8	48	8.03	8.20	8.38
6	50.1	51.4	53	8.54	8.81	9.25
7	49.3	50	51.6	8.41	8.57	9.01
8	51.7	50	54.5	8.82	8.57	9.52
9	54	54.2	58.4	9.21	9.29	10.20
10	49.1	48.2	49.8	8.37	8.26	8.69
11	52.5	53	54.5	8.95	9.09	9.52
12	53	54.4	56.6	9.04	9.33	9.88
13	53.5	54.1	57.4	9.12	9.28	10.02
14	54.2	55	55.7	9.24	9.43	9.72
15	53.9	54.7	55.4	9.19	9.38	9.67
16	52.1	51.1	53.5	8.88	8.76	9.34
17	53.9	53.4	57.4	9.19	9.16	10.02
18	54.6	56.8	61.1	9.31	9.74	10.67
19	53.4	53.9	58.3	9.11	9.24	10.18
20	49.9	50.8	54.6	8.51	8.71	9.53
21	50.8	50.6	48.6	8.66	8.68	8.49
22	51.8	51.8	54.2	8.83	8.88	9.46
23	50.1	50.9	55.4	8.54	8.73	9.67
24	50.3	49.8	51.9	8.58	8.54	9.06
25	51.6	51	55.2	8.80	8.74	9.64
26	50.5	52	54.8	8.61	8.92	9.57
27	52.8	55	57.2	9.00	9.43	9.99
28	52.2	52.5	56.6	8.90	9.00	9.88
29	54.4	52.5	60.4	9.28	9.00	10.55
30	50.8	52.2	54.8	8.66	8.95	9.57
31	52.4	52.4	56.6	8.94	8.98	9.88
32	51.1	54.6	58.5	8.71	9.36	10.21
33	50.5	50.3	57	8.61	8.62	9.95
34	50.2	54.4	58.3	8.56	9.33	10.18

35	51	54.8	60.6	8.70	9.40	10.58
36	53.1	52.7	56.7	9.05	9.04	9.90
37	53.6	53.1	58	9.14	9.10	10.13
38	53.9	55.7	57.6	9.19	9.55	10.06
39	53.5	53.3	57.7	9.12	9.14	10.07
40	53	54.9	58.2	9.04	9.41	10.16
45	53.2	56.5	65.7	9.07	9.69	11.47
50	56	56.6	60.3	9.55	9.71	10.53
55	57	57.9	62.5	9.72	9.93	10.91
60	55.1	58.1	58.9	9.40	9.96	10.28
65	57.2	59.3	60.9	9.75	10.17	10.63
70	59.8	58.6	62.9	10.20	10.05	10.98
75	60.9	61.5	64.6	10.38	10.55	11.28
80	60.9	63.2	68.8	10.38	10.84	12.01

Appendix H - Bulk Resistivity Results – w/c 0.45, Sample #1-#27, #31-#36

Bulk resistivity – w/c 0.45 (kOhm/cm)						
	Sample #	Upper foam	Lower foam & cylinder	Cylinder & foams	NET	Calculated
Cycle 0	#01	4.5	1.4	53.8	47.9	7.99
	#02	4.5	1.5	52.3	46.3	7.96
	#03	4.5	1.2	57.9	52.2	8.70
Cycle 05	#04	4.1	1.1	50.3	45.1	7.72
	#05	5.6	1.3	55.3	48.4	8.29
	#06	4.4	1.1	50.9	45.4	7.84
Cycle 10	#07	5.1	1.3	52.7	46.3	7.96
	#08	5.2	1.3	54.1	47.6	8.17
	#09	5.3	1.5	56.5	49.7	8.28
Cycle 15	#10	5.8	1.2	56.7	49.7	8.57
	#11	5.1	1.3	55.4	49	8.48
	#12	4.3	1	59.9	54.6	9.05
Cycle 20	#13	5.3	1.4	54.3	47.6	8.17
	#14	5.1	1.5	55.5	48.9	8.07
	#15	5.8	1.6	51.1	43.7	7.54
Cycle 30	#16	3.8	1.2	51.5	46.5	8.07
	#17	3.3	1.4	50.3	45.6	7.80
	#18	3.3	1.3	49.1	44.5	7.65
Cycle 40	#19	2.6	1.3	57	53.1	9.14
	#20	3	1.2	53.1	48.9	8.42
	#21	3	1	56.1	52.1	9.00
Cycle 50	#22	1.7	1	67.8	65.1	10.80
	#23	1.9	1.3	61.3	58.1	9.92
	#24	2.6	1.1	60.4	56.7	9.74
Cycle 60	#25	1.9	1.1	60.6	57.6	9.97
	#26	2.7	1	63.2	59.5	10.20
	#27	2.6	1	60.5	56.9	9.81
Cycle 70	#31	2.1	0	64.1	62	10.37
	#32	3.1	0	59.9	56.8	9.57
	#33	2.5	0	61.6	59.1	10.25
Cycle 80	#34	2.6	0	66.4	63.8	10.78
	#35	2.4	0	69.3	66.9	11.50
	#36	3.1	0	66.1	63	10.83

Appendix I - UPV Results – w/c 0.65, Control Samples

UPV- w/c 0.65 (m/s)						
Cycle#	Control#1 Measured	Control#2 Measured	Control#3 Measured	Control#1 Calculated	Control#2 Calculated	Control#3 Calculated
0	44.53	46.10	44.07	4373.13	4240.78	4368.38
1	46.40	48.47	45.87	4197.20	4033.70	4196.95
2	46.10	47.87	46.23	4224.51	4084.26	4163.66
3	46.37	47.83	46.13	4200.22	4087.11	4172.69
4	45.87	47.50	44.93	4246.00	4115.79	4284.12
5	46.30	47.53	45.90	4206.26	4112.90	4193.90
6	47.07	48.10	46.77	4137.75	4064.45	4116.18
7	47.00	48.33	47.00	4143.62	4044.83	4095.74
8	46.70	48.40	45.37	4170.24	4039.26	4243.20
9	46.60	47.63	46.17	4179.18	4104.27	4169.68
10	45.97	47.40	46.80	4236.77	4124.47	4113.25
11	45.30	47.30	45.43	4299.12	4133.19	4236.98
12	45.67	47.13	45.90	4264.60	4147.81	4193.90
13	47.23	48.37	46.77	4123.15	4042.04	4116.18
14	45.80	46.90	45.53	4252.18	4168.44	4227.67
15	46.67	48.07	46.93	4173.21	4067.27	4101.56
16	45.57	46.93	45.53	4273.96	4165.48	4227.67
17	47.10	48.00	46.83	4134.82	4072.92	4110.32
18	45.83	47.80	46.23	4249.09	4089.96	4163.66
19	46.23	47.60	46.60	4212.33	4107.14	4130.90
20	45.93	47.30	46.47	4239.84	4133.19	4142.75
21	46.67	48.10	46.90	4173.21	4064.45	4104.48
22	47.33	49.00	47.53	4114.44	3989.80	4049.79
23	47.17	48.80	47.70	4128.98	4006.15	4035.64
24	47.37	48.60	47.13	4111.54	4022.63	4084.16
25	47.73	49.53	48.27	4079.96	3946.84	3988.26
26	47.00	48.83	47.90	4143.62	4003.41	4018.79
27	47.33	48.90	48.30	4114.44	3997.96	3985.51
28	48.17	49.97	50.00	4043.25	3912.61	3850.00
29	47.80	48.90	48.63	4074.27	3997.96	3958.19
30	48.57	49.83	50.13	4009.95	3923.08	3839.76
31	48.40	50.33	50.53	4023.76	3884.11	3809.37
32	48.40	49.63	50.60	4023.76	3938.89	3804.35
33	48.67	50.10	51.13	4001.71	3902.20	3764.67
34	48.63	50.07	50.90	4004.46	3904.79	3781.93

35	49.00	51.17	52.47	3974.49	3820.85	3669.00
36	49.73	50.77	52.97	3915.88	3850.95	3634.36
37	49.40	50.67	52.00	3942.31	3858.55	3701.92
38	49.53	50.77	53.07	3931.70	3850.95	3627.51
39	50.97	52.10	54.73	3821.12	3752.40	3517.05
40	51.67	52.33	54.43	3769.35	3735.67	3536.44

Appendix J - UPV Results – w/c 0.65, Sample #1-#27, #31-#36

UPV- w/c 0.65 (m/s)					
	Sample #	Measurement 1	Measurement 2	Measurement 3	Calculated average
Cycle 0	#01	44.8	44.7	44.7	4314.46
	#02	44	43.7	43.3	4396.95
	#03	44	44.2	44.1	4376.42
Cycle 05	#04	46.1	46.1	46.4	3998.92
	#05	46.4	45.9	45.8	4236.06
	#06	46.2	45.9	45.9	4157.61
Cycle 10	#07	44.4	44.4	44.4	4228.60
	#08	45.5	45.5	46	4204.38
	#09	45.9	46.2	46.3	4151.01
Cycle 15	#10	47.6	47.7	48.1	4037.66
	#11	49	49	48.5	3993.17
	#12	51.2	51.2	52.1	3747.57
Cycle 20	#13	50.5	49.7	49.7	3877.59
	#14	47.4	47.3	47.2	4117.34
	#15	59.7	60.5	60.6	3231.47
Cycle 25	#16	60	59.8	59.9	3238.73
	#17	64	66.9	64	2970.75
	#18	51.1	50.8	51	3826.03
Cycle 30	#19	61.7	62.2	63.1	3112.30
	#20	55.7	55.2	55	3535.26
	#21	60.8	59.7	60.2	2963.48
Cycle 35	#22	72.8	73.5	74.7	2582.58
	#23	44.1	44.1	44.1	4223.36
	#24	64.3	63.8	65.7	3018.58
Cycle 40	#25	75	77.5	77	2571.90
	#26	49.9	49.6	49.9	3875.50
	#27	64.9	63.7	64.9	2934.11

Appendix K - UPV Results – w/c 0.45, Control Samples

UPV- w/c 0.45 (m/s)						
Cycle#	Control#1 Measured	Control#2 Measured	Control#3 Measured	Control#1 Calculated	Control#2 Calculated	Control#3 Calculated
0	46.87	46.80	47.10	4304.77	4321.58	4219.75
1	48.27	48.10	47.87	4179.90	4204.78	4152.16
2	48.50	49.10	48.03	4159.79	4119.14	4137.75
3	48.70	48.63	48.80	4142.71	4158.67	4072.75
4	49.03	49.73	49.20	4114.55	4066.69	4039.63
5	49.23	49.27	49.20	4097.83	4105.21	4039.63
6	48.77	48.77	49.10	4137.05	4147.30	4047.86
7	49.60	49.60	49.17	4067.54	4077.62	4042.37
8	49.10	48.90	49.17	4108.96	4135.99	4042.37
9	48.63	48.17	48.27	4148.39	4198.96	4117.75
10	48.67	48.93	48.37	4145.55	4133.17	4109.24
11	48.27	48.13	48.60	4179.90	4201.87	4089.51
12	48.43	48.97	48.43	4165.52	4130.36	4103.58
13	49.27	50.10	49.80	4095.06	4036.93	3990.96
14	47.97	47.83	47.73	4206.05	4228.22	4163.76
15	49.07	48.97	48.63	4111.75	4130.36	4086.70
16	47.60	48.00	47.80	4238.45	4213.54	4157.95
17	49.07	48.60	48.40	4111.75	4161.52	4106.40
18	47.97	48.03	48.17	4206.05	4210.62	4126.30
19	47.83	47.57	47.60	4217.77	4251.93	4175.42
20	47.90	47.33	47.57	4211.90	4272.89	4178.35
21	48.03	47.90	48.27	4200.21	4222.34	4117.75
22	47.93	48.80	48.50	4208.97	4144.47	4097.94
23	47.53	47.67	47.83	4244.39	4243.01	4155.05
24	48.27	47.90	47.93	4179.90	4222.34	4146.38
25	47.70	47.97	47.83	4229.56	4216.47	4155.05
26	47.70	47.17	47.33	4229.56	4287.99	4198.94
27	47.53	47.73	47.20	4244.39	4237.08	4210.81
28	47.70	47.60	47.57	4229.56	4248.95	4178.35
29	47.33	47.03	46.87	4262.32	4300.14	4240.75
30	48.37	48.03	48.00	4171.26	4210.62	4140.63
31	47.93	47.70	49.07	4208.97	4240.04	4050.61
32	48.07	48.03	47.67	4197.30	4210.62	4169.58
33	47.87	47.83	47.87	4214.83	4228.22	4152.16
34	47.47	47.33	46.97	4250.35	4272.89	4231.72

35	47.70	48.00	47.73	4229.56	4213.54	4163.76
36	48.17	47.73	47.47	4188.58	4237.08	4187.15
37	48.07	47.43	48.00	4197.30	4263.88	4140.63
38	47.53	47.10	47.17	4244.39	4294.06	4213.78
39	47.93	47.87	47.47	4208.97	4225.28	4187.15
40	47.97	47.93	47.87	4206.05	4219.40	4152.16
45	48.03	47.93	47.87	4200.21	4219.40	4152.16
50	48.13	48.17	47.77	4191.48	4198.96	4160.85
55	48.17	48.03	47.87	4188.58	4210.62	4152.16
60	48.20	48.77	48.17	4185.68	4147.30	4126.30
65	47.83	47.83	47.17	4217.77	4228.22	4213.78
70	47.73	47.20	46.87	4226.61	4284.96	4240.75
75	47.40	47.63	47.27	4256.33	4245.98	4204.87
80	47.13	47.07	46.97	4280.41	4297.10	4231.72

Appendix L - UPV Results – w/c 0.45, Samples #1-#27, #31-#36

	Sample #	Measurement 1	Measurement 2	Measurement 3	Calculated average
Cycle 0	#01	47	46.7	46.9	4246.09
	#02	46.6	46.9	46.6	4304.07
	#03	46.7	47.3	46.9	4242.37
Cycle 05	#04	48.9	48.9	48.9	4115.54
	#05	48.2	48	48.1	4158.00
	#06	49.5	49.1	49	4059.96
Cycle 10	#07	48.4	48.4	48.3	4155.75
	#08	48	47.9	48.3	4181.69
	#09	47.2	47.2	47.3	4223.71
Cycle 15	#10	49	49	49.2	4096.47
	#11	49.6	49.8	50.1	4018.39
	#12	48.2	48.6	48.3	4135.08
Cycle 20	#13	48.1	47.8	48.3	4181.69
	#14	46.9	47.1	46.9	4268.99
	#15	48.5	48.1	48.1	4162.06
Cycle 30	#16	47.2	47.1	47.7	4198.94
	#17	48.8	48.2	48.2	4183.88
	#18	49.3	49.6	49.6	4055.56
Cycle 40	#19	48.4	48.3	48.4	4171.26
	#20	47.9	47.9	47.7	4186.41
	#21	46.7	46.6	46.4	4289.55
Cycle 50	#22	49.1	48.6	48.1	4125.51
	#23	48.9	48.5	48.3	4159.23
	#24	48.8	48.5	48.2	4154.64
Cycle 60	#25	47.8	47.7	47.2	4183.60
	#26	49	49.1	48.6	4105.32
	#27	49	48.9	48.6	4131.40
Cycle 70	#31	46.5	46.8	46.8	4245.18
	#32	45.4	45.4	45.6	4321.85
	#33	47.1	47.1	47.2	4216.76
Cycle 80	#34	45.4	45.5	45.5	4338.34
	#35	46.6	46.8	46.7	4320.13
	#36	46.9	46.9	46.8	4304.77

Appendix M - Pressure Tension Test Results– w/c 0.65

Cycle #	Sample #	Strength (Mpa)	Average (Mpa)
Cycle 0	1	4.000291	4.5765123
	2	5.714385	
	3	4.014861	
Cycle 05	4	1.999911 (BAD DATA)	4.123497
	5	4.123497	
	6	1.459808 (BAD DATA)	
Cycle 10	7	5.467313	3.553363
	8	3.001593	
	9	2.191183	
Cycle 15	10	N/A	2.363957
	11	2.40554	
	12	2.322374	
Cycle 20	13	1.8103155	1.3629387
	14	N/A	
	15	0.9155619	
Cycle 25	16	0.98364	1.0446723
	17	1.12051	
	18	1.029867	
Cycle 30	19	1.674314	1.170044
	20	0.81599	
	21	1.019828	
Cycle 35	22	0.743083	0.9223727
	23	1.305733	
	24	0.718302	
Cycle 40	25	0.456869	0.7053813
	26	0.7349	
	27	0.924375	

Appendix N - Pressure Tension Test Results– w/c 0.45

Cycle #	Sample #	Strength (Mpa)	Average (Mpa)
Cycle 0	1	4.51691	4.179613
	2	4.068905	
	3	3.953024	
Cycle 05	4	4.879714	5.035915
	5	5.192116	
	6	0.741776 (BAD DATA)	
Cycle 10	7	5.467313	5.487558
	8	5.507803	
	9	N/A	
Cycle 15	10	5.042412	5.5499895
	11	N/A	
	12	6.057567	
Cycle 20	13	5.42453	5.534079
	14	6.220217	
	15	4.95749	
Cycle 30	16	5.57721	5.860544
	17	5.407488	
	18	6.596934	
Cycle 40	19	6.808085	5.43497333
	20	5.667506	
	21	3.829329	
Cycle 50	22	6.249140741	6.329
	23	6.669169464	
	24	6.067629313	
Cycle 60	25	7.118287176	6.567
	26	6.589479839	
	27	5.994489709	
Cycle 70	31	2.50093	4.17217333
	32	3.50916	
	33	6.50643	
Cycle 80	34	3.78852	5.35997245
	35	7.014727895	
	36	5.276669445	

Appendix O - Surface Resistivity – Temperature (w/c 0.65)

ALT01-0.65

core tem	Surface temerature (°C)			average	Surface resistivity (kOhm/cm)			average
1.9	3.8	4.1	4.1	4.025	8.2	8.3	8.1	7.825
5.7	7.8	7.8	7.8	7.8	7.1	7.2	7.1	6.85
8.3	10.2	10.6	10.3	10.375	6.5	6.7	6.5	6.3
10.5	12.4	12.5	12.4	12.45	6.1	6.3	6.1	5.9
12.1	14.3	14.3	14.3	14.3	5.9	5.9	5.7	5.6
14.6	16.7	16.7	16.7	16.65	5.5	5.6	5.4	5.25
18.2	18.7	18.7	18.7	18.7	5.1	5.2	5	4.9
20.3	21.8	21.7	21.8	21.6	4.8	4.9	4.7	4.6
22.3	23.8	23.7	23.7	23.5	4.5	4.7	4.5	4.375
25	26.3	26.2	26.3	26.1	4.3	4.4	4.2	4.125
27	28.6	28.3	28.2	28	4.1	4.2	4.1	3.95
29	30.1	30.1	30	29.8	3.9	3	3.9	3.525

ALT02-0.65

core tem	Surface temerature (°C)			average	Surface resistivity (kOhm/cm)			average
0.8	2.4	2.5	2.5	2.45	8.3	7.6	8	7.975
2.8	4.8	4.8	4.8	4.8	7.7	7.1	7.5	7.425
5.1	7.5	7.5	7.6	7.525	7	6.5	6.9	6.8
7.1	10	10	10	10.05	6.5	6	6.3	6.275
9.1	12.1	12.2	12.2	12.175	6.1	5.7	6	5.925
11.3	14.6	14.5	14.5	14.5	5.7	5.3	5.6	5.525
13.4	16.5	16.4	16.6	16.475	5.4	5	5.2	5.2
15.4	19.2	19.3	19.2	19.2	5.1	4.7	4.9	4.9
17.7	22	21.9	21.7	21.8	4.7	4.4	4.5	4.55
20.1	24.2	23.8	23.7	23.825	4.5	4.2	4.4	4.35
22.1	27.6	27.5	27.4	27.45	4.2	3.9	4.1	4.075
24.1	28.6	28.4	28.3	28.35	4.1	3.7	4	3.925
26.7	30.3	30.1	29.8	30	3.9	3.7	3.8	3.775
28.8	31.6	31.8	31.7	31.675	3.7	3.5	3.7	3.625

AGT01-0.65

water tem	Surface temerature (°C)			average	Surface resistivity (kOhm/cm)			average
3	2.9	2.3	2.1	2.425	8.1	9.5	9.1	8.8
5	4.9	4.7	5.6	5.05	7.7	9	8.5	8.35
7	6.8	6.8	7	6.825	7.5	8.3	8	7.8
9	8.5	8.5	8.9	8.625	6.9	8	7.6	7.4
11	10.6	10.4	11.6	10.9	6.4	7.4	7.2	6.9
13.5	12.6	12.5	12.5	12.55	6	6.8	6.7	6.425
15.5	14.8	14.8	14.8	14.8	5.8	6.5	6.2	6.075
17.5	16.9	16.9	16.9	16.9	5.4	6.2	6	5.775
19.5	19	18.9	18.9	18.925	5	5.8	5.6	5.4
22	21.2	21.2	21.2	21.175	4.7	5.5	5.2	5.075
24	22.3	22.2	22.2	22.225	4.6	5.2	5	4.875
26	25.2	25.2	25	25.1	4.4	5	4.8	4.65
28.5	27.5	27.6	27.6	27.575	4.1	4.8	4.5	4.4
30	28.9	28.8	28.8	28.825	3.9	4.5	4.3	4.1
32	31.1	31.1	30.9	30.925	3.7	4.2	4	3.95

AGT02-0.65

water tem	Surface temerature (°C)			average	Surface resistivity (kOhm/cm)			average
2.5	2.6	2.6	2.6	2.625	9.1	8.5	9.6	8.9	9.025
5	5.2	5.1	5.3	5.35	8.4	7.9	8.9	8.5	8.425
7	7	6.9	7.1	6.975	8	7.5	8.4	7.9	7.95
9	9	9	9	9.025	7.6	7	7.9	7.5	7.5
11	10.9	10.6	10.6	10.675	7.2	6.7	7.5	7	7.1
13	12.6	12.5	12.9	12.675	6.7	6.3	7	6.6	6.65
15	15.3	15.2	15.2	15.175	6.2	5.9	6.5	6.2	6.2
17	17.2	16.9	17.1	17.075	5.8	5.6	6.2	5.8	5.85
19	19.2	19.2	19	19.025	5.6	5.3	5.8	5.6	5.575
21	21.1	20.8	20.7	20.825	5.3	5	5.6	5.3	5.3
23	23	22.7	22.7	22.775	5	4.7	5.3	5	5
25	25	24.9	24.9	25.025	4.8	4.5	5	4.7	4.75
27	26.8	26.8	26.7	26.625	4.6	4.3	4.8	4.5	4.55
29	28.6	28.7	28.7	28.625	4.4	4.1	4.6	4.4	4.375
31	30.8	30.7	30.4	30.6	4.3	3.9	4.4	4.1	4.175

NLT01-0.65

water tem	Surface temerature (°C)			average	Surface resistivity (kOhm/cm)			average
3	2.6	3.1	3	2.925	8	7.1	7.2	7.8	7.525
5.5	5.2	5.2	5.2	5.225	7.5	6.7	6.8	7.1	7.025
7.5	7.3	7.2	7.3	7.35	7	6.3	6.3	6.7	6.575
9	8.5	8.5	8.5	8.5	6.9	6	6.1	6.5	6.375
11	10.8	11	11	10.9	6	5.7	5.8	6.1	5.9
13	12.5	12.5	12.4	12.45	6.1	5.4	5.5	5.9	5.725
15	14.9	14.9	14.8	14.925	5.8	5.1	5.2	5.6	5.425
17	16.8	16.7	16.7	16.725	5.5	4.9	5	5.2	5.15
19	18.6	18.5	18.4	18.475	5.2	4.7	4.7	5	4.9
21.5	20.6	20.7	20.6	20.625	4.9	4.5	4.5	4.8	4.675
24	23	22.9	22.8	22.8	4.7	4.2	4.3	4.5	4.425
25.5	24.5	24.5	24.6	24.4	4.6	4	4.1	4.3	4.25
27.5	26.4	26.4	26.1	26.1	4.4	4	4.1	4.2	4.175
29.5	28.6	28.2	28.2	28	4.3	3.8	3.8	4.1	4
31.5	30.5	30.6	30.5	30.2	4	3.6	3.7	3.9	3.8

NLT02-0.65

water tem	Surface temerature (°C)			average	Surface resistivity (kOhm/cm)			average
2.5	2.6	2.6	2.7	2.65	8	8.1	8.2	7.8	8.025
4.5	4.5	4.5	4.3	4.45	7.6	7.7	7.8	7.6	7.675
6.5	6.5	6.3	6.7	6.625	7.3	7.2	7.4	7.2	7.275
8.5	8	8	8.8	8.35	6.7	6.9	6.9	6.8	6.825
10.5	10.5	10.3	10.6	10.425	6.2	6.3	6.5	6.3	6.325
13	12.8	12.3	12.5	12.55	6	6	6.2	6.1	6.075
15	14.8	14.8	14.7	14.75	5.6	5.7	5.7	5.6	5.65
17	16.9	16.8	16.8	16.825	5.4	5.4	5.5	5.5	5.45
19	18.4	18.2	18.2	18.25	5.1	5.2	5.3	5	5.15
21	20.9	20.9	20.7	20.75	4.8	4.9	4.9	4.9	4.875
23.5	22.8	23	22.8	22.725	4.6	4.7	4.7	4.5	4.625
25.5	24.9	24.9	24.4	24.65	4.4	4.5	4.4	4.4	4.425
27.5	26.8	26.9	26.5	26.675	4.2	4.2	4.4	4.3	4.275
29.5	28.7	28.9	27.6	28.2	4.1	4.1	4.1	3.9	4.05
31.5	30.7	30.6	29.3	30.225	3.9	4	4	3.9	3.95
32.5	31.2	31.4	30.8	31.05	3.8	3.9	3.9	3.7	3.825

NGT01-0.65

water tem	Surface temerature (°C)			average	Surface resistivity (kOhm/cm)			average
3	3.3	3.1	3	3.1	7.5	7.3	7.5	7.3	7.4
5	5.1	4.9	4.8	4.925	7.3	7	7.1	7	7.1
7	7.1	6.9	6.9	6.9	6.7	6.5	6.6	6.5	6.575
9	9	8.9	9.1	8.925	6.3	6.1	6.3	6.1	6.2
11	11	10.8	10.8	10.875	6	5.7	5.9	5.7	5.825
13	13	12.8	12.8	12.85	5.8	5.4	5.5	5.4	5.525
15	15.1	14.9	14.9	14.975	5.4	5.1	5.2	5.1	5.2
17	17	17	17	17	5	4.8	4.9	4.9	4.9
19	18.8	18.8	18.7	18.75	4.9	4.6	4.8	4.6	4.725
21	20.8	20.5	20.2	20.425	4.7	4.5	4.6	4.5	4.575
23	22.6	22.5	22.4	22.475	4.2	4.2	4.3	4.2	4.225
25	24.9	24.8	24.8	24.75	4.2	4	4.1	4	4.075
27	26.7	26.6	26.6	26.6	4	3.8	3.9	3.8	3.875
30	28.9	29.1	28.7	28.8	3.7	3.6	3.8	3.7	3.7
32	31.1	31.1	31.1	31.05	3.5	3.4	3.6	3.5	3.5

NGT02-0.65

water tem	Surface temerature (°C)			average	Surface resistivity (kOhm/cm)			average
3	3.1	3	3.1	3.125	8.3	8.3	8.3	8.1	8.25
5	5.4	5.4	5.4	5.45	7.8	7.9	7.9	7.7	7.825
7	7	7	6.9	7	7.4	7.5	7.5	7.2	7.4
9	9.1	9.2	9.1	9.125	7	7	7	6.8	6.95
11	11.1	11	11.3	11.175	6.5	6.6	6.7	6.4	6.55
13.5	13.6	13.6	13.6	13.6	6.2	6.2	6.3	5.9	6.15
15.5	15.5	15.5	15.5	15.5	5.8	5.8	5.9	5.7	5.8
17.5	17.4	17.4	17.4	17.4	5.5	5.4	5.6	5.4	5.475
20	19.9	19.7	19.7	19.75	5.1	5.2	5.3	5	5.15
22.5	22.4	22.4	22.4	22.4	4.8	4.9	4.9	4.7	4.825
24.5	24.1	24.1	24.1	24.1	4.7	4.7	4.8	4.5	4.675
26.5	26.3	26.3	26.2	25.8	4.5	4.5	4.5	4.3	4.45
28.5	28.1	28.1	28.1	28	28.075	4.3	4.3	4.4	4.1	4.275
30.5	29.9	29.3	29.7	29.5	29.6	4.1	4.1	4.1	3.9	4.05
32	31.5	31.5	31.3	31.1	31.35	3.9	3.9	4	3.8	3.9

Appendix P - Surface Resistivity – Temperature (w/c 0.45)

ALT01-0.45

core tem	Surface temperature (°C)			average	Surface resistivity (kOhm/cm)			average
2.4	3.4	3.8	3.4	3.525	13.7	15	14.6	14.225
4.4	5.4	5.4	5.5	5.45	12.6	13.9	13.7	13.25
6.4	7.9	8	7.9	7.925	11.7	12.7	12.6	12.175
8.5	10	10	9.8	9.925	10.9	11.9	11.7	11.3
10.4	11.6	11.6	11.5	11.55	10.2	11	11	10.6
12.5	14.1	14.1	14.1	14.1	9.4	10.3	10.1	9.8
14.4	15.9	15.9	15.9	15.9	8.8	9.8	9.5	9.225
16.4	17.8	17.7	17.7	17.725	8.3	9	9	8.65
18.5	20.4	20.4	20.3	20.35	7.7	8.4	8.3	8.025
20.4	21.9	21.9	21.9	21.9	7.3	8	7.9	7.625
22.4	24.1	24	24	24.025	6.8	7.4	7.4	7.125
24.5	25.9	25.9	25.8	25.85	6.5	7.1	7	6.8
26.5	27.8	27.7	27.7	27.6	6.1	6.8	6.7	6.45
28.5	29.3	29.2	29.2	29.1	5.8	6.5	6.4	6.15

ALT02-0.45

core tem	Surface temperature (°C)			average	Surface resistivity (kOhm/cm)			average
2	3.7	3.5	3.4	3.525	13	13.4	14.3	13.625
4	4.5	4.4	4.2	4.35	12.5	12.9	13.6	13.075
6	7	6.9	7	6.925	11.4	11.8	12.6	12
8	8.8	8.8	8.8	8.825	10.6	11	11.8	11.375
10	11.6	11.2	11.3	11.375	9.8	10.1	10.8	10.225
12	13.9	13.9	13.8	13.825	9	9.5	10.1	9.55
14	15.8	15.8	15.7	15.75	8.6	8.8	9.3	8.925
16	18	17.8	17.9	17.9	8	8.3	8.8	8.375
18	20.6	20.6	20.6	20.6	7.4	7.6	8.1	7.75
20	23	23	22.8	22.875	7	7.2	7.7	7.325
22.5	25	25	24.8	24.95	6.4	6.6	7.1	6.7
25.5	28.5	28.4	28.2	28.3	5.8	6.1	6.5	6.2
27.5	29.9	29.8	29.7	29.675	5.5	5.8	6.2	5.9
29.3	31	31	30.8	30.875	5.3	5.6	5.9	5.7

AGT01-0.45

water tem	Surface temperature (°C)			average	Surface resistivity (kOhm/cm)			average
4	4.7	4.8	4.8	4.775	15.5	14.1	14.9	14.775
6	6.2	6.2	6.3	6.25	14.8	13.5	14.2	14.05
9	8.6	8.6	8.6	8.6	12.7	13.6	12.6	13.025
10.5	10.6	10.6	10.6	10.6	11.9	12.6	11.8	12.2
13	13.1	13.1	13.2	13.15	11	11.9	10.8	11.4
15	15.1	15.1	15.2	15.175	10.2	10.9	10.1	10.7
17	17.3	17.5	17.5	17.4	9.5	10.3	9.4	9.9
19	18.9	18.9	18.9	18.9	9.1	9.8	8.9	9.3
21	20.9	20.6	20.9	21	8.6	8.8	8.3	8.9
23	22.9	22.9	22.5	22.7	8	8.4	7.8	8.2
25	25.3	25.3	25	25.15	7.6	8	7.4	7.8
27	26.7	27	26.7	26.7	7.2	7.6	7	7.3
29	28.7	28.4	28.4	28.425	6.7	7.3	6.6	7
30	29.8	29.9	29.7	29.7	6.5	7	7.4	6.8
31	30.6	30.6	30.6	30.625	6.3	6.7	6.2	6.6

AGT02-0.45

water tem	Surface temperature (°C)			average	Surface resistivity (kOhm/cm)			average
3	3.9	3.8	3.8	3.825	17.8	17.1	16.7	17.025
5	4.9	4.8	4.8	4.95	17.4	16.2	15.5	16.15
7	6.9	6.8	7	6.925	16.1	15.2	14.3	15.05
9	9.1	8.9	8.9	8.95	14.9	14.1	13.3	13.95
11	11.1	11.1	11.1	11.1	13.6	13.1	12.3	12.5
13	12.7	12.7	12.7	12.7	12.7	12.4	11.7	11.9
15	15	15	15	15	12.1	11.4	10.9	11
17	16.7	16.7	16.7	16.7	11.1	10.7	10.3	10.4
19	18.4	18.4	18.4	18.4	10.9	10.3	9.6	9.8
21	20.8	20.5	20.5	20.6	10.2	9.5	9	9.1
23.5	23.1	23.3	23.1	23.15	9.3	8.8	8.2	8.4
25	25	24.9	24.8	24.9	8.7	8.4	7.9	8
27	26.7	26.7	26.4	26.55	8.2	7.9	7.5	7.5
29.5	28.8	28.8	29.1	28.875	7.8	7.4	7	7
31	30.4	30.3	30	30.2	7.4	7	6.7	6.8

NLT01-0.45

water tem	Surface temperature (°C)			average	Surface resistivity (kOhm/cm)			average
3	2.8	3.3	3	2.95	14.1	12.8	13.9	13.6
5.5	5.3	5.4	5.4	5.375	13.1	11.9	12.9	12.4
7	7	7	7	7.025	12.3	11.3	12.1	11.8
9.5	9.5	9.3	9.3	9.4	11.4	10.3	11	10.7
11	10.7	10.7	10.7	10.725	10.8	9.9	10.5	10.3
13	12.7	12.7	12.6	12.675	10.2	9.2	9.9	9.7
15	14.4	14.4	14.8	14.525	9.4	8.6	9.3	9
17.5	17.2	17.2	17.3	17.25	8.6	7.8	8.4	8.2
19.5	19	18.9	18.9	18.925	8.1	7.4	8	7.7
21	20.4	20.3	20.4	20.375	7.8	7	7.7	7.4
23	22.7	22.7	22.8	22.8	7.3	6.6	7.1	6.9
25	24.4	24.4	24.4	24.4	6.9	6.2	6.6	6.6
27.5	27.2	27	27.2	27.1	6.3	5.8	6.3	6.1
29.5	28.5	28.5	28.3	28.4	6	5.5	6	5.7
31.5	31	30.7	30.8	30.8	5.6	5.1	5.5	5.4

NLT02-0.45

water tem	Surface temperature (°C)			average	Surface resistivity (kOhm/cm)			average
3	4	3.5	4	3.875	13.9	14.5	15	14.6
5	4.9	5.6	5.7	5.275	13.5	13.9	14.2	13.7
7	6.4	6.4	6.4	6.4	12.9	13.3	13.5	13.1
9.5	8.9	8.9	9	8.95	11.9	12.4	12.5	12.2
11.5	10.3	10.3	10.3	10.3	11.3	11.5	11.8	11.6
14	13.1	13.1	13	13.05	10.2	10.4	10.8	10.5
16.5	15.5	15.5	15.5	15.5	9.4	9.5	10	9.7
18.5	17.5	17.5	17.3	17.4	8.8	9	9.2	9
20.5	19.3	19.2	19.2	19.225	8.2	8.4	8.8	8.5
22.5	21.1	21.1	21.2	21.15	7.7	7.9	8.1	7.9
24.5	23.4	23.1	23.1	23.175	7.3	7.5	7.7	7.4
26.5	25	25	25	25.1	6.7	6.9	7.1	6.9
28.5	26.9	26.5	26.3	26.6	6.3	6.5	6.7	6.5
30.5	29.6	29.4	29	29.175	5.9	6.1	6.4	6.1
32.5	31	31	30.7	30.775	5.7	5.9	6.1	5.8

NGT01-0.45

water tem	Surface temperature (°C)			average	Surface resistivity (kOhm/cm)			average
3	3.4	3.3	3.7	3.6	13.2	14.2	14	13.7
5.5	5.5	5.5	6.2	5.6	12.3	13.2	13.2	13.1
7.5	7.4	7.1	7.2	7.2	11.6	12.7	12.2	12.2
9.5	8.8	8.8	9	9	10.9	11.7	11.6	11.6
12	11.4	11.4	11.5	11.5	10	11	10.7	10.6
15	14.6	14.6	14.6	14.6	9.2	9.9	9.7	9.8
17	16.2	16.2	16.1	16.2	8.7	9.4	9.4	9.2
18.5	17.7	17.7	17.7	17.7	8.2	8.7	8.9	8.8
20.5	19.4	19.4	19.6	19.5	7.7	8.2	8.3	8.3
23	22	22	22	22	7.2	7.5	7.7	7.7
24.5	23.3	23.2	23.3	23.3	6.8	7.5	7.2	7.3
26.5	25.3	25.3	25	24.8	6.5	7	6.8	6.9
28.5	27.2	27.1	26.7	26.8	6	6.5	6.5	6.4
31	29.7	29.5	29.3	29.5	5.6	6.1	6	6.1
32.5	31.2	31.1	30.7	30.7	5.5	5.9	5.7	5.8

NGT02-0.45

water tem	Surface temperature (°C)			average	Surface resistivity (kOhm/cm)			average
3	2.4	2.5	2.9	2.6	15.9	15.8	13.9	13.8
5	5.1	5.1	6.1	5.6	14.5	14.5	12.9	12.6
7	7.2	7	7.1	7.1	13.4	13.3	11.7	11.8
9.5	9.3	9.3	9.3	9.3	12.4	12.6	10.9	10.8
11.5	11	10.8	11.1	11.4	11.7	11.8	10.4	10.4
13.5	13.1	12.9	13.1	13.3	11.9	11.2	9.6	9.7
15.5	15.4	15.2	15.2	15.2	10.2	10.2	9	9
17.5	16.6	16.7	16.6	16.8	9.7	9.8	8.5	8.6
19.5	19	18.9	18.9	18.9	9.1	9.1	7.9	7.9
22	21.5	21.4	21.4	21.4	8.2	8.4	7.4	7.3
23.5	23.3	23.3	23.3	23.2	7.8	7.8	6.9	6.9
25.5	25.1	25.1	25.2	25.3	7.4	7.4	6.4	6.5
27.5	27	27.1	26.3	26.4	6.9	7	6.1	6.1
29.5	29.2	29.2	29.1	29.1	6.5	6.5	5.7	5.7
31.5	30.8	31.1	31.1	31	6.1	6.1	5.4	5.5